Thermoacoustic-wave equation and its application to marginal conditions for the onset of gas oscillations in a looped tube

Hiroaki HYODO

March 2014

Thermoacoustic-wave equation and its application to marginal conditions for the onset of gas oscillations in a looped tube

A dissertation submitted to
THE GRADUATE SCHOOL OF ENGINEERING SCIENCE
OSAKA UNIVERSITY
in partial fulfillment of the requirements for the degree of
DCOTOR OF PHILOSOPHY IN ENGINEERING

BY

Hiroaki HYODO

March 2014

Abstract

When a quiescent gas enclosed by a wall is subjected to temperature gradient, it may become unstable and begin to oscillate spontaneously in spite of the diffusive effects by viscosity and thermal conductivity. This phenomena are called thermoacoustic ones, in which interconversion between mechanical and thermal energy is taking place. Recently, much attention has been paid to heat engines using the phenomenon, in particular, to the heat engines exploiting a gas-filled, looped tube. Main features of this engine are in emergence of a traveling wave transporting acoustic energy flux, and yielding higher efficiency than a heat engine exploiting a standing wave. However, because physical mechanisms occurring in the engine are not well understood, it is difficult but important not only to identify marginal conditions for the onset of oscillations but also to quantify the phenomena, especially, in order to construct large-scaled engines.

This thesis deals with the marginal conditions based on the thermo- acoustic-wave equation and clarifies quantitatively the marginal state of oscillations. This equation is derived in the linear framework and based on the narrow-tube approximation that a typical span length is much smaller than a typical axial length. While Rott's equation in a frequency domain is well known in thermoacoustics and useful in deriving marginal conditions, the thermoacoustic-wave equation corresponds to the equation expressed in the space- and time-domain and enables to solve a transient behavior of an initial disturbance. The equation may be approximated by the ratio of a thickness of thermoviscous diffusion layer to a span length of a gas passage.

Before deriving marginal conditions, effects of heat conduction in a wall are examined on the thermoacoustic-wave equation, though the effects are usually regarded as being negligible. It is revealed that the effects have no substantial influence in the case of thin diffusion layer, whereas they give rise to substantial influence in the case of thick diffusion layer. However, it is also revealed that the effects introduce no new terms so that their effects may be taken into account by adjusting the coefficients of the approximate equation for the thick diffusion layer. Using the approximate equations for thick and thin diffusion layers, attempt is made to derive analytically marginal conditions for a gas in a looped tube with a stack which consists of many pores axially inserted. For plausible temperature distributions along the stack and the buffer tube, analytical solutions are obtained and a frequency equation is derived. Seeking a real solution for a frequency, marginal conditions are obtained numerically. By using the conditions, marginal states of oscillations are obtained. Finally the marginal conditions are checked against the ones derived by solving Rott's equation numerically. It is shown that the approximate equations can give the conditions and the marginal state of oscillations adequately. As this comparison implies, it is concluded that the approximate equations simplify the complicated Rott's theory and clarify physical mechanisms involved in the thermoacoustic phenomena.

Contents

1 Introduction

It happens that a gas enclosed by a wall with temperature gradient axially begins to oscillate in spite of diffusive effects by the viscosity and the thermal conductivity of the gas. Such phenomena are called thermoacoustic ones. The representative example is Taconis oscillation (Taconis *et al.* (1949)). This phenomenon occurs when a narrow tube with one end open is inserted to a dewar and the open end approaches the surface of liquid helium, the gaseous helium in the tube begins to oscillate spontaneously. This is merely an example of thermoacoustic phenomena so these may be happen even in the region other than the low temperature one.

Essence of the phenomena is in the interconversion between the thermal energy and kinematic one. Because energy of gas oscillations is supplied by ambient heat source, energy conversion takes place from thermal energy to mechanical one. This is the very action of a prime mover. On the contrary, when a gas is subjected to forced oscillations, it happens that a heat flux flows against a temperature gradient along the tube wall. This is the very action of the heat pump.

Recently application of thermoacoustic phenomena to heat engine has been attempted (Swift (2002), Garrett (2004)). Especially, thermoacoustic heat engines exploiting a gas-filled, looped tube have attracted much attention (Yazaki *et al.* (1998), Backhaus & Swift (1999), (2000), Yazaki *et al.* (2002)). Main features are in emergence of a traveling wave transporting acoustic energy flux, and yielding higher efficiency as a heat engine. Most of all approaches are experimental ones, by which, however, it is difficult to derive the marginal conditions of the onset of the gas thoroughly. Therefore it is helpful to derive the marginal conditions theoretically and the establishment of the theory of thermoacoustics is required in order to comprehend these phenomena and develop the devices.

Theoretical approach to thermoacoustic phenomena based on fluid dynamics was initiated by Rott (Rott (1969), (1973)). He derived an equation for a complex pressure amplitude of the gas under the temperature gradient, which has no limitation of the thickness of diffusion layer to the tube radius. This equation is derived in the linear theory for a harmonic component under a narrow tube approximation that a typical span length is much smaller than a typical axial length. Stability analysis of Taconis oscillation was performed by setting a step temperature distribution to solve the equation analytically in spite of physical irrelevance of the step. Although observed thermoacoustic phenomena are nonlinear ones, it is a first step to make a linear stability analysis for an infinitely small disturbance. The marginal curves are compared with the experimental results later, and shown to agree quantitatively (Yazaki *et al.* (1998)). Recently, the boundary-layer theory is developed in the axial space- and time-domain to this problem by assuming that the diffusion layer is thinner than the span width, and marginal conditions of the Taconis oscillations are derived by Sugimoto & Yoshida (2007). It is revealed that the conditions agree qualitatively with the ones by Rott's theory. The boundary-layer theory has also been applied to derive marginal conditions of the Sondhauss tube by Sugimoto & Takeuchi (2009).

The boundary-layer theory has an advantage in that it may be extended to nonlinear regime, and it can capture unstable and transient behaviors leading to nonlinear saturation of oscillations (Sugimoto & Shimizu (2008), Shimizu & Sugimoto (2010), Shimizu *et al.* (2012)). Recently, though in linear frame works, a thermoacoustic-wave equation has

been derived based on the narrow tube approximation [Sugimoto(2010) referred to as paper I]. This is a one-dimensional wave equation for an excess pressure of the gas in a two-dimensional channel or a circular tube with temperature gradient and given in the space- and time-domain, by taking into account the history effect due to diffusion one.

When a single time-harmonic component is considered, the wave equation is reduced to Rott's equation. However, because the equation is valid for any temporal behavior than the harmonic one, it enables to unveil an unstable transient behavior before nonlinearity sets in. This theory is expected to be extended to nonlinear regime, as in the case of the boundary-layer theory in which the diffusion layer is thin.

This thesis is organized as follows. The first part deals with effects of heat conduction in a wall on the thermoacoustic-wave equation. This equation focuses on the gas in one flow passage and ignores the temperature fluctuation of the wall by assuming that the heat capacity of the wall is larger than that of gas. However, the actual thermoacoustic devices exploit a so-called stack consisting of the narrow pores where the wall thickness is comparable with the span of the flow passage. Then it is expected that the effect of the thermal conductivity of the solid wall can not be ignored. Therefore, it is necessary to clarify the effect of thermal conductivity of the wall on the thermoacoustic-wave equation. Assuming the flow passages are arranged periodically, the temperature variations in the solid wall are solved simultaneously with the variations in the gas to derive the thermoacoustic-wave equation. Approximation of the equation is also discussed by the thickness of diffusion layer to unveil influences of the heat conduction in the wall.

The second part applies the approximate wave equations to derivation of marginal conditions for the onset of thermoacoustic oscillations of a gas-filled looped tube with a stack inserted. For the gas in the pore in the stack, the approximate equation for the thick diffusion layer theory is applied, while for the gas elsewhere, the approximate theory for the thin diffusion layer theory is employed. Given physically plausible and mathematically amenable temperature distributions along the loop, analytical solutions are derived to seek marginal conditions of instability in the gas-filled looped tube.

The last part verifies the marginal conditions obtained in the part 2 against the ones obtained by solving Rott's equation, which is assumed to be valid for the gas everywhere in the looped tube. Because Rott's equation is difficult to solve analytically for smooth temperature distributions, it is solved numerically by Runge-Kutta method combined with a shooting method. It is shown that the marginal conditions obtained by the asymptotic theories agree with the ones by Rott's theory.

Usefulness of the asymptotic theories is demonstrated. Although the asymptotic theories cannot cover a whole domain of the thickness of the diffusion layer against a span length of the flow passage, they are simple and are able to provide insights into mechanisms of thermoacoustic phenomena which cannot be seen in Rott's theory. In addition, they allow us to impose an initial-value problem to clarify a transient behavior. The approaches by the thermoacoustic-wave equation in the space- and time-domain have advantages over Rott's theory.

2 Thermoacoustic-wave equation with effects of heat conduction in wall

Influences of heat conduction in solid wall on thermoacoustic-wave propagation in gas-filled channels or tubes subject to temperature gradient axially are examined. Neglecting the effects, thermoacoustic-wave equation for excess pressure by using the narrow-tube approximation have been already derived. Effects of heat conduction in wall are regarded to be negligible because when the heat capacity of the wall is regarded as infinitely large, no variations in the wall temperature occur irrespective of temperature variations in gas. This assumption may be relevant usually in the context of classical acoustics.

In recent thermoacoustic devices, however, so-called stacks are exploited (e.g. Swift (2002)), in which ceramics or polymers are used for wall materials, or a wall thickness is comparable with a span length of the channels or the tubes. In such a situation, it is unclear as to whether or not the above assumptions are satisfied fully.

But studies on the effects of heat conduction in wall are not many. Rott Rott (1973) included the effects of heat conduction. Later Swift (1988) also included them in developing the linear theory for two-dimensional channels bounded by plates taking account of finite thickness of them. The effects appear through the square root of product of the ratio of the heat capacities of the gas to the solid per volume, and the ratio of the thermal conductivities of the gas to the solid. Because this ratio, denoted by ε, is usually very small of order, the effects were considered to be negligible.

It is seen in Swift's theory (1988) in a frequency domain that the effects of heat conduction in the wall introduce a following factor to Rott's equation

$$\{1 + \varepsilon \tanh[H(-\mathrm{i}\omega/\kappa_e)^{1/2}]/\tanh[d(-\mathrm{i}\omega/\kappa_s)^{1/2}]\}^{-1},$$

where H and d denote, respectively, half the width of the channel and of the solid wall, and κ_e and κ_s denote, respectively, the thermal diffusivities of the gas and of the solid, ω being a typical angular frequency and i imaginary unit. For a small value of ε, it appears to be appropriate to expand the factor asymptotically in terms of ε and to take account of its first-order effects. But because the factor has poles in a complex plane of the frequency, there arises non-uniformity in the expansion, depending on values of d/H and κ_e/κ_s. This implies a sort of resonance occurs. In this case, effects may not be within the order ε.

We examine the effects of heat conduction in solid wall on thermoacoustic-wave equation by considering the stack model placed periodically. And thermoacoustic-wave equation is approximated based on asymptotic theories. There are two cases that the ratio of thickness of diffusion layer to the span length of gas passage is thick or thin. Effects on asymptotic theories are examined. Effects of resonance case and the conditions at which it occurs are examined.

2.1 Model of problem

To examine effects of heat conduction in wall on thermoacoustic-wave propagation, two models are considered. One is for propagation in two-dimensional channels between parallel plates of thickness $2d$ stacked in the direction normal to the plates periodically with distance $2H$ apart. Taking the y-axis along this direction, the x-axis is taken in parallel

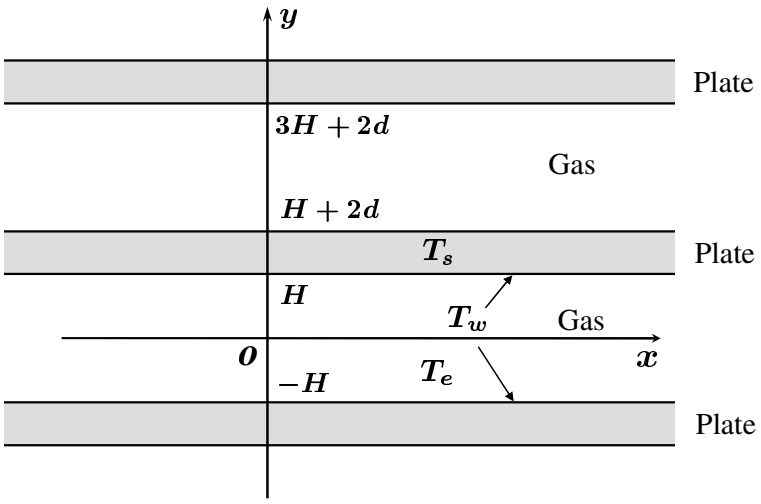

Figure 1: Illustration of two-dimensional channels of width $2H$ separated by an infinite stack of solid plates of thickness $2d$ subjected to non-uniform temperature distribution in the x-direction where T_e, T_s and T_w denote, respectively, the temperatures of gas, solid plate and wall surfaces in a quiescent state, and the origin of the coordinate axes x and y is chosen in one cell of the channels.

to the plates along the direction of wave propagation. The origin of the axes is taken at a midpoint spanwise in one 'cell' of the channels in the stack of plates. Figure 1 shows geometrical configuration of the channels where no variations are assumed in the direction normal to the sheet of paper.

The other model is for propagation in a periodic array of circular tubes. Two arrangements are conceivable, one being a square array in a plane normal to the axis of the tubes, and the other a staggered array, as shown in figures $2(a)$ and $2(b)$, respectively. In the square array, circular tubes of radius R and of thickness d are embedded in a solid matrix. The centres of the tubes are located at four corners of square of side length $2(R + d)$. In the staggered array, the centres are located at three corners of triangle of side length $2(R+d)$. If the material of tubes is the same as the one of the matrix, then a term 'pores' may rather be suitable.

In both models, the channels and the tubes extend infinitely not only in the x-direction but also periodically in a plane normal to the x-axis so that no outer boundaries are considered. Solid walls are assumed to be rigid with smooth surface. A phenomenon occurring in one cell of the channels or the tubes is assumed to be identical to those in the other cells. Because of the spatial periodicity in arrangements, only a unit cell with the origin of the coordinate axes taken is considered.

2.2 Steady temperature fields

The solid wall is subjected to temperature gradient in the x-direction. In a quiescent state of the gas where no gravity is assumed, steady temperature fields in the gas and the solid

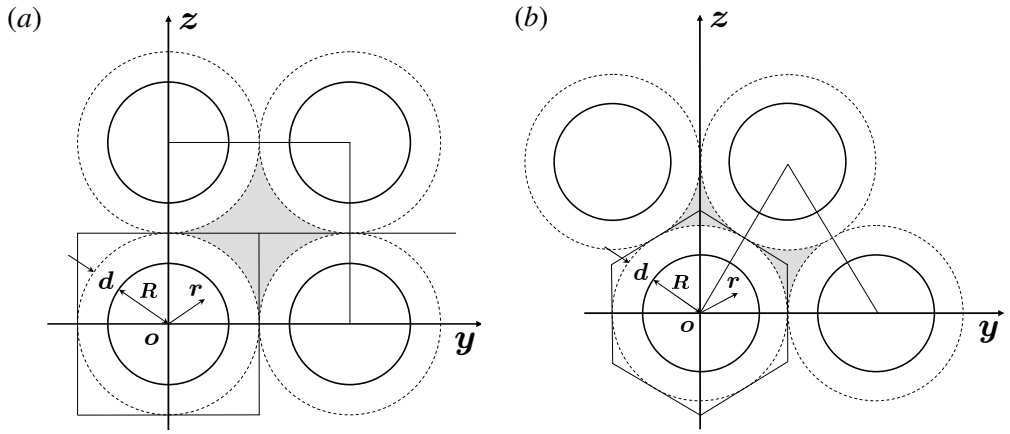

Figure 2: Arrangements of the circular tubes in the axial cross-section where (a) and (b) show, respectively, the square and staggered arrays of the tubes of radius R and of thickness d, which are embedded in a solid matrix (shaded area), and the origin of the radial coordinate r is chosen in one cell bounded by the square in (a) and the hexagon in (b).

are sought. Letting the temperature at the wall surface between the gas and the solid be T_w, axial variation of this is assumed to be gentle enough over a distance comparable with a span length to satisfy a following condition:

$$\frac{H^2}{T_w}\left|\frac{\partial^2 T_w}{\partial x^2}\right| \ll \frac{H}{T_w}\left|\frac{\partial T_w}{\partial x}\right| \ll 1, \tag{2.1}$$

where T_w is a function of x only for the channels. For the tubes, H is replaced by R but T_w will depend not only on x but on a circumferential coordinate of the tube. This will be discussed later. No boundary conditions in the axial direction are considered since the channels and tubes are assumed to be long enough.

The temperature field in the solid, denoted by T_s, is first sought. Because the heat flux $-k_s\nabla T_s$ must be divergence-free, where k_s is a thermal conductivity of the solid and is assumed to be a constant independent of the temperature, T_s satisfies the Laplace equation $\Delta T_s = 0$. As long as the assumption (2.1) is valid, T_s is obtained for the case of the channels as

$$T_s = T_w + \frac{1}{2}\frac{\mathrm{d}^2 T_w}{\mathrm{d}x^2}\left[d^2 - (y - H - d)^2\right] + \cdots, \tag{2.2}$$

for $H < y < H + 2d$, where $T_w(x)$ denotes a temperature on the wall surfaces at $y = H$ and $y = H + 2d$ (also at $y = -H$), which is an unknown function of x, and the symmetry with respect to $y = H + d$ has been used.

For the gas, the temperature field also satisfies $\nabla \cdot (k\nabla T) = 0$, k being a thermal conductivity of gas. This conductivity and a shear viscosity μ are assumed to be dependent on the temperature in the form of a power law given by

$$\frac{k}{k_0} = \left(\frac{T}{T_0}\right)^{\beta} \quad \text{and} \quad \frac{\mu}{\mu_0} = \left(\frac{T}{T_0}\right)^{\beta}, \tag{2.3}$$

where β is a positive constant between 0.5 and 0.7 for air, and the subscript 0 is used to imply a value of a quantity or a variable attached in a quiescent, reference state. With (2.3), $T^{1+\beta}$ satisfies the Laplace equation $\Delta T^{1+\beta} = 0$.

In the same way as that leading to (2.2), $T^{1+\beta}$ may be obtained as

$$T^{1+\beta} = T_w^{1+\beta} + \frac{1}{2}\frac{\mathrm{d}^2}{\mathrm{d}x^2}(T_w^{1+\beta})\left(H^2 - y^2\right) + \cdots, \tag{2.4}$$

where T is equal to T_w at the wall surfaces $y = \pm H$. Since the second term is assumed to be small, (2.4) is expanded into

$$T = T_w + \frac{T_w^{-\beta}}{2(1+\beta)}\frac{\mathrm{d}^2}{\mathrm{d}x^2}(T_w^{1+\beta})\left(H^2 - y^2\right) + \cdots. \tag{2.5}$$

For this distribution, the continuity of heat fluxes through the wall surfaces is required, i.e. $-k\partial T/\partial y = -k_s\partial T_s/\partial y$. Thus it follows that

$$\frac{k_0 H T_0}{1+\beta}\frac{\mathrm{d}^2}{\mathrm{d}x^2}\left(\frac{T_w}{T_0}\right)^{1+\beta} = -k_s d\frac{\mathrm{d}^2 T_w}{\mathrm{d}x^2}. \tag{2.6}$$

Equation (2.6) is readily integrated to yield an equation which determines the temperature distribution T_w on the wall as

$$\frac{1}{1+\beta}\left(\frac{T_w}{T_0}\right)^{1+\beta} + \frac{k_s}{k_0}\frac{d}{H}\frac{T_w}{T_0} = c_1 + c_2 x, \tag{2.7}$$

where c_1 and c_2 are arbitrary constants to be determined by boundary conditions at both ends of the channels, though not specified in the present context.

If $k_s d/k_0 H \gg 1$, $(T_w/T_0)^{1+\beta}$ is negligible so that T_w/T_0 may be approximately given by a linear function of x as $(k_0 H/k_s d)(c_1 + c_2 x)$. If $k_s d/k_0 H$ is comparable with unity, then (2.7) should be solved for T_w/T_0, which is given by a nonlinear function of x. Note that this distribution is monotonic in x.

For the case of tubes or bores, the temperature fields are not so easily obtained. The temperature field of the solid must satisfy, by symmetry, no heat flux $-k_s\partial T_s/\partial n = 0$ along each side of the square or hexagonal cell, n denoting the normal coordinate along the periphery of the cell. While the temperature field is uniform over a cross-section to the lowest approximation, higher-order corrections similar to (2.2) and (2.4) are no longer functions of radial coordinate r only, but periodic functions in a circumferential coordinate. They are difficult to be obtained.

If the boundary conditions are replaced by $\partial T_s/\partial r = 0$ at $r = R + d$, then the axisymmetric temperature field is readily obtained as

$$T_s = T_w + \frac{1}{4}\frac{\mathrm{d}^2 T_w}{\mathrm{d}x^2}\left[R^2 - r^2 + 2(R+d)^2\log\left(\frac{r}{R}\right)\right], \tag{2.8}$$

where $T_w(x)$ stands for a temperature along the wall surface at $r = R$. This is a situation in which the circular tubes having thickness d and thermal conductivity k_s are embedded in non-heat-conducting matrix (shaded area in figure 2). Such a model will be treated in the following for the sake of simplicity. This will be closer to a situation in the staggered array than that in the square array because the fraction of the shaded area to the total area of the unit cell is smaller in the former case.

For the gas, the temperature field is obtained as

$$T = T_w + \frac{T_w^{-\beta}}{4(1+\beta)}\frac{\mathrm{d}^2}{\mathrm{d}x^2}({T_w}^{1+\beta})\left(R^2 - r^2\right). \tag{2.9}$$

The continuity of heat fluxes at $r = R$ leads to

$$\frac{1}{1+\beta}\left(\frac{T_w}{T_0}\right)^{1+\beta} + \frac{k_s}{k_0}\frac{[(R+d)^2 - R^2]}{R^2}\frac{T_w}{T_0} = c_1 + c_2 x, \tag{2.10}$$

c_1 and c_2 being arbitrary constants. Although the coefficient in the second term is different from (2.7), the analysis will be made in parallel.

2.3 Narrow-tube approximation and dimensionless parameters

At first, we explain the narrow-tube approximation. We consider the situation that the gas is in the tube of which the wall is subject to temperature gradient. There are three length scales in the problem. One is a typical span length, H, another a typical axial length L in temperature gradient or a typical axial wavelength of pressure disturbances a_0/ω, a_0 and ω being an adiabatic sound speed and a typical angular frequency, and the other a typical thickness of viscous diffusion layer $\sqrt{\nu/\omega}$ or thermal one $\sqrt{\kappa/\omega}$, respectively, ν being a kinematic viscosity. Because the Prandtl number Pr $(= \nu/\kappa)$ is of order unity for gases, the diffusion layer is represented by the viscous one. The three dimensionless parameters are introduced as follows:

$$\frac{H}{L} \equiv \lambda \ll 1, \quad \frac{\omega L}{a_0} \equiv \frac{1}{\chi} \le O(1) \quad \text{and} \quad \frac{\sqrt{\nu/\omega}}{H} \equiv \delta = O(1), \tag{2.11}$$

where χ takes a value larger than unity but it takes unity if temperature gradient is absent. It should be emphasized here that the term 'narrow tube' in this paper means a case with $\lambda \ll 1$ not $\delta \gg 1$. The latter will be called a case of thick diffusion layer.

When the heat conduction in wall is taken into account, it will be revealed that introduction of following parameters combined is useful rather than simple ratios:

$$\frac{k_s/\rho_s c_s}{k_e/\rho_e c_p} = \frac{\kappa_s}{\kappa_e} \equiv K, \quad \sqrt{\frac{\rho_e c_p k_e}{\rho_s c_s k_s}} = \sqrt{K}\,\frac{k_e}{k_s} \equiv \varepsilon \quad \text{and} \quad \sqrt{\frac{\kappa_e}{\kappa_s}}\frac{d}{H} = \frac{1}{\sqrt{K}}\frac{d}{H} \equiv Ge, \tag{2.12}$$

where the subscripts e and s designate value of quantities for the gas in quiescent state and the one for the solid, respectively, and these parameters vary along the channels or tubes, since the quantities with e are dependent on temperature. While necessity of introduction of K is obvious, ε measures the square root of product of two ratios, one being the ratio of the heat capacity of gas per volume $\rho_e c_p$ to the one of solid $\rho_s c_s$, and the other the ratio of the thermal conductivity of gas k_e to the one of solid k_s. Because both ratios are very small, admittedly, ε is a small parameter. The last parameter Ge measures geometry of the two-dimensional channels. For the case of the circular tubes, Ge will be defined later by (2.99).

Here we refer to the value of dimensionless parameters related to thermal properties of gases and solids used in thermoacoustic heat engines.

The values for the gases are taken from the database of the National Institute of Standards and Technology (NIST, US Department of Commerce), Thermophysical properties of pure fluids–NIST12 Version 5.2 (see also Turns (2006)). The values of the pure copper and the stainless steel (AISI 304) are taken from Incropera & DeWitt (1990). The values

K	ceramics	copper	polyimide	steel
air	3.61	5.234	3.48×10^{-3}	0.178
argon	3.82	5.532	3.68×10^{-3}	0.188
helium	0.44	0.631	4.19×10^{-4}	0.0214
nitrogen	3.67	5.319	3.54×10^{-3}	0.180

Table 1: Numerical values of K $(= \kappa_s/\kappa_e)$ for combinations of the gas in the left column and the solid in the top row at 1 atm and 300K.

$\varepsilon \times 10^4$	ceramics	copper	polyimide	steel
air	2.95	1.505	130	7.46
argon	2.05	1.046	90.2	5.19
helium	6.06	3.090	266	15.3
nitrogen	2.93	1.494	129	7.40

Table 2: Numerical values of ε $(= \sqrt{\rho_e c_p k_e/\rho_s c_s k_s})$ times 10^4 for combinations of the gas in the left column and the solid in the top row at 1 atm and 300K.

of the ceramics are taken from Zhou *et al.* (2004). The values of the polyimide are taken from the Technical Data Sheet of DuPont Kapton HN.

Tables 1 and 2 show numerical values of K and ε, respectively, calculated for 16 combinations of the gases and the solids. It is seen that K takes values of order unity except for the case of polyimide and for the combination of the helium with steel. It is remarked that K for the ceramics is close to the one for the copper. On the other hand, ε takes a small value of order 10^{-4} except for the case of polyimide. Even for this case, ε takes a value of order 10^{-2}. This fact suggests us to use ε as a small parameter and to expand solutions in terms of it.

2.4 Basic equations and boundary conditions

In a quiescent state, let the pressure in the gas p take a uniform value p_0 throughout, while let the temperature of gas be equal to the one of solid wall, as long as $\mathrm{d}^2T_w/\mathrm{d}x^2$ is neglected. According to our notation used so far, the temperature of gas in the quiescent state is denoted by T_e rather than T_w so that $T = T_e$ and $T_s = T_e$. The linearized equations for the gas in the narrow-tube approximation are given in I. In presenting the equations again here, the integer j is prepared to distinguish between the cases of channels and of tubes by $j = 0$ and $j = 1$, respectively. Although the notation of y and H is often used even for the case of $j = 1$, they should be understood to be replaced by r (≥ 0) and R, respectively. All field variables are written without the subscript j because no confusion would occur.

The equations for the gas are given by the following equations of continuity, motion and energy together with equation of state for ideal gas as

$$\frac{\partial \rho'}{\partial t} + \frac{\partial}{\partial x}(\rho_e u') + \frac{1}{y^j}\frac{\partial}{\partial y}(y^j \rho_e v') = 0, \tag{2.13}$$

$$\rho_e \frac{\partial u'}{\partial t} = -\frac{\partial p'}{\partial x} + \frac{\mu_e}{y^j}\frac{\partial}{\partial y}\left(y^j \frac{\partial u'}{\partial y}\right), \tag{2.14}$$

$$0 = -\frac{\partial p'}{\partial y}, \tag{2.15}$$

$$\rho_e c_p \left(\frac{\partial T'}{\partial t} + u' \frac{\mathrm{d}T_e}{\mathrm{d}x}\right) = \frac{\partial p'}{\partial t} + \frac{k_e}{y^j}\frac{\partial}{\partial y}\left(y^j \frac{\partial T'}{\partial y}\right), \tag{2.16}$$

$$\frac{p'}{p_0} = \frac{\rho'}{\rho_e} + \frac{T'}{T_e}, \tag{2.17}$$

in $|x| < \infty$ and $|y| < H$ where ρ', p', T', u' and v' denote, respectively, disturbances in density, pressure, temperature, axial velocity in the x-direction and spanwise velocity in the y-direction from those in the quiescent state, t being the time $-\infty < t$, and the subscript e for the quiescent state implying functions of x determined by T_e.

These equations are now supplemented by the equation for the heat conduction in the solid walls. Because a span length of the wall is assumed to be comparable with that of the channels or tubes and much shorter than the typical axial length L, the narrow-tube approximation is also employed. Then the equation is approximated as

$$\rho_s c_s \frac{\partial T_s'}{\partial t} = \frac{k_s}{y^j}\frac{\partial}{\partial y}\left(y^j \frac{\partial T_s'}{\partial y}\right), \tag{2.18}$$

in $|x| < \infty$ and $H < y < H + d$ where T_s' denotes disturbance in temperature of the solid wall from T_e, and ρ_s, c_s and k_s are assumed to be constant.

Boundary conditions on the wall surface(s) require non-slip of the gas as

$$u' = v' = 0 \quad \text{at} \quad y = H \quad \text{and} \quad y = (-1)^{j+1}H, \tag{2.19}$$

and the continuity of the temperatures and of the heat fluxes as

$$T' = T_s' \quad \text{and} \quad -k_e \frac{\partial T'}{\partial y} = -k_s \frac{\partial T_s'}{\partial y} \quad \text{at} \quad y = H \quad \text{and} \quad y = (-1)^{j+1}H. \tag{2.20}$$

In addition, no heat flux is required as

$$-k_s \frac{\partial T_s'}{\partial y} = 0 \quad \text{at} \quad y = H + d. \tag{2.21}$$

Noting that p' is uniform in y from (2.15), and averaging (2.13) to (2.17) over the cross-section, the system of equations is reduced to a prototype of the thermoacoustic-wave equation for p' with a dipole s and a monopole q as

$$\frac{\partial^2 p'}{\partial t^2} - \frac{\partial}{\partial x}\left(a_e^2 \frac{\partial p'}{\partial x}\right) = \frac{2^{2j-1}}{H}\left[-\frac{\partial}{\partial x}\left(a_e^2 s\right) + \frac{a_e^2}{c_p T_e}\frac{\partial q}{\partial t}\right], \tag{2.22}$$

where a_e denotes a local adiabatic sound speed defined by $\sqrt{\gamma p_0/\rho_e}$, γ being the ratio of specific heats, and s and q denote, respectively, shear stress acting on the gas at the wall surface(s) and heat flux flowing into the gas from the wall as

$$s = \mu_e \left.\frac{\partial u'}{\partial y}\right|_{y=+H} + (j-1)\mu_e \left.\frac{\partial u'}{\partial y}\right|_{y=-H}, \tag{2.23}$$

and

$$q = k_e \frac{\partial T'}{\partial y}\bigg|_{y=+H} + (j-1) k_e \frac{\partial T'}{\partial y}\bigg|_{y=-H}. \tag{2.24}$$

Integrating (2.18) over the thickness, on the other hand, it follows that

$$\frac{\partial}{\partial t}\left(\int_H^{H+d} \rho_s c_s T_s' \, y^j \mathrm{d}y \right) = -2^{j-1} H^j q, \tag{2.25}$$

where (2.21) and (2.24) have been used. Equation (2.22) for p' is coupled with the temperature variation in the solid wall through q in (2.25). If the heat capacity of solid per volume $\rho_s c_s$ is very large, then T_s' does not change against the heat flux q. If the thermal conductivity k_s is very large in comparison with k_e, then the second condition of (2.20) suggests no temperature gradient normal to the wall surface.

2.5 Derivation of equation by Fourier transform

To derive the closed form of the thermoacoustic-wave equation, we proceed to express s and q in terms of p'. Following the same way as demonstrated in I, the method of Fourier transform is employed. It is defined by

$$\mathscr{F}\{u'\} = \frac{1}{\sqrt{2\pi}} \int_{-\infty}^{\infty} u'(x,y,t) \mathrm{e}^{\mathrm{i}\omega t} \mathrm{d}t \equiv \hat{u}'(x,y,\omega), \tag{2.26}$$

with its inverse transform given by

$$\mathscr{F}^{-1}\{\hat{u}'\} = \frac{1}{\sqrt{2\pi}} \int_{-\infty}^{\infty} \hat{u}'(x,y,\omega) \mathrm{e}^{-\mathrm{i}\omega t} \mathrm{d}\omega = u'(x,y,t). \tag{2.27}$$

Making use of the result that p' is uniform over a cross-section, a first step is to express an axial velocity u' in terms of p' by solving (2.14) together with (2.19). Next step is to express temperature T' and T_s' by solving (2.16) with u' obtained and simultaneously (2.18) so as to satisfy the boundary conditions (2.20) and (2.21). With both velocity and temperature fields available, a final step is to express s and q in terms of p' and to substitute them into (2.22). Then a thermoacoustic-wave equation for p' is derived. This equation may alternatively be derived without use of (2.22) by solving v' on substituting u' and ρ' (from (2.17)) into (2.13) and applying the boundary condition (2.19) for v'.

2.5.1 Case of the two-dimensional channels

At the outset, the axial velocity $\hat{u}'$ is obtained from (2.14). Even when the effects of heat conduction in the walls are taken into account, it is unchanged and given by

$$\hat{u}' = -\frac{1}{\rho_e} \sigma^{-1} \frac{\partial \hat{p}'}{\partial x} f, \tag{2.28}$$

with $\sigma = -\mathrm{i}\omega$ where f is defined as

$$f(x,y) = 1 - \frac{\cosh(y/H\delta_e)}{\cosh(1/\delta_e)}, \tag{2.29}$$

and δ_e is defined by

$$\delta_e(x) = \frac{1}{H}\left(\frac{\nu_e}{\sigma}\right)^{\frac{1}{2}}, \tag{2.30}$$

with $\nu_e(x) = \mu_e/\rho_e$. Here the dependence of f on σ has been suppressed and $\sigma^{-\frac{1}{2}}$ is defined to take a positive real part for a positive value of ω.

On the other hand, the temperature of gas $\hat{T}'$ must be sought by solving (2.16) simultaneously with (2.18) for that of solid wall so that the boundary conditions (2.20) may be fulfilled. Making use of the smallness of ε, an asymptotic expansion with respect to it is made and terms proportional to ε^2 or higher than it are neglected. It then follows that

$$\hat{T}' = \frac{1}{\rho_e c_p}\hat{p}' f_P + \frac{1}{\rho_e}\frac{\mathrm{d}T_e}{\mathrm{d}x}\sigma^{-2}\frac{\partial \hat{p}'}{\partial x}\left(-\frac{Pr}{1-Pr}f + \frac{1}{1-Pr}f_{\mathrm{P}}\right) + \varepsilon\hat{T}'_{\varepsilon}, \tag{2.31}$$

with $Pr = \nu_e/\kappa_e$ and

$$f_P(x,y) = 1 - \frac{\cosh(y\sqrt{Pr}/H\delta_e)}{\cosh(\sqrt{Pr}/\delta_e)}, \tag{2.32}$$

where $\varepsilon\hat{T}'_{\varepsilon}$ is a modification due to the thermal coupling with the solid wall, and the subscript P implies the Prandtl number and thermal origin. In passing, no subscript implies viscous origin. The lowest terms in (2.31) correspond to the solution without the coupling and they vanish at $y = H$ where $f = f_P = 0$. The modification is given by

$$\varepsilon\hat{T}'_{\varepsilon} = \frac{\varepsilon}{\rho_e c_p}\hat{p}' f_{KP} + \frac{\varepsilon}{\rho_e}\frac{\mathrm{d}T_e}{\mathrm{d}x}\sigma^{-2}\frac{\partial \hat{p}'}{\partial x}\left(-\frac{\sqrt{Pr}}{1-Pr}f_K + \frac{1}{1-Pr}f_{KP}\right) + O(\varepsilon^2), \tag{2.33}$$

where f_K and f_{KP} are defined, respectively, by

$$\begin{bmatrix} f_K(x,y) \\ f_{KP}(x,y) \end{bmatrix} = \begin{bmatrix} \mathcal{C} \\ \mathcal{C}_P \end{bmatrix} \frac{\cosh(y\sqrt{Pr}/H\delta_e)}{\cosh(\sqrt{Pr}/\delta_e)}, \tag{2.34}$$

with

$$\mathcal{C} = \frac{\tanh(1/\delta_e)}{\tanh(1/\delta_s)}, \tag{2.35}$$

$$\mathcal{C}_P = \frac{\tanh(\sqrt{Pr}/\delta_e)}{\tanh(1/\delta_s)}, \tag{2.36}$$

and

$$\delta_s = \frac{1}{d}\left(\frac{\kappa_s}{\sigma}\right)^{1/2}. \tag{2.37}$$

Here $\mathcal{C}$ stands for the coupling between the viscous diffusion and the thermal one in the solid wall, while $\mathcal{C}_{\mathcal{P}}$ stands for the one between the thermal diffusions of the gas and the solid, and δ_s is independent of x because κ_s is assumed to be a constant.

In consistent with (2.31) and (2.33), T'_s is obtained as

$$\hat{T}'_s = \frac{\varepsilon}{\rho_e c_p}\hat{p}' f_{SP} + \frac{\varepsilon}{\rho_e}\frac{\mathrm{d}T_e}{\mathrm{d}x}\sigma^{-2}\frac{\partial \hat{p}'}{\partial x}\left(-\frac{\sqrt{Pr}}{1-Pr}f_S + \frac{1}{1-Pr}f_{SP}\right) + O(\varepsilon^2), \tag{2.38}$$

where f_S and f_{SP} are defined, respectively, by

$$\begin{bmatrix} f_S(x,y) \\ f_{SP}(x,y) \end{bmatrix} = \begin{bmatrix} \mathcal{C} \\ \mathcal{C}_P \end{bmatrix} \frac{\cosh[(y-H-d)/d\delta_s]}{\cosh(1/\delta_s)}, \tag{2.39}$$

in $H < y < H + 2d$, and $\varepsilon\hat{T}'_\varepsilon$ matches with $\hat{T}'_s$ at $y = H$ where $f_K = f_S$ and $f_{KP} = f_{SP}$.

With $\hat{u}'$ and $\hat{T}'$ available, the shear stress on the wall surfaces is obtained as

$$\hat{s} = 2\sqrt{\nu_e}\sigma^{-\frac{1}{2}}\frac{\partial\hat{p}'}{\partial x}g(x,H), \tag{2.40}$$

while the heat flux through the wall surfaces is obtained as

$$\begin{aligned}\sigma\hat{q} = &-\frac{2c_pT_e\sqrt{\nu_e}}{a_e^2}\Bigg\{\frac{\gamma-1}{\sqrt{Pr}}\sigma^{3/2}\hat{p}'g_P(x,H) - \frac{a_e^2}{T_e}\frac{\mathrm{d}T_e}{\mathrm{d}x}\sigma^{-1/2}\frac{\partial\hat{p}'}{\partial x} \\ &\times\Big[\frac{1}{1-Pr}g(x,H) - \frac{1}{(1-Pr)\sqrt{Pr}}g_P(x,H)\Big]\Bigg\} + \varepsilon\sigma\hat{q}_w,\end{aligned} \tag{2.41}$$

with

$$\sigma\hat{q}_w = -\mathcal{C}_P\sigma\hat{q} + O(\varepsilon), \tag{2.42}$$

where g and g_P are defined, respectively, as

$$g(x,y) = \frac{\sinh(y/H\delta_e)}{\cosh(1/\delta_e)}, \tag{2.43}$$

$$g_P(x,y) = \frac{\sinh(y\sqrt{Pr}/H\delta_e)}{\cosh(\sqrt{Pr}/\delta_e)}. \tag{2.44}$$

It is found from these relations that the effects of heat conduction in wall on the gas appear in the temperature field and therefore the heat flux, but not in the velocity field and the shear stress. If the temperature gradient $\mathrm{d}T_e/\mathrm{d}x$ is absent, the heat flux is determined only by the thermal diffusivity κ_e and the pressure $\hat{p}'$ itself. This is seen in (2.41) by noting $\sqrt{\nu_e/Pr} = 1/\sqrt{\kappa_e}$ and $\sqrt{Pr}/\delta_e = (\sigma/\kappa_e)^{1/2}H$. But when the gradient is present, the viscous diffusivity ν_e comes into play in the heat flux through $g(x,H)$ together with the pressure gradient $\partial\hat{p}'/\partial x$. This is because the temperature field is affected by convection due to the second term on the left-hand side of (2.16). This convection yields one of the very features of thermoacoustic phenomena.

By the lowest temperature distribution in $\hat{T}'$, i.e. without the thermal coupling, there flows the lowest heat flux q in (2.41). This gives rise to temperature variation in the walls through (2.25). Because the heat capacity of solid per volume or its thermal conductivity is large, $\hat{T}'_s$ is much smaller than $\hat{T}'$ by the order of ε. This feeds back to $\hat{T}'_\varepsilon$ in the gas and the heat flux $\varepsilon\hat{q}_w$ flows through the wall surface. This heat flux gives rise to temperature variation in wall of order ε^2 and, in turn, to temperature variation in gas and heat flux of ε^2, and this cycle continues. The expansion is truncated at the order of ε, and no higher-order coupling between the gas and the solid is taken account. Remark that if $\mathcal{C}_P$ in (2.42) diverges, then a strong coupling is expected to take place.

Since $\hat{s}$ and $\hat{q}$ are now available, the next step is to make their inverse transforms. To do this, use is made of the following formula ((2.39) in I):

$$\frac{1}{\sqrt{2\pi}}\mathscr{F}^{-1}\left\{\sigma^{-\frac{1}{2}}\tanh(\sqrt{Pr}/\delta_e)\right\} = \Phi\left(\frac{\nu_e t}{PrH^2}\right)h(t), \tag{2.45}$$

$h(t)$ being a unit step function, where Φ is defined by

$$\Phi\left(\frac{\nu_e t}{PrH^2}\right) = \frac{2\sqrt{\nu_e}}{\sqrt{Pr}H}\sum_{n=1}^{\infty}\exp\left[-\frac{(2n-1)^2\pi^2}{4}\frac{\nu_e t}{PrH^2}\right]h(t). \tag{2.46}$$

Because this sum diverges as $t \to 0$, (2.46) is alternatively written as

$$\Phi = \frac{1}{\sqrt{\pi t}}G\left(\frac{\nu_e t}{PrH^2}\right) = \frac{1}{\sqrt{\pi t}}\left[1 + 2\sum_{n=1}^{\infty}(-1)^n\exp\left(-n^2\frac{PrH^2}{\nu_e t}\right)\right]. \tag{2.47}$$

To obtain q_w, transforms of $\sigma^{-1/2}\mathcal{C}_P g(x,H)$ and $\sigma^{-1/2}\mathcal{C}_P g_P(x,H)$ must be evaluated. They are given by the following two inverse transforms, which are set formally as

$$\frac{1}{\sqrt{2\pi}}\mathscr{F}^{-1}\left\{\sigma^{-\frac{1}{2}}\frac{\tanh(\sqrt{Pr}/\delta_e)}{\tanh(1/\delta_s)}\tanh(1/\delta_e)\right\} = M_T(t)h(t), \tag{2.48}$$

$$\frac{1}{\sqrt{2\pi}}\mathscr{F}^{-1}\left\{\sigma^{-\frac{1}{2}}\frac{\tanh(\sqrt{Pr}/\delta_e)}{\tanh(1/\delta_s)}\tanh(\sqrt{Pr}/\delta_e)\right\} = M_D(t)h(t), \tag{2.49}$$

where explicit expressions of M_T and M_D will be given in §5. Here M_T represents the triple coupling among the viscous diffusion, the thermal diffusion of the gas and the one of the solid, while M_D represents the double coupling between the thermal diffusions of the gas and of the solid.

Using these formulas, the inverse transform of $\hat{s}$ is expressed in the form of a convolution integral given by

$$s = 2\sqrt{\nu_e}\mathscr{M}\left(\frac{\partial p'}{\partial x}\right), \tag{2.50}$$

where $\mathscr{M}(\phi)$ designates a functional of a function $\phi(x,t)$, which is defined as a special case of a following functional $\mathscr{M}_P(\phi)$ by setting Pr to be equal to unity formally:

$$\mathscr{M}_P\left[\phi(x,t)\right] \equiv \frac{1}{\sqrt{\pi}}\int_{-\infty}^{t}\frac{G[\nu_e(t-\tau)/PrH^2]}{\sqrt{t-\tau}}\phi(x,\tau)\mathrm{d}\tau. \tag{2.51}$$

Using the transforms (2.48) and (2.49), new functionals $\mathscr{M}_T(\phi)$ and $\mathscr{M}_D(\phi)$ are defined, respectively, as

$$\mathscr{M}_I\left[\phi(x,t)\right] \equiv \int_{-\infty}^{t}M_I(t-\tau)\phi(x,\tau)\mathrm{d}\tau, \tag{2.52}$$

where the subscript I takes T or D.

With these definitions of the functionals, the inverse transform of $\sigma\hat{q}$ is expressed as

$$\begin{aligned}\frac{\partial q}{\partial t} = &-\frac{2c_pT_e\sqrt{\nu_e}}{a_e^2}\left\{\frac{\gamma-1}{\sqrt{Pr}}\mathscr{M}_P\left(\frac{\partial^2 p'}{\partial t^2}\right)\right.\\ &\left.-\frac{a_e^2}{T_e}\frac{\mathrm{d}T_e}{\mathrm{d}x}\left[\frac{1}{1-Pr}\mathscr{M}\left(\frac{\partial p'}{\partial x}\right)-\frac{1}{(1-Pr)\sqrt{Pr}}\mathscr{M}_P\left(\frac{\partial p'}{\partial x}\right)\right]\right\}+\varepsilon\frac{\partial q_w}{\partial t},\end{aligned} \tag{2.53}$$

where q_w is set in the form of

$$\frac{\partial q_w}{\partial t} = \frac{2c_p T_e H}{a_e^2} W + O(\varepsilon), \tag{2.54}$$

with

$$W = \frac{\sqrt{\nu_e}}{H}\left\{ \frac{\gamma-1}{\sqrt{Pr}} \mathscr{M}_D \left(\frac{\partial^2 p'}{\partial t^2} \right) \right. \\ \left. - \frac{a_e^2}{T_e}\frac{\mathrm{d}T_e}{\mathrm{d}x}\left[\frac{1}{1-Pr}\mathscr{M}_T\left(\frac{\partial p'}{\partial x}\right) - \frac{1}{(1-Pr)\sqrt{Pr}}\mathscr{M}_D\left(\frac{\partial p'}{\partial x}\right)\right]\right\}. \tag{2.55}$$

While the subscripts T and D attached to $\mathscr{M}$ imply the origin from the heat flux, respectively, due to the triple and double couplings among the three diffusions, P implies the one from the heat flux without the coupling and $\mathscr{M}$ without the subscript implies the one from the shear stress. Each term in εW has the counterpart on the left-hand side. A reason of this will be revealed later.

Substituting s and q into (2.22), the thermoacoustic-wave equation for the case of the two-dimensional channels is obtained up to the first-order terms in ε as

$$\frac{\partial^2 p'}{\partial t^2} - \frac{\partial}{\partial x}\left(a_e^2 \frac{\partial p'}{\partial x}\right) + \frac{\partial}{\partial x}\left[\frac{a_e^2\sqrt{\nu_e}}{H}\mathscr{M}\left(\frac{\partial p'}{\partial x}\right)\right] + \frac{\sqrt{\nu_e}}{H}\left\{ \frac{\gamma-1}{\sqrt{Pr}}\mathscr{M}_P\left(\frac{\partial^2 p'}{\partial t^2}\right)\right. \\ \left. -\frac{a_e^2}{T_e}\frac{\mathrm{d}T_e}{\mathrm{d}x}\left[\frac{1}{1-Pr}\mathscr{M}\left(\frac{\partial p'}{\partial x}\right) - \frac{1}{(1-Pr)\sqrt{Pr}}\mathscr{M}_P\left(\frac{\partial p'}{\partial x}\right)\right]\right\} = \varepsilon W. \tag{2.56}$$

2.5.2 Case of the circular tubes

Analyses in this case can be executed in parallel to the previous case but are a little complicated. The transformed solutions $\hat{u}'$ and $\hat{T}'$ are given by (2.28), (2.31) and (2.33), respectively, with f, f_P, f_K and f_{KP} replaced by the following functions:

$$f(x,r) = 1 - \frac{I_0(r/R\delta_e)}{I_0(1/\delta_e)}, \tag{2.57}$$

$$f_P(x,r) = 1 - \frac{I_0(r\sqrt{Pr}/R\delta_e)}{I_0(\sqrt{Pr}/\delta_e)} = 1 - \frac{I_0(r/R\delta_\kappa)}{I_0(1/\delta_\kappa)}, \tag{2.58}$$

$$\begin{bmatrix} f_K(x,r) \\ f_{KP}(x,r) \end{bmatrix} = \begin{bmatrix} \mathcal{C} \\ \mathcal{C}_P \end{bmatrix} \frac{I_0(r/R\delta_\kappa)}{I_0(1/\delta_\kappa)}, \tag{2.59}$$

with

$$\begin{bmatrix} \mathcal{C} \\ \mathcal{C}_P \end{bmatrix} = \begin{bmatrix} I_1(1/\delta_e)/I_0(1/\delta_e) \\ I_1(1/\delta_\kappa)/I_0(1/\delta_\kappa) \end{bmatrix} Z(R, 1/\delta_s) \tag{2.60}$$

where I_i and K_i below $(i = 0, 1)$ denote the modified Bessel functions of the i-th order, respectively, and $Z(r, z)$ is a solution of (2.18) transformed with (2.21) and is given by

$$Z(r,z) = \frac{I_1(\zeta)K_0(rz/R) + K_1(\zeta)I_0(rz/R)}{I_1(\zeta)K_1(z) - K_1(\zeta)I_1(z)}, \tag{2.61}$$

with $z = 1/\delta_s$, $\zeta = (1+\eta)z$ and $\eta = d/R$. Here δ_e is defined by (2.30) with H replaced by R, while δ_κ is newly introduced to avoid use of the factor $\sqrt{Pr}$ in $\sqrt{Pr}/\delta_e$, and δ_s is defined differently from (2.37) as

$$\delta_e = \frac{1}{R}\left(\frac{\nu_e}{\sigma}\right)^{\frac{1}{2}}, \quad \delta_\kappa = \frac{1}{R}\left(\frac{\kappa_e}{\sigma}\right)^{\frac{1}{2}} = \frac{\delta_e}{\sqrt{Pr}} \quad \text{and} \quad \delta_s = \frac{1}{R}\left(\frac{\kappa_s}{\sigma}\right)^{\frac{1}{2}}. \tag{2.62}$$

For $\hat{T}_s'$, f_{S_1} and f_{S_2} are replaced, respectively, by

$$\begin{bmatrix} f_S(x,r) \\ f_{SP}(x,r) \end{bmatrix} = \begin{bmatrix} \mathcal{C} \\ \mathcal{C}_P \end{bmatrix} \frac{Z(r, 1/\delta_s)}{Z(R, 1/\delta_s)} \tag{2.63}$$

The shear stress and heat flux are given by half of (2.40) and (2.41) with g and g_P replaced, respectively, by

$$g(x,r) = \frac{I_1(r/R\delta_e)}{I_0(1/\delta_e)}, \tag{2.64}$$

$$g_P(x,r) = \frac{I_1(r\sqrt{Pr}/R\delta_e)}{I_0(\sqrt{Pr}/\delta_e)}. \tag{2.65}$$

To make inverse transforms of them, the following relation ((4.13) in I) is used:

$$\frac{1}{\sqrt{2\pi}}\mathscr{F}^{-1}\left\{\sigma^{-\frac{1}{2}}\frac{I_1(\sqrt{Pr}/\delta_e)}{I_0(\sqrt{Pr}/\delta_e)}\right\} = \Theta\left(\frac{\nu_e t}{PrR^2}\right)h(t), \tag{2.66}$$

where Θ is defined as

$$\Theta\left(\frac{\nu_e t}{PrR^2}\right) = \frac{2\sqrt{\nu_e}}{\sqrt{Pr}R}\sum_{n=1}^{\infty}\exp\left(-j_n^2\frac{\nu_e t}{PrR^2}\right), \tag{2.67}$$

and j_n $(n = 1, 2, 3, \cdots)$ denote roots of $J_0(j_n) = 0$ $(0 < j_1 \approx 2.40 < j_2 \approx 5.52 < j_3 \approx 8.65\cdots)$. As this sum diverges as $t \to 0$, its asymptitic behaviour is already available as

$$\Theta\left(\frac{\nu_e t}{PrR^2}\right) = \frac{1}{\sqrt{\pi t}} - \frac{\sqrt{\nu_e}}{2\sqrt{Pr}R} - \frac{\nu_e}{4PrR^2}\sqrt{\frac{t}{\pi}} + \cdots. \tag{2.68}$$

Using (2.66), the functional $\mathscr{N}_P$ is introduced as

$$\mathscr{N}_P[\phi(x,t)] \equiv \int_{-\infty}^{t}\Theta\left[\frac{\nu_e(t-\tau)}{PrR^2}\right]\phi(x,\tau)\mathrm{d}\tau, \tag{2.69}$$

and the functional $\mathscr{N}(\phi)$ denotes $\mathscr{N}_P(\phi)$ with $Pr = 1$ set equal to unity formally.

After the case of the channels, new functionals are defined by

$$\mathscr{N}_I[\phi(x,t)] \equiv \int_{-\infty}^{t} N_I(t-\tau)\phi(x,\tau)\mathrm{d}\tau, \tag{2.70}$$

where I stands for T and D, and N_T and N_D are defined in terms of the following inverse transforms, respectively, as

$$\frac{1}{\sqrt{2\pi}}\mathscr{F}^{-1}\left\{\sigma^{-\frac{1}{2}}\frac{I_1(1/\delta_e)}{I_0(1/\delta_e)}\frac{I_1(1/\delta_\kappa)}{I_0(1/\delta_\kappa)}Z(R,1/\delta_s)\right\} = N_T(t)h(t), \tag{2.71}$$

$$\frac{1}{\sqrt{2\pi}}\mathscr{F}^{-1}\left\{\sigma^{-\frac{1}{2}}\frac{I_1^2(1/\delta_\kappa)}{I_0^2(1/\delta_\kappa)}Z(R,1/\delta_s)\right\} = N_D(t)h(t). \tag{2.72}$$

Here explicit expressions of N_T and N_D will be given later.

Using these definitions, the shear stress and the heat flux on the wall surface are expressed by (2.50), (2.53) and (2.54) with the functionals designated by $\mathscr{M}$ replaced by their corresponding ones by $\mathscr{N}$. But remark that the factor 2 in (2.50) and in front of $c_pT_e\sqrt{\nu_e}$ in (2.53) and (2.54) should be removed. Substituting these into (2.22) for $j=1$, the thermoacoustic-wave equation for the case of the circular tubes is obtained up to the first-order terms in ε as

$$\begin{aligned}\frac{\partial^2 p'}{\partial t^2} - \frac{\partial}{\partial x}\left(a_e^2\frac{\partial p'}{\partial x}\right) + \frac{\partial}{\partial x}\left[\frac{2a_e^2\sqrt{\nu_e}}{R}\mathscr{N}\left(\frac{\partial p'}{\partial x}\right)\right] + \frac{2\sqrt{\nu_e}}{R}\left\{\frac{\gamma-1}{\sqrt{Pr}}\mathscr{N}_{\mathrm{P}}\left(\frac{\partial^2 p'}{\partial t^2}\right)\right.\\ \left. - \frac{a_e^2}{T_e}\frac{\mathrm{d}T_e}{\mathrm{d}x}\left[\frac{1}{1-Pr}\mathscr{N}\left(\frac{\partial p'}{\partial x}\right) - \frac{1}{(1-Pr)\sqrt{Pr}}\mathscr{N}_{\mathrm{P}}\left(\frac{\partial p'}{\partial x}\right)\right]\right\} = \varepsilon W\end{aligned} \tag{2.73}$$

with

$$\begin{aligned}W = \frac{2\sqrt{\nu_e}}{R}\left\{\frac{\gamma-1}{\sqrt{Pr}}\mathscr{N}_D\left(\frac{\partial^2 p'}{\partial t^2}\right)\right.\\ \left. - \frac{a_e^2}{T_e}\frac{\mathrm{d}T_e}{\mathrm{d}x}\left[\frac{1}{1-Pr}\mathscr{N}_T\left(\frac{\partial p'}{\partial x}\right) - \frac{1}{(1-Pr)\sqrt{Pr}}\mathscr{N}_D\left(\frac{\partial p'}{\partial x}\right)\right]\right\}.\end{aligned} \tag{2.74}$$

2.6 Evaluation of the relaxation functions

The thermoacoustic-wave equations have been derived formally by introducing the functionals $\mathscr{M}_I$ and $\mathscr{N}_I$ where the subscript I takes T or D. Since explicit expressions of the functions involved are left unspecified, they are evaluated in §2.6. The kernel functions M_I in $\mathscr{M}_I$ and N_I in $\mathscr{N}_I$ where I takes T or D, are called relaxation functions in this paper. Just as in the case of the inverse transforms of (2.45) and (2.66), they are reduced to the inverse Laplace transforms along the imaginary axis in the complex σ-plane, which are easily evaluated by Cauchy's theorem (see (4.17) in I). Looking for simple poles of the integrands, it is found that they are located on the negative axis so that the integrals vanish for $t<0$. In all cases, no branch point exists at $\sigma=0$.

2.6.1 Case of two-dimensional channels

For $M_T(t)$, there are simple poles at $\sigma = -(n-1/2)^2\pi^2\nu_e/H^2$, $\sigma = -(n-1/2)^2\pi^2\kappa_e/H^2$ and $\sigma = -(n\pi)^2\kappa_s/d^2$, $(n = 1, 2, 3, \cdots)$, which originate from the zeros of $\cosh(1/\delta_e) = 0$, $\cosh(\sqrt{Pr}/\delta_e) = 0$ and $\sinh(1/\delta_s) = 0$, respectively. When they are different from each other, then the theorem yields

$$
\begin{aligned}
M_T(t) = {} & \frac{2\sqrt{\nu_e}}{H}\sum_{n=1}^{\infty}\frac{\tan[(n-1/2)\pi\sqrt{\nu_e/\kappa_e}]}{\tan[(n-1/2)\pi\sqrt{\nu_e/\kappa_e}Ge]}\exp\left[-\frac{(2n-1)^2\pi^2}{4}\frac{\nu_e t}{H^2}\right] \\
& + \frac{2\sqrt{\kappa_e}}{H}\sum_{n=1}^{\infty}\frac{\tan[(n-1/2)\pi\sqrt{\kappa_e/\nu_e}]}{\tan[(n-1/2)\pi Ge]}\exp\left[-\frac{(2n-1)^2\pi^2}{4}\frac{\kappa_e t}{H^2}\right] \\
& - \frac{2\sqrt{\kappa_s}}{d}\sum_{n=1}^{\infty}\tan\left(\frac{n\pi}{Ge}\right)\tan\left(\frac{n\pi}{\sqrt{\nu_e/\kappa_e}Ge}\right)\exp\left[-(n\pi)^2\frac{\kappa_s t}{d^2}\right].
\end{aligned}
\tag{2.75}
$$

Here all coefficients of the exponential functions are assumed to be finite, which is a non-resonant case. It is found that there appears a new relaxation time d^2/κ_s due to the heat conduction in the solid wall in addition to the viscous and thermal ones of gas H^2/ν_e and H^2/κ_s, respectively. Note that because d^2/κ_s is written as Ge^2PrH^2/ν_e, this time becomes longer in proportion to Ge^2 compared with H^2/ν_e as the wall becomes thicker and the diffusion in the solid wall lasts longer.

For M_D, the poles of second order exist at $\sigma = -(n-1/2)^2\pi^2\kappa_e/H^2$ so that the theorem yields

$$
\begin{aligned}
M_D(t) = {} & \frac{2\sqrt{\kappa_e}}{H}\sum_{n=1}^{\infty}\frac{(2n-1)\pi}{\tan[(n-1/2)\pi Ge]}\frac{\kappa_e t}{H^2}\exp\left[-\frac{(2n-1)^2\pi^2}{4}\frac{\kappa_e t}{H^2}\right] \\
& + \frac{2\sqrt{\kappa_e}}{H}\sum_{n=1}^{\infty}\frac{Ge}{\sin^2[(n-1/2)\pi Ge]}\exp\left[-\frac{(2n-1)^2\pi^2}{4}\frac{\kappa_e t}{H^2}\right] \\
& - \frac{2\sqrt{\kappa_s}}{d}\sum_{n=1}^{\infty}\tan^2\left(\frac{n\pi}{Ge}\right)\exp\left[-(n\pi)^2\frac{\kappa_s t}{d^2}\right].
\end{aligned}
\tag{2.76}
$$

The poles of second order contribute to algebraic growth $\kappa_e t/H^2$, though multiplied by the decaying exponential function, and give rise to a slower behaviour. For a moderate or large value of t (> 0), the exponential functions decay rapidly as n increases so that the sums converge quickly. For a small value of t, however, the convergence becomes so slow that they tend to diverge as $t \to 0$. Further it may occur that the sums do not converge if one of the coefficients of the exponential functions happens to diverge. This is called a resonant case and will be examined in detail in the next section.

To examine their asymptotic behaviours as $t \to 0$, their Fourier transforms are useful. Expanding them in δ_e^{-1}, δ_k^{-1} and δ_s^{-1} by using $\tanh X = 1 + 2\sum_{n=1}^{\infty}(-1)^n\exp(-2nX)$ for $|X| \gg 1$, and transforming inversely each exponential function, it then follows that

$$
M_T(t) = \frac{1}{\sqrt{\pi t}}\left[1 - 2\exp\left(-\frac{H^2}{\nu_e t}\right) - 2\exp\left(-\frac{H^2}{\kappa_e t}\right) + 2\exp\left(-\frac{d^2}{\kappa_s t}\right) + ...\right], \tag{2.77}
$$

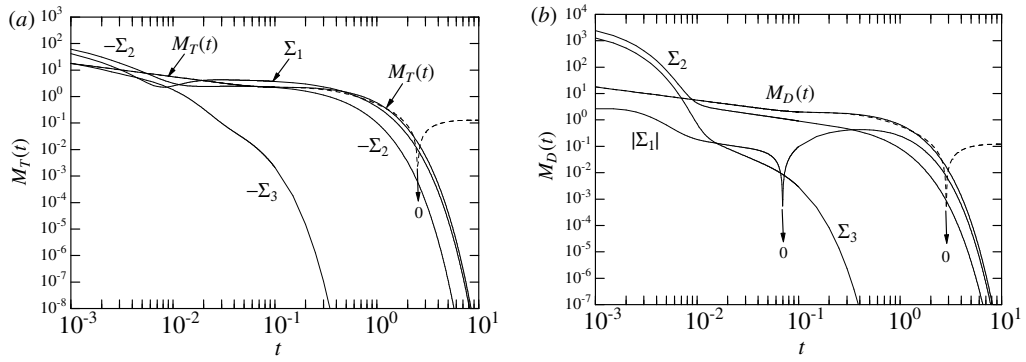

Figure 3: Logarithmic plots of the functions $M_T(t)$ and $M_D(t)$ against t over the interval $10^{-3} \leq t \leq 10$ in (a) and (b), respectively, where the abscissa and ordinate in (a) measure $\nu_e t/H^2$ and $(H/\sqrt{\nu_e})M_T(t)$, while those in (b) measure $\kappa_e t/H^2$ and $(H/\sqrt{\kappa_e})M_D(t)$, but the both factors ν_e/H^2 and κ_e/H^2 are omitted for simplicity. Here the subscripts 1, 2 and 3 of the summation symbol labelled to the curves designate, respectively, the first, second and third sums in (2.75) and (2.76), the symbol $|\cdots|$ or the minus sign designating the absolute value or the value with sign reversed, and the broken lines represent the asymptotic expressions (2.77) and (2.78).

and

$$M_D(t) = \frac{1}{\sqrt{\pi t}}\left[1 - 4\exp\left(-\frac{H^2}{\kappa_e t}\right) + 2\exp\left(-\frac{d^2}{\kappa_s t}\right) + ...\right], \tag{2.78}$$

as $t \to 0$. Thus it is found that M_T and M_D tend to diverge as $(\pi t)^{-1/2}$ as $t \to 0$ and this behaviour is the same as that in (2.47).

For air enclosed by the ceramic plates with $d/H = 1$, $Pr = \nu_e/\kappa_e = 0.72$, $K = \kappa_s/\kappa_e = 3.61$ and $Ge = d/H\sqrt{K} = 0.526$ (see table 2), figures 3(a) and 3(b) show the logarithmic plots of $M_T(t)$ and $M_D(t)$ against t over the range $10^{-3} \leq t \leq 10$, respectively, where the factor ν_e/H^2 in the abscissa $\nu_e t/H^2$ and ordinate $(H/\sqrt{\nu_e})M_T$ is omitted in figure 3(a), while the one κ_e/H^2 is omitted in figure 3(b), for simplicity. The functions M_T and M_D consist of three respective sums. The first sum in (2.76) changes sign so that the absolute value is shown with the label $|\sum_1|$ attached to the curve. The arrow indicates the vanishing point. The last sums (excluding the minus sign in front of the summation symbol) are negative in M_T and positive in M_D. The broken curves represent the asymptotic expressions (2.77) and (2.78) but they are invisible for $t < 0.5$ because they almost coincide with M_T and M_D.

The figures show which sum contributes to each function most. For a small value of t, the first sums in (2.75) and (2.76) are much smaller than the others, while the second and third sums cancel with each other to yield the asymptotic expressions $1/\sqrt{\pi t} + \cdots$. For a large value of t, on the other hand, both functions decay rapidly and the first sums survive over the others.

2.6.2 Case of the circular tubes

The functions N_T and N_D can be evaluated by the same method. For N_T, the simple poles occur at $\sigma = -j_n^2\nu_e/R^2$ and $\sigma = -j_n^2\kappa_e/R^2$ $(n = 1, 2, 3, \cdots)$ from the zeros of $I_0[(\sigma/\nu_e)^{1/2}R]$ and $I_0[(\sigma/\kappa_e)^{1/2}R]$, respectively. Further because $Z(R, 1/\delta_s)$ has poles,

their contributions should be included. Setting $1/\delta_s = z$, it is found that the logarithmic singularity at $z = 0$ in K_i $(i = 0, 1)$ cancels out to disappear and a simple pole appears at $z = 0$. As $z \to 0$, Z behaves as

$$Z(R, z) = A\left(\frac{1}{z} + Bz + \cdots\right), \tag{2.79}$$

with

$$A = \frac{2}{[(1+\eta)^2 - 1]} \quad \text{and} \quad B = \frac{1}{8} - \frac{3}{8}(1+\eta)^2 + \frac{(1+\eta)^4 \log(1+\eta)}{2[(1+\eta)^2 - 1]^2}, \tag{2.80}$$

while as $|z| \to \infty$, Z behaves as

$$Z(R, z) = 1 - \frac{1}{2z} + \frac{3}{8z^2} + ..., \tag{2.81}$$

if $\mathrm{Re}\{z\} > 0$. There exist infinite number of simple poles at $z = z_n = \pm \mathrm{i}k_n$ $(n = 1, 2, 3, \cdots)$ where z_n satisfies $I_1(z)/I_1(\zeta) = K_1(z)/K_1(\zeta)$ with $\zeta = (1+\eta)z$. From the asymptotic expressions of the ratios of the two modified Bessel functions for $|z| \gg 1$ (e.g. Abramowitz & Stegun (1972)), k_n are approximated to be given by $(n\pi/\eta)\{1+3\eta^2/[8n^2\pi^2(1+\eta)]+\cdots\}$.

Taking account of the residues, thus, N_T is evaluated as

$$\begin{aligned} N_T(t) = {} & \frac{2\sqrt{\nu_e}}{R} \sum_{n=1}^{\infty} X(\mathrm{i}j_n\sqrt{\nu_e/\kappa_e}) Z(R, \mathrm{i}j_n\sqrt{\nu_e/\kappa_s}) \exp\left(-j_n^2 \frac{\nu_e t}{R^2}\right) \\ & + \frac{2\sqrt{\kappa_e}}{R} \sum_{n=1}^{\infty} X(\mathrm{i}\, j_n\sqrt{\kappa_e/\nu_e}) Z(R, \mathrm{i}j_n\sqrt{\kappa_e/\kappa_s}) \exp\left(-j_n^2 \frac{\kappa_e t}{R^2}\right) \\ & + \frac{2\sqrt{\kappa_s}}{R} \sum_{n=1}^{\infty} X(\mathrm{i}\, k_n\sqrt{\kappa_s/\nu_e}) X(\mathrm{i}\, k_n\sqrt{\kappa_s/\kappa_e}) Y_n \exp\left(-k_n^2 \frac{\kappa_s t}{R^2}\right), \end{aligned} \tag{2.82}$$

where X stands for $I_1(z)/I_0(z)$, and Y_n stands for $\lim_{z\to z_n}(z - z_n)Z(R, z)$, which is evaluated as

$$Y_n = \frac{I_1(\zeta_n)K_0(z_n) + K_1(\zeta_n)I_0(z_n)}{(1+\eta)[I_0(\zeta_n)K_1(z_n) + K_0(\zeta_n)I_1(z)] - K_1(\zeta_n)I_0(z_n) - I_1(\zeta_n)K_0(z_n)}, \tag{2.83}$$

with $\zeta_n = (1+\eta)z_n$, z_n being $\mathrm{i}k_n$ $(n = 1, 2, 3, \cdots)$. For evaluation of N_D, on the other hand, there appear poles of second order at $\sigma = -j_n^2\kappa_e/R^2$ from zeros of $I_0^2[(\sigma/\kappa_e)^{1/2}R]$, which give rise to a slower decay. Taking account of them, N_D is expressed as

$$\begin{aligned} N_D(t) = {} & \frac{2\sqrt{\kappa_e}}{R} \sum_{n=1}^{\infty} \frac{\mathrm{i}}{j_n} \left(1 + 2j_n^2 \frac{\kappa_e t}{R^2}\right) Z(R, \mathrm{i}j_n\sqrt{\kappa_e/\kappa_s}) \exp\left(-j_n^2 \frac{\kappa_e t}{R^2}\right) \\ & + \frac{2\sqrt{\kappa_e}}{R} \sum_{n=1}^{\infty} \sqrt{\frac{\kappa_e}{\kappa_s}} \frac{\mathrm{d}}{\mathrm{d}z} Z(R, z)\Big|_{z=\mathrm{i}j_n\sqrt{\kappa_e/\kappa_s}} \exp\left(-j_n^2 \frac{\kappa_e t}{R^2}\right) \\ & + \frac{2\sqrt{\kappa_s}}{R} \sum_{n=0}^{\infty} X^2(\mathrm{i}\, k_n\sqrt{\kappa_s/\kappa_e})\ Y_n \exp\left(-k_n^2 \frac{\kappa_s t}{R^2}\right). \end{aligned} \tag{2.84}$$

Because the sums on the right-hand sides of (2.82) and (2.84) diverge as $t \to 0$, their asymptotic behaviours are examined by expanding the transformed expressions in terms of δ_e^{-1}, δ_κ^{-1} and δ_s^{-1}. Then it follows that

$$\sigma^{-\frac{1}{2}} \frac{I_1(1/\delta_e)}{I_0(1/\delta_e)} \frac{I_1(1/\delta_\kappa)}{I_0(1/\delta_\kappa)} Z(R, 1/\delta_s) = \sigma^{-1/2} - \frac{\upsilon_{11}}{2R}\sigma^{-1} - \frac{\upsilon_{12}}{8R^2}\sigma^{-3/2} + \cdots, \tag{2.85}$$

with

$$\upsilon_{11} = \sqrt{\nu_e} + \sqrt{\kappa_e} + \sqrt{\kappa_s}, \tag{2.86}$$

$$\upsilon_{12} = \nu_e + \kappa_e - 3\kappa_s - 2(\sqrt{\nu_e\kappa_e} + \sqrt{\kappa_e\kappa_s} + \sqrt{\kappa_s\nu_e}), \tag{2.87}$$

and

$$\sigma^{-\frac{1}{2}} \frac{I_1^2(1/\delta_\kappa)}{I_0^2(1/\delta_\kappa)} Z(R, 1/\delta_s) = \sigma^{-1/2} - \frac{\upsilon_{21}}{2R}\sigma^{-1} + \frac{\upsilon_{22}}{8R^2}\sigma^{-3/2} + \cdots, \tag{2.88}$$

with $\upsilon_{21} = 2\sqrt{\kappa_e} + \sqrt{\kappa_s}$ and $\upsilon_{22} = 4\sqrt{\kappa_e\kappa_s} + 3\kappa_s$. The inverse transforms yield the asymptotic expressions of N_T and N_D respectively as

$$N_T = \frac{1}{\sqrt{\pi t}} - \frac{\upsilon_{11}}{2R} - \frac{\upsilon_{12}}{4R^2}\sqrt{\frac{t}{\pi}} + \cdots, \tag{2.89}$$

$$N_D = \frac{1}{\sqrt{\pi t}} - \frac{\upsilon_{21}}{2R} + \frac{\upsilon_{12}}{4R^2}\sqrt{\frac{t}{\pi}} + \cdots, \tag{2.90}$$

for $t \to 0$. The leading asymptotic expressions are found to be given commonly by $1/\sqrt{\pi t}$.

Figures 4(a) and 4(b) show the logarithmic plots of $N_T(t)$ and $N_D(t)$ against t over the range $10^{-3} \le t \le 5$, respectively, where the factor ν_e/R^2 in the abscissa $\nu_e t/R^2$ and ordinate $(R/\sqrt{\nu_e})N_T$ is omitted in figure 4(a), while the one κ_e/R^2 is omitted in figure 4(b), for simplicity. Here concerned is the case with air enclosed in the ceramic tube with $d/R = \eta = 1$ where the values of Pr and K are the same as employed in figure 3.

As N_T and N_D consist of three respective sums, each sum is designated by the summation symbol consecutively from the first one. As the sum changes sign, the absolute value or the value with sign reversed is shown with the labels attached to the curves. The broken curves represent the asymptotic expressions (2.89) and (2.90). Unlike the case of M_T and M_D, three terms are necessary to find agreements with the numerical values.

2.7 Influence on the thin diffusion layer theory

For a thin diffusion layer, i.e. $\delta_e \ll 1$, the asymptotic expressions of the relaxation functions are truncated at the leading terms. But if a value of Ge is very small, as (2.77) and (2.78) suggest, this condition should be replaced by $d^2/\kappa_s t \gg 1$, i.e. $Ge^2 PrH^2/\nu_e t \gg 1$. Then all functionals for $j = 0$ are reduced to the derivatives of minus half-order as (Gel'fand & Shilov (1964))

$$\mathscr{M}(\phi) \approx \mathscr{M}_I(\phi) \approx \frac{1}{\sqrt{\pi}} \int_{-\infty}^{t} \frac{\phi(x,\tau)}{\sqrt{t-\tau}} \mathrm{d}\tau \equiv \frac{\partial^{-\frac{1}{2}}\phi}{\partial t^{-\frac{1}{2}}}, \tag{2.91}$$

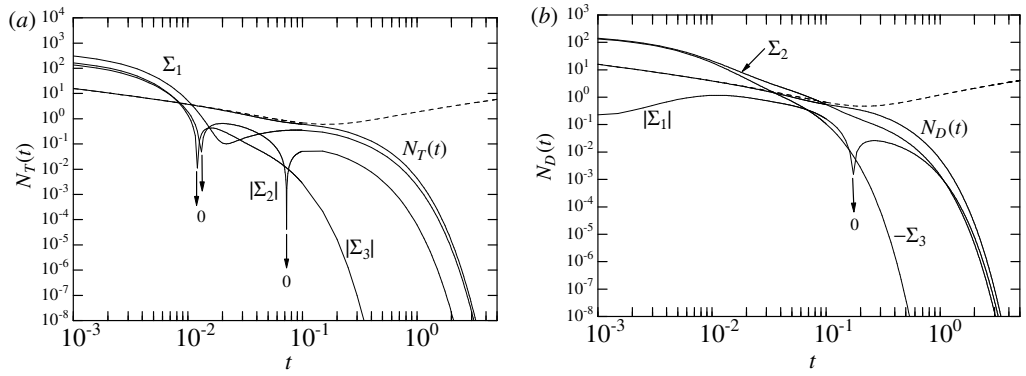

Figure 4: Logarithmic plots of the functions $N_T(t)$ and $N_D(t)$ against t over the interval $10^{-3} \leq t \leq 5$ in (a) and (b), respectively, where the abscissa and ordinate in (a) measure $\nu_e t/R^2$ and $(R/\sqrt{\nu_e})N_T(t)$, while those in (b) measure $\kappa_e t/R^2$ and $(R/\sqrt{\kappa_e})N_D(t)$, but the both factors ν_e/R^2 and κ_e/R^2 are omitted for simplicity. Here the subscripts 1, 2 and 3 of the summation symbol labelled to the curves designate, respectively, the first, second and third sums in (2.82) and (2.84), the symbol $|\cdots|$ or the minus sign designating the absolute value or the value with sign reversed, and the broken lines indicate the asymptotic expressions (2.89) and (2.90).

where I takes P, T and D, and so is the case with $j = 1$ by replacing $\mathscr{M}$ by $\mathscr{N}$.

Using (2.91), the thermoacoustic-wave equations are approximated into

$$\frac{\partial^2 p'}{\partial t^2} - \frac{\partial}{\partial x}\left(a_e^2 \frac{\partial p'}{\partial x}\right) + \frac{2^j a_e^2 \sqrt{\nu_e}}{H}\left[C \frac{\partial^{-\frac{1}{2}}}{\partial t^{-\frac{1}{2}}}\left(\frac{\partial^2 p'}{\partial x^2}\right) + \frac{(C + C_T)}{T_e}\frac{\mathrm{d}T_e}{\mathrm{d}x}\frac{\partial^{-\frac{1}{2}}}{\partial t^{-\frac{1}{2}}}\left(\frac{\partial p'}{\partial x}\right)\right] = 0, \tag{2.92}$$

with

$$C = 1 + \frac{(1-\varepsilon)(\gamma - 1)}{\sqrt{Pr}} \quad \text{and} \quad C_T = \frac{1}{2} + \frac{\beta}{2} + \frac{1-\varepsilon}{\sqrt{Pr} + Pr}. \tag{2.93}$$

Here since the contributions from the functionals remain small, the leading balance occurs between the first two terms so that $\partial^2 p'/\partial t^2$ involved in $\mathscr{M}_P$ in (2.56) and $\mathscr{N}_P$ in (2.73) has been replaced by $(\partial/\partial x)(a_e^2 \partial p'/\partial x)$ and the relation $(a_e^2\sqrt{\nu_e})^{-1}(\mathrm{d}/\mathrm{d}x)(a_e^2\sqrt{\nu_e}) = (3/2 + \beta/2)T_e^{-1}\mathrm{d}T_e/\mathrm{d}x$ has been used. It is revealed that the effect of the heat conduction in the wall gives rise to only small corrections of order ε in the coefficients C and C_T and therefore the thin diffusion layer theory is affected little, as expected. In passing, as was found by Henry and remarked by Rott, it is interesting to find that because C is engaged in damping in the absence of the temperature gradient, the effects of heat conduction decreases the values of C (and also C_T) to reduce the damping, though very slightly.

2.8 Influence on the thick diffusion layer theory

Next concerned is approximation for a thick diffusion layer. This corresponds to the case in which the span length is much smaller than the thickness of diffusion layer, i.e. $|\delta_e| \gg 1$. But if a value of Ge is very large, this condition should be replaced by $Ge^2 PrH^2/\nu_e t \ll 1$. To derive the approximate equations, it is convenient to work with (2.22) transformed.

Treating both cases for $j = 0$ and $j = 1$ simultaneously, and replacing H with R for $j = 1$, $\hat{s}$ in (2.40) is expanded in terms of $1/\delta_e$ up to $1/\delta_e^4$ as

$$\hat{s} = \frac{H}{2^{2j-1}} \left(1 - \frac{1}{3+5j} \frac{H^2\sigma}{\nu_e} + \frac{2}{15+81j} \frac{H^4\sigma^2}{\nu_e^2} + \cdots \right) \frac{\partial \hat{p}'}{\partial x}, \tag{2.94}$$

while $\sigma\hat{q}$ in (2.41) is expanded in a similar fashion as

$$\begin{aligned} \sigma\hat{q} = \frac{c_p T_e H}{2^{2j-1} a_e^2} \Bigg\{ & -(\gamma-1) \left(1 - \frac{Pr}{3+5j} \frac{H^2\sigma}{\nu_e} + \cdots \right) \sigma^2 \hat{p}' \\ & - \frac{a_e^2}{T_e} \frac{\mathrm{d}T_e}{\mathrm{d}x} \left[\frac{1}{3+5j} - \frac{2(1+Pr)}{15+81j} \frac{H^2\sigma}{\nu_e} + \cdots \right] \frac{H^2\sigma}{\nu_e} \frac{\partial \hat{p}'}{\partial x} \Bigg\} + \varepsilon\sigma\hat{q}_w. \end{aligned} \tag{2.95}$$

Since $\hat{q}_w = -\mathcal{C}_P \hat{q}$ in (2.42), $\mathcal{C}_P$ is expanded similarly so that $\hat{q}_w$ is obtained as

$$\begin{aligned} \varepsilon\sigma\hat{q}_w = \frac{\varepsilon c_p T_e H}{2^{3j-1} a_e^2 Ge} \Bigg\{ & (\gamma-1) \left[1 - \left(\frac{2Pr}{3+5j} - Q_j \right) \frac{H^2\sigma}{\nu_e} + \cdots \right] \sigma^2 \hat{p}' + \frac{a_e^2}{T_e} \frac{\mathrm{d}T_e}{\mathrm{d}x} \\ & \times \left[\frac{1}{3+5j} - \left(\frac{Pr}{(3+5j)^2} + \frac{2(1+Pr)}{15+81j} - \frac{Q_j}{3+5j} \right) \frac{H^2\sigma}{\nu_e} + \cdots \right] \frac{H^2\sigma}{\nu_e} \frac{\partial \hat{p}'}{\partial x} \Bigg\}, \end{aligned} \tag{2.96}$$

where Q_j are defined as

$$Q_0 = \frac{\nu_e d^2}{3\kappa_s H^2} = \frac{1}{3} Pr Ge^2, \tag{2.97}$$

$$Q_1 = \frac{\nu_e}{\kappa_s} \left\{ \frac{1}{8} - \frac{3}{8}(1+\eta)^2 + \frac{(1+\eta)^4 \log(1+\eta)}{2[(1+\eta)^2 - 1]} \right\}, \tag{2.98}$$

and Ge for the case of the circular tubes is defined as

$$Ge = \sqrt{\frac{\kappa_e}{\kappa_s}} \frac{[(1+\eta)^2 - 1]}{2} = \sqrt{\frac{\kappa_e}{\kappa_s}} \left[\frac{d}{R} + \frac{1}{2} \left(\frac{d}{R} \right)^2 \right]. \tag{2.99}$$

For $\eta \ll 1$, $Q_1 \approx Q_0 = Pr(\kappa_e/\kappa_s)\eta^2/3$.

Before deriving the approximate equations, note that, in (2.22), the first term on the left-hand side stems from the adiabatic density change in the equation of continuity, while the second term stems from the pressure gradient in the equation of motion. When the span length is very narrow, the pressure gradient almost balances with the shear stress on the wall surfaces. Substituting $\hat{s}$ in (2.94) into (2.22), in fact, it is seen that the first term in (2.94) cancels with the term due to the pressure gradient.

On the other hand, the form of heat flux (2.95) (more generally from (2.41)) depends not only on the pressure but also on the product of the temperature gradient $\mathrm{d}T_e/\mathrm{d}x$ and the pressure gradient $\partial p'/\partial x$. The magnitude of the latter is of order $(\chi/|\delta_e|)^2$ in comparison with the former and is comparable if χ becomes of order $|\delta_e|$. Given a pressure gradient, the heat flux changes its sense of flow according to a local value of the temperature gradient. This is another feature of the thermoacoustic phenomena.

For a very small span length, the temperature of the gas is almost equal to the local temperature of the wall so that the temperature variation in the gas is negligible and the thermal process is regarded as being isothermal locally. Yet the heat flux flows through the wall surface. Noting the sign of the heat flux (taken positive into the gas), and $c_pT_e = a_e^2/(\gamma-1)$, it flows into the solid when the pressure tends to increase temporarily because q is given by $-2^{1-2j}H\partial p'/\partial t$ to the lowest relation of (2.95).

Substituting (2.95) into (2.22), the first term in (2.95), i.e. the term proportional to $-(\gamma-1)\sigma^2\hat{p}'$, and the first term on the left-hand side of (2.22) yield $\gamma\sigma^2\hat{p}'$. The factor γ implies the isothermal sound speed a_e^2/γ jointly with the second term due to the pressure gradient if the shear stress were absent. However, the shear stress does exist to cancel with the pressure gradient. Thus the lowest relation of (2.22) is reduced to $\gamma\sigma^2\hat{p}' = 0$, i.e. $\gamma\partial^2 p'/\partial t^2 = 0$, not to the wave equation $\gamma\partial^2 p'/\partial t^2 - (\partial/\partial x)(a_e^2\partial p'/\partial x) = 0$. This means that the isothermal sound speed $a_e/\sqrt{\gamma}$ has no meaning physically.

Keeping these relations in mind, we proceed to seek higher-order terms in (2.22). Substituting (2.94) and (2.95) with (2.96) into (2.22) transformed, and dividing it by $\gamma\sigma$, we arrive at an equation in the same form as (3.17) in I but with an additional term on the right-hand side, denoted by $\varepsilon\hat{w}_j$, due to the effects of heat conduction in wall. To treat both cases with $j = 0$ and $j = 1$ simultaneously, α is now replaced by α_j given by

$$\alpha_j = \frac{a_e^2 H^2}{(3+5j)\gamma\nu_e}, \tag{2.100}$$

while the coefficient $2/5$ in (3.17) in I is replaced by $(6+10j)/(15+81j)$.

Transforming these inversely, the approximate equations for the thick diffusion layer are obtained as

$$\begin{aligned}&\frac{\partial p'}{\partial t} - \frac{\partial}{\partial x}\left(\alpha_j\frac{\partial p'}{\partial x}\right) + \frac{\alpha_j}{T_e}\frac{\mathrm{d}T_e}{\mathrm{d}x}\frac{\partial p'}{\partial x} - (\gamma-1)Pr\frac{\alpha_j}{a_e^2}\frac{\partial^2 p'}{\partial t^2}\\ &+\frac{6+10j}{15+81j}\left[\frac{\partial}{\partial x}\left(\frac{\alpha_j H^2}{\nu_e}\frac{\partial^2 p'}{\partial t\partial x}\right) - (1+Pr)\frac{\alpha_j H^2}{\nu_e T_e}\frac{\mathrm{d}T_e}{\mathrm{d}x}\frac{\partial^2 p'}{\partial t\partial x}\right] = \varepsilon w_j,\end{aligned} \tag{2.101}$$

where εw_j are given by

$$\begin{aligned}\varepsilon w_j = \frac{\varepsilon}{2^j Ge}\Bigg\{&\frac{\gamma-1}{\gamma}\frac{\partial p'}{\partial t} + \frac{\alpha_j}{T_e}\frac{\mathrm{d}T_e}{\mathrm{d}x}\frac{\partial p'}{\partial x} - (\gamma-1)Pr[2-(3+5j)Q_j]\frac{\alpha_j}{a_e^2}\frac{\partial^2 p'}{\partial t^2}\\ &-\left[\frac{Pr}{3+5j} + \frac{6+10j}{15+81j}(1+Pr) - Q_j\right]\frac{\alpha_j H^2}{\nu_e T_e}\frac{\mathrm{d}T_e}{\mathrm{d}x}\frac{\partial^2 p'}{\partial t\partial x}\Bigg\}.\end{aligned} \tag{2.102}$$

Because each term in εw_j has a counterpart on the left-hand side of (2.101), and no new terms in form appear, the effects of heat conduction in wall will not give rise qualitative changes. But quantitative differences will occur through the coefficients. Their effects appears through the parameter Ge. As Ge becomes smaller to be comparable with ε,

they give rise to an appreciable difference from those without their effects. Noting that

$$\frac{\varepsilon}{2^j Ge} = \begin{cases} \dfrac{\rho_e c_p}{\rho_s c_s}\dfrac{H}{d} & \text{for } \ j=0, \\ \dfrac{\rho_e c_p}{\rho_s c_s}\dfrac{R^2}{[(R+d)^2-d^2]} & \text{for } \ j=1, \end{cases} \tag{2.103}$$

by (2.12) and (2.99), $\varepsilon/2^j Ge$ implies the heat capacity of the wall per unit axial length. Thus the effects of heat conduction in wall become pronounced admittedly as the thickness of wall becomes thinner.

2.9 Resonant case and unusual diffusion

2.9.1 Relations in the case without expansion in terms of ε

When the resonance takes place, the expansion in terms of ε becomes invalid and the temperature distributions should be sought without expansion. Then $\hat{T}'$ in (2.31) is modified by replacing f_P in (2.32) with

$$f_P = 1 - \frac{1}{\mathcal{A}}\,\frac{\cosh(y\sqrt{Pr}/H\delta_e)}{\cosh(\sqrt{Pr}/\delta_e)}, \tag{2.104}$$

where

$$\mathcal{A} = 1 + \varepsilon\frac{\tanh(\sqrt{Pr}/\delta_e)}{\tanh(1/\delta_s)} = 1 + \varepsilon\mathcal{C}_P, \tag{2.105}$$

while $\varepsilon\hat{T}'_\varepsilon$ in (2.33) is modified by replacing f_K in (2.34) with

$$f_K = \frac{1}{\mathcal{A}}\,\frac{\tanh(1/\delta_e)}{\tanh(1/\delta_s)}\frac{\cosh(y\sqrt{Pr}/H\delta_e)}{\cosh(\sqrt{Pr}/\delta_e)}, \tag{2.106}$$

and setting f_{KP} to be zero. For $\hat{T}_s{}'$, on the other hand, f_S and f_{SP} in (2.39) are replaced by $\mathcal{A}^{-1}f_S$ and $\mathcal{A}^{-1}f_{SP}$, respectively. Since the replacements above give exact expressions to $\hat{T}'$ and $\hat{T}_s{}'$, the symbol $O(\varepsilon^2)$ in (2.33) and (2.38) is unnecessary.

For the case of the tubes, f_P is replaced by

$$f_P = 1 - \frac{1}{\mathcal{A}}\frac{I_0(r/R\delta_\kappa)}{I_0(1/\delta_\kappa)} \tag{2.107}$$

with

$$\mathcal{A} = 1 + \varepsilon\,\frac{I_1(1/\delta_\kappa)}{I_0(1/\delta_\kappa)}Z(R,1/\delta_s) = 1 + \varepsilon\mathcal{C}_P, \tag{2.108}$$

and f_K is replaced by

$$f_K = \frac{1}{\mathcal{A}}\left[\frac{I_1(1/\delta_e)}{I_0(1/\delta_e)}Z(R,1/\delta_s)\right]\frac{I_0(r/R\delta_\kappa)}{I_0(1/\delta_\kappa)}, \tag{2.109}$$

with setting $f_{KP} = 0$, while f_S and f_{SP} in (2.63) are replaced by $\mathcal{A}^{-1}f_S$ and $\mathcal{A}^{-1}f_{SP}$, respectively.

By expanding $1/\mathcal{A}$ as $1-\varepsilon\mathcal{C}_P+O(\varepsilon^2)$, it is verified that $\hat{T}'$ and $\hat{T}_s'$ in §4 are recovered. Thus each term in W on the right-hand side of (2.56) has the counterpart on the left-hand side. The replacements by $1/\mathcal{A}$ modify the heat flux in (2.41) through g_P, which affect the thermoacoustic-wave equations. But no changes occur in f and therefore in the shear stress and g. Noting that g_P results from differentiation of f_P with respect to y, g_P is multiplied by $\mathcal{A}^{-1}$. In addition, (2.42) is replaced by

$$\sigma\hat{q}_w = -\frac{2c_pT_e\sqrt{\nu_e}}{a_e^2}\left[\frac{1}{1-Pr}\frac{a_e^2}{T_e}\frac{\mathrm{d}T_e}{\mathrm{d}x}\sigma^{-1/2}\frac{\partial\hat{p}'}{\partial x}\frac{\mathcal{C}_P}{\mathcal{A}}g(x,H)\right], \tag{2.110}$$

without the symbol $O(\varepsilon)$. For the case of the circular tube, the factor 2 should be deleted.

2.9.2 Modifications of relaxation functions

To derive the thermoacoustic-wave equations, the inverse transform of the heat flux (2.41) is necessary, and the inverse transform (2.45) is modified by $1/\mathcal{A}$. Thus the following transform must be evaluated:

$$\frac{1}{\sqrt{2\pi}}\mathscr{F}^{-1}\left\{\frac{\sigma^{-1/2}}{1+\varepsilon\tanh(\sqrt{Pr}/\delta_e)/\tanh(1/\delta_s)}\tanh(\sqrt{Pr}/\delta_e)\right\}. \tag{2.111}$$

It is readily seen that the poles of $\tanh(\sqrt{Pr}/\delta_e)$ and $\tanh(1/\delta_s)$ are no longer poles of the integrand. Instead new poles appear from zeros of the denominator by competition between $\tanh(\sqrt{Pr}/\delta_e)$ and $\tanh(1/\delta_s)$.

For the denominator to vanish: $\tanh(1/\delta_s)+\varepsilon\tanh(\sqrt{Pr}/\delta_e)=0$, there are two cases, one being a case in which $\tanh(\sqrt{Pr}/\delta_e)$ takes a large value of order ε^{-1}, or the other a case in which $\tanh(1/\delta_s)$ takes a small value of order ε. In the former case, simple poles are located near the ones of $\tanh(\sqrt{Pr}/\delta_e)$ and are given by $-\{(2n-1)^2\pi^2/4-\varepsilon(2n-1)\pi/\tan[(n-1/2)\pi G_e]+O(\varepsilon^2)\}\kappa_e/H^2$. The poles are shifted by the order of ε. Noting that the factor $1/\tan[(n-1/2)\pi Ge]$ results from $1/\tanh(1/\delta_s)$ and assuming this does not vanish for any positive integer of n, these poles yield the inverse transform as

$$\begin{aligned}&\frac{2\sqrt{\kappa_e}}{H}\sum_{n=1}^{\infty}\left\{1+\varepsilon\frac{Ge}{\sin^2[(n-1/2)\pi Ge]}+O(\varepsilon^2)\right\}^{-1}\\&\times\exp\left\{-\frac{(2n-1)^2\pi^2}{4}\frac{\kappa_e t}{H^2}-\varepsilon\frac{(2n-1)\pi}{\tan[(n-1/2)\pi Ge]}\frac{\kappa_e t}{H^2}+O(\varepsilon^2)\right\}.\end{aligned} \tag{2.112}$$

In the latter case, simple poles are located near the zeros of $\tanh(1/\delta_s)$. They are found to be given by $\sigma=-(n\pi)^2[1-2\varepsilon\tan(n\pi/Ge)/n\pi+O(\varepsilon^2)]\kappa_s/d^2$ and shifted by the order of ε. Noting that $\tan(n\pi/Ge)$ results from $\tanh(\sqrt{Pr}/\delta_e)$ and assuming this does not diverge for any n, these poles yield

$$\varepsilon\frac{2\sqrt{\kappa_s}}{d}\sum_{n=1}^{\infty}\tan^2\left(\frac{n\pi}{Ge}\right)\exp\left[-n^2\pi^2\frac{\kappa_s t}{d^2}+2\varepsilon n\pi\tan\left(\frac{n\pi}{Ge}\right)\frac{\kappa_s t}{d^2}+O(\varepsilon^2)\right]. \tag{2.113}$$

Thus the inverse transform of (2.111) is given by the sum of (2.112) and (2.113). If the exponential function in (2.112) is expanded in terms of ε, the leading term of order ε^0 corresponds to (2.46), which yields the functional $\mathscr{M}_P$. The first-order terms in ε correspond to the first and second sums of $M_D(t)$ in (2.76) with sign reversed, respectively, while (2.113) corresponds to the third sum with sign reversed.

For the heat flux q, there is another contribution from $\hat{q}_w$ given in (2.110), though small of order ε. To evaluate this, the following inverse transform must be executed:

$$\frac{1}{\sqrt{2\pi}}\mathscr{F}^{-1}\left\{\frac{\sigma^{-1/2}}{1+\varepsilon\tanh(\sqrt{Pr}/\delta_e)/\tanh(1/\delta_s)}\frac{\tanh(\sqrt{Pr}/\delta_e)\tanh(1/\delta_e)}{\tanh(1/\delta_s)}\right\}. \tag{2.114}$$

This is reduced to (2.48) to the lowest order in ε. The transform (2.114) can be evaluated in a similar fashion to the one (2.111). In this case, however, there occur poles of $\tanh(1/\delta_e)$ in addition to those in (2.111), and there are contributions from three types of poles. It is verified that these correspond to the three sums in (2.75) to the lowest order in ε.

It is found from (2.112) and (2.113) that the coefficients of ε diverge when $\tan[(n-1/2)\pi Ge]$ vanishes or $\tan(n\pi/Ge)$ diverges for a special value Ge. These are the resonant cases seen in (2.76). For $Ge=2$, for example, they correspond to cases where the zeros of $\cosh(\sqrt{Pr}/\delta_e)$ coincide with the ones of $\sinh(1/\delta_s)$ and $\kappa_e/H^2=4\kappa_s/d^2$. Then the simple poles of the integrand in (2.111) are located at $\sigma=-[(n-1/2)^2\pi^2\pm(2n-1)\pi\sqrt{\varepsilon/2}+\cdots]\kappa_e/H^2$, and the integral is evaluated as

$$\frac{2\sqrt{\kappa_e}}{H}\sum_{n=1}^{\infty}\exp\left[-\frac{(2n-1)^2\pi^2}{4}\frac{\kappa_e t}{H^2}\right]\cosh\left[(2n-1)\pi\sqrt{\frac{\varepsilon}{2}}\frac{\kappa_e t}{H^2}\right]+O(\varepsilon). \tag{2.115}$$

The relaxation becomes slower by the order of $\sqrt{\varepsilon}$ in the hyperbolic function than the order of ε in (2.112) and (2.113) in the non-resonant case. At resonance, the diffusion is unusual in the sense that the effects of heat conduction no longer remains to be of order ε. This difference manifests significant as the value of ε becomes larger.

Profiles of the relaxation function are displayed in non-resonant cases. Taking the value of ε to be 0.01, figure 5 depicts logarithmic plots of the function $\Phi(t)-\varepsilon M_D(t)$ for four values of Ge (= 1.5, 2.5, 3.5 and 4.5), where the factor κ_e/H^2 in the abscissa $\kappa_e t/H^2$ and ordinate $(H/\sqrt{\kappa_e})(\Phi-\varepsilon M_D)$ is omitted. For t less than 5, all behaviours are almost the same as $1/\sqrt{\pi t}$. For t greater than 5, it is seen that as the value of Ge becomes larger, slower relaxation appear. The curve of $\Phi(t)$ without the effects of heat conduction almost coincides with the curve for $Ge=1.5$.

The relaxation function in the resonant case for $Ge=2$ is compared with the ones in non-resonance cases in the vicinity of it. Figure 6 displays the logarithmic plots of the function determined by (2.115) and $\Phi(t)-\varepsilon M_D(t)$ for the values of $Ge=1.95$ and 2.05 against t over the interval $0.1\le t\le 100$ where ε is chosen to be 0.2 and the factor κ_e/H^2 is omitted from the abscissa and ordinate.

For reference, $\Phi(t)$ is drawn in the broken curve. The open and solid dots represent, respectively, the inverse Laplace transforms of (2.45), and (2.111) for $Ge=2$ and $\varepsilon=0.2$ evaluated numerically by the double exponential formulas (Ooura & Mori (1991)). The open dots almost lie on the broken curve for $\Phi(t)$ but the dots in both cases scatter for

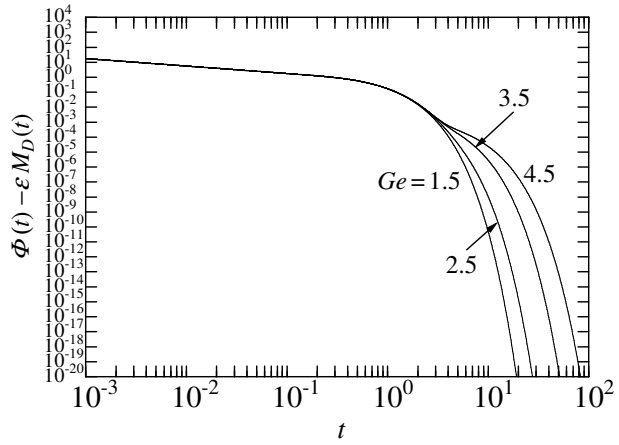

Figure 5: Logarithmic plots of the relaxation function $\Phi(t)-\varepsilon M_D(t)$ in the non-resonant cases with $\varepsilon = 0.01$ and $Ge = 1.5$, 2.5, 3.5 and 4.5 against t over the interval $10^{-3} \le t \le 10^2$ where the abscissa and ordinate measure $\kappa_e t/H^2$ and $(H/\sqrt{\kappa_e})(\Phi - \varepsilon M_D)$, respectively, but the factor κ_e/H^2 being omitted.

the ordinate below 10^{-15}, which is the limit of accuracy in double precision. Because the formulas provide very accurate results just as seen from the agreements between the open dots and the broken curve, it is conjectured that differences between the curve for $Ge = 2$ and the dots would stem from higher-order terms in (2.115). When (2.111) is evaluated numerically for $Ge = 1.95$ and $Ge = 2.05$, they are close to the solid dots away from the curves with $Ge = 1.95$ and 2.05.

2.9.3 Resonance conditions and modified thermoacoustic-wave equations

Resonance conditions are found from the coefficients of the exponential functions in M_T and M_D. They are given as follows: $\tan[(n-1/2)\pi\sqrt{Pr}Ge] = \tan[(n-1/2)\pi Ge] = 0$ and $\cot(n\pi/Ge) = \cot(n\pi/\sqrt{Pr}Ge) = \cot[(n-1/2)\pi\sqrt{Pr}] = \cot[(n-1/2)\pi/\sqrt{Pr}] = 0$ for any integer n. It is noted that because the value of Ge varies with x, the resonance conditions are met at somewhere along the channel. For the resonance conditions in the case of the tubes, they are identified by the relaxation functions N_T and N_D. The resonance occurs when $j_n\sqrt{Pr}$ or $j_n/\sqrt{Pr}$ hit one of the roots of J_0 or when $k_n\sqrt{\kappa_s/\nu_e}$ or $k_n\sqrt{\kappa_s/\kappa_e}$ hit one of those roots. Further $j_n\sqrt{\nu_e/\kappa_s}$ or $j_n\sqrt{\kappa_e/\kappa_s}$ hit the poles of Z.

To derive the thermoacoustic-wave equation valid both in non-resonant and resonant cases, the asymptotic expansion in ε should be abandoned. Then the functionals $\mathscr{M}_P - \varepsilon\mathscr{M}_D$ and $\mathscr{M}_T$ in (2.56) and (2.55) are replaced, respectively, by $\tilde{\mathscr{M}}_P$ and $\tilde{\mathscr{M}}_T$, whose relaxation functions $\tilde{M}_P$ and $\tilde{M}_T$ are to be determined by the inverse transforms of (2.111) and (2.114), respectively. Then the thermoacoustic-wave equation takes the following form:

$$\frac{\partial^2 p'}{\partial t^2} - \frac{\partial}{\partial x}\left(a_e^2\frac{\partial p'}{\partial x}\right) + \frac{\partial}{\partial x}\left[\frac{a_e^2\sqrt{\nu_e}}{H}\mathscr{M}\left(\frac{\partial p'}{\partial x}\right)\right] + \frac{\sqrt{\nu_e}}{H}\left\{\frac{\gamma-1}{\sqrt{Pr}}\tilde{\mathscr{M}}_P\left(\frac{\partial^2 p'}{\partial t^2}\right)\right.$$

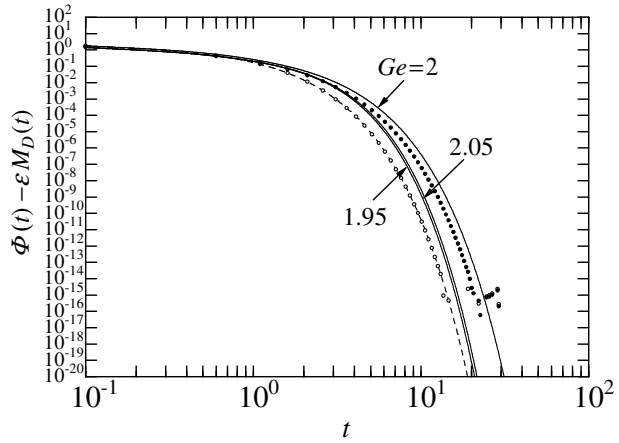

Figure 6: Differences of the relaxation functions in the vicinity of the resonance at $Ge = 2$ for $\varepsilon = 0.2$. Logarithmic plots of the relaxation function determined by (2.115) in the resonant case and $\Phi(t) - \varepsilon M_D(t)$ in the non-resonant cases for $Ge = 1.95$ and 2.05 against t over the interval $0.1 \le t \le 100$ where the abscissa and ordinate measure $\kappa_e t/H^2$ and $(H/\sqrt{\kappa_e})(\Phi - \varepsilon M_D)$, respectively, but the factor κ_e/H^2 is omitted. The open and solid dots represent, respectively, the inverse Laplace transforms of (2.45) and (2.111) evaluated numerically by the double exponential formulas where the former almost lie on the curve $\Phi(t)$ in the broken line but both dots scatter for the ordinate below 10^{-15}.

$$- \frac{a_e^2}{T_e}\frac{\mathrm{d}T_e}{\mathrm{d}x}\left[\frac{1}{1-Pr}\mathscr{M}\left(\frac{\partial p'}{\partial x}\right) - \frac{1}{(1-Pr)\sqrt{Pr}}\tilde{\mathscr{M}}_P\left(\frac{\partial p'}{\partial x}\right) - \frac{\varepsilon}{1-Pr}\tilde{\mathscr{M}}_T\left(\frac{\partial p'}{\partial x}\right)\right]\Bigg\} = 0. \tag{2.116}$$

Although explicit expressions of $\tilde{M}_P$ and $\tilde{M}_T$ are not given, they are determined by the zeros of the functions $\tanh(1/\delta_s) + \varepsilon\tanh(\sqrt{Pr}/\delta_e)$ and the poles of $\tanh(1/\delta_e)$. Equation (2.116) is the full thermoacoustic-wave equation taking account of the effects of heat conduction without making an expansion in terms of ε, and therefore it is valid for any value of Ge. For the case of the circular tubes, similar replacements are necessary in (2.73) and (2.74). The relaxation functions in $\tilde{\mathscr{N}_P}$ and $\tilde{\mathscr{N}_T}$ are simply replaced by the inverse transforms of (2.71) and (2.72) with the factor $1/\mathcal{A}$ multiplied.

Equation (2.116) has been derived by evaluating the heat flux fully. Using this heat flux, the mean temperature of the solid wall $\bar{T}_s'$ is obtained from (2.25) as

$$\frac{\partial^2 \bar{T}_s{}'}{\partial t^2} = \frac{\varepsilon}{Ge}\frac{T_e}{\rho_e a_e^2}\frac{\sqrt{\nu_e}}{H}\left\{\frac{\gamma-1}{\sqrt{Pr}}\tilde{\mathscr{M}}_P\left(\frac{\partial^2 p'}{\partial t^2}\right) - \frac{a_e^2}{T_e}\frac{\mathrm{d}T_e}{\mathrm{d}x}\left[\frac{1}{1-Pr}\mathscr{M}\left(\frac{\partial p'}{\partial x}\right) - \frac{1}{(1-Pr)\sqrt{Pr}}\tilde{\mathscr{M}}_P\left(\frac{\partial p'}{\partial x}\right) - \frac{\varepsilon}{1-Pr}\tilde{\mathscr{M}}_T\left(\frac{\partial p'}{\partial x}\right)\right]\right\}. \tag{2.117}$$

The terms in the curl brackets may be replaced by the first three terms in (2.116) with sign reversed. The relation (2.117) holds for the case of the circular tubes by replacing $\mathscr{M}$ with $\mathscr{N}$, and H with $2R$. Then the mean temperature is defined by integrating $2\pi r T_s'$

over the thickness and dividing it by $\pi[(1+\eta)^2-1]R^2$, whereby the integral of rZ over the thickness is equal to δ_s^{-1}.

2.10 Conclusion of the heat conduction in wall

We examined the effects of the thermal conduction in the wall on the thermoacoustic wave equation and its approximated theory. The effects appear through the parameter ε defined by the square root of the product of two ratios, one being the ratio of the heat capacities per volume and the other the ratio of the thermal conductivities. This is not the only parameter for the effects but they are determined by the ratio of thermal diffusivities and especially the geometry parameter Ge defined by the relative thickness of the wall. Because the heat capacity per volume and thermal conductivity of the solid wall are usually greater than the ones of gas, the value of ε is very small so that the effects of heat condition have been taken into account to the first order of ε. However it has been unveiled that when the geometry parameter takes special values, the expansion exhibits nonuniformity, i.e. resonance, and then the effects become enhanced up to the order of $\sqrt{\varepsilon}$. In comparison with the diffusion of ε in non-resonant case, the effects give rise to unusual diffusion in a transient behavior and modify the thermoacoustic-wave equations.

In thin diffusion layer theory, the effects of heat conduction appear only through ε, however in the thick diffusion layer theory, they appear through ε and Ge. The effects of heat conduction in wall may be neglected as long as the value of ε is small enough. But it may happen that the effects appear enhanced, depending through Ge on the geometry of the tubes, and the combination between the gas and the solid. However, in thick and thin diffusion layer theory, terms obtained by the heat conduction have the same form of terms as the equation without temperature variation. Therefore we can summarize them in the coefficients of the main equation.

3 Marginal conditions for the onset of thermoacoustic oscillations in a looped tube

Essence of the phenomena is in the interconversion between the thermal energy and kinematic one. Because energy of gas oscillations is supplied by ambient heat source, energy conversion takes place from thermal energy to mechanical one. This may be regarded as prime mover . Recently application of thermoacoustic phenomena to heat engine has attracted much attention and interest from a viewpoint of energy and environmental problems, especially, heat engines exploiting a gas-filled, looped tube (Swift (2002), Garrett (2004)). This prime mover with looped tube is characterized by emergence of a travelling wave, which yields a favourable phasing between pressure and velocity of a gas particle to enhance efficiency as a heat engine in comparison with that exploiting a standing wave. For further increase in efficiency and power to put it into practical use, physical processes occurring especially in narrow pores in the stack must be clarified. At present, however, even marginal conditions of instability are not well established.

Marginal conditions of instability are shown experimentally by Yazaki *et al.* (1998), a first attempt to derive it analytically is made by Penelet *et al.* (2005) by using the transmission matrix method by solving a pressure field based on Rott's equation (Rott (1969)). Later Ueda & Kato (2008) also solved Rott's equation by a transmission matrix method to derive marginal conditions and compared them with their experimental results. Although all these analyses are based on Rott's equation, this equation is desperately difficult to be solved analytically so that they must rely on numerical computations to solve the differential equation. This foreshadows understanding of mechanisms of instability and physical processes involved.

Essence of thermoacoustic phenomena lies in thermoviscous diffusion of a gas in contact with a solid wall. To understand the phenomena as easily as possible, it seems to be reasonable to consider them by limiting a situation concerned. The diffusion effects will occur differently depending on a span length of a flow passage, therefore situation may be classify by the ratio of thickness of diffusion layer to a span length. Rott's equation covers all situation in frequency domain. Thermoacoustic-wave equation also covers all situation classified by thickness of diffusion layer, but this is in the space and time domain. This equation is reduced to Rott's equation if a time-harmonic disturbance is considered. The equation enables to unveil a unstable transient behavior and is expected to be extended to nonlinear regime. This equation may be approximated by the thickness of diffusion layer and asymptotic equations may be obtained for thick or thin diffusion layer.

In the case of thin diffusion layer, marginal conditions for the Taconis oscillations and for the Sondhaus tube are derived Sugimoto & Yoshida (2007) and Sugimoto & Takeuchi (2009). Nonlinear problem also have been already done. On the other hand, in the case of thick diffusion layer, applications to the specific problem have not been done yet.

In this section, Marginal conditions of onset of thermoacoustic oscillations in the looped tube based on asymptotic theories. For the gas outside of the pores, the theory for thin diffusion layer is applied. Recently Shimizu *et al.* (2012) applied this theory of thin diffusion layer even to the gas in the pores to obtain a right branch of marginal curves up to the minimum temperature ratio. However, since it is obviously inapplicable to a left branch, this paper employs the theory of thick diffusion layer by expecting to derive a left branch.

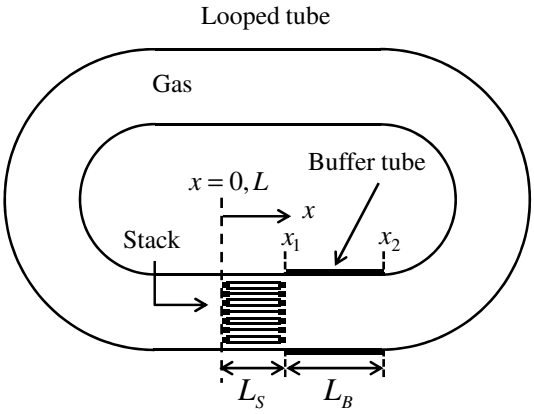

Figure 7: Illustration of a gas-filled, looped tube of inner radius R and axial length L with a stack of length L_S inserted where the x-axis is taken along the tube's central axis counterclockwise. The stack is assumed to consist of many pores of radius $R_S(\ll R)$ and to be subjected to a temperature gradient axially by keeping the left end of the stack ($x = 0$) at a room temperature T_0 while the right end ($x = x_1(= L_S)$) at a temperature T_1 higher than T_0, and the temperature relaxes from T_1 at $x = x_1$ to T_0 at $x = x_2(= L_S + L_B \ll L)$ over a buffer tube of length L_B, the temperature being at T_0 elsewhere in the tube.

3.1 Model of looped tube

Now we apply asymptotic equations derived in §2 to the looped tube and derive the marginal conditions. Results from the approximate equations for thick and thin diffusion layer, new form of terms does not appear in equation. Therefore we use approximate equations taking ε to 0 for simplicity. We consider a model of a gas-filled, looped tube with a stack inserted as shown in figure 7. For sake of simplicity, the tube has a uniform cross section of inner radius R except for a section of the stack. The stack is assumed to consist of many long pores of radius $R_S(\ll R)$ and of length L_S axially. The stack wall is subjected to a temperature gradient by keeping the left end of the stack at a room temperature T_0 while the right end at a temperature T_1 higher than T_0. This temperature gradient is imposed, in reality, by hot and cold heat exchangers installed close to both ends of the stack. However, because of the short axial length of the heat exchangers, the present model does not take them into account but assumes simply the temperature at both ends of the stack to be held constant. In a section of the tube except for the stack, the temperature of gas and wall relaxes from the highest one at the hot end of the stack to resume the room temperature over an axial length of L_B. Such a section is called a buffer tube. Except for the sections of the stack and the buffer tube, the temperature is assumed to be at the room temperature.

In figure 7, the x-axis is taken along the tube's central axis counterclockwise and the origin is set at the cold end of the stack. Let the tube length along the centerline be L. The hot end of the stack is located at $x = x_1(= L_S)$, which is the left end of the buffer tube. The right end of the buffer tube is located at $x = x_2(= L_S + L_B \ll L)$. The loop is not necessarily circular but a typical loop radius $L/2\pi$ is assumed to be much larger than the inner radius R. Then curvature effects of the x-axis may be negligible in

thermoviscous effects and also the centrifugal force, which is quadratic in velocity. Hence following arguments are based on the assumption that the loop may be regarded as a straight tube locally.

Assuming an ideal gas, the pressure takes a uniform value p_0 throughout in a quiescent state where no gravity is assumed. Then the temperature of gas T_e is regarded as being equal to that of the wall and uniform over the cross section. Thus T_e is a function of x only, and the local density of the gas is denoted by ρ_e with $\rho_e T_e$ being constant. Even when the gas is in motion, no account of temporal variations in the wall temperature is taken. The subscript e implying mechanical equilibrium, i.e. the quiescent state is attached to designate a quantity of a function of x determined by T_e.

3.2 Derivation of frequency equation

We now derive a frequency equation which determines marginal oscillations. Employing the theories for thick and thin diffusion layer for the gas in the stack and that in the other sections, respectively, we attempt to seek analytical solutions to the respective equations. By imposing them on matching conditions at each junction of the sections, the frequency equation is derived.

To do this, the temperature distribution T_e must be specified. As the theory of thick diffusion layer suggests, it is assumed that T_e in the stack is given by (3.13). Note that since $(1-L_S/x_\infty)^{-2/(1+2\beta)}$ determines the temperature ratio T_1/T_0, the stack length varies slightly with the temperature ratio. When the temperature gradient is absent, its length shrinks to zero. In the buffer tube, as will be shown later, T_e is assumed to decrease from T_1 to T_0 in the form of a parabolic function in x given by (3.44) below because analytical solutions are available in this case. Elsewhere in the tube, T_e is assumed to be T_0. Figure 8 shows an example of the temperature distribution T_e/T_0 in the section $0 \le x \le 0.25L$ for the case with $T_1/T_0 = 2$, $L_S = 0.02L$, $L_B = 0.21L$ and $\beta = 0.5$ where the stack and the buffer tube occupy the sections $0 < x < 0.02L$ and $0.02L < x < 0.23L$, respectively. The distribution in the stack and the one in the buffer tube are concave upward, though the latter appears to be linear in this scale.

3.2.1 Relations for the gas in the pores of the stack

Suppose that the thickness of thermoviscous diffusion layer in the pore of the stack is much thicker than the pore radius. Then the thermoacoustic-wave equation is approximated to be the diffusion wave equation to the lowest approximation in the ratio of the radius to the thickness. As long as this equation is used, however, no instability can be expected and therefore employed is the higher-order equation taking account of the finiteness of the ratio.

The higher-order equation is given by (2.101) ($\varepsilon \to 0, j = 1$) for an excess pressure $p'(x,t)$ over p_0 in the case of the circular tube of radius R, which corresponds to R_S in the present context. For integrity's sake, the higher-order equation is written in the following form:

$$\frac{\partial p'}{\partial t} - \frac{\partial}{\partial x}\left(\alpha_e \frac{\partial p'}{\partial x}\right) + \frac{\alpha_e}{T_e}\frac{\mathrm{d}T_e}{\mathrm{d}x}\frac{\partial p'}{\partial x}$$

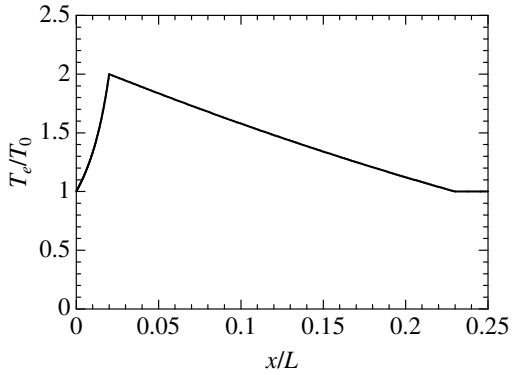

Figure 8: Example of the temperature distribution T_e/T_0 in the section $0 \leq x \leq 0.25L$ for the case with $T_1/T_0 = 2$, $L_S = 0.02L$, $L_B = 0.21L$ and $\beta = 0.5$ where the stack and the buffer tube extend in the sections $0 < x < 0.02L$ and $0.02L < x < 0.23L$, respectively. The distribution in the stack is given by (3.13) with $\beta = 0.5$, while that in the buffer tube is given by (3.44) with $\lambda = \sqrt{2} - 1$.

$$+ \frac{\alpha_e}{a_e^2}\frac{\partial}{\partial t}\left\{\left[\frac{4}{3}\gamma - (\gamma-1)Pr\right]\frac{\partial p'}{\partial t} - \frac{1}{6}(1+\beta+Pr)\frac{a_e^2R^2}{\nu_e T_e}\frac{\mathrm{d}T_e}{\mathrm{d}x}\frac{\partial p'}{\partial x}\right\} = 0, \tag{3.1}$$

Remark that α_e gives the diffusivity of acoustic waves in the narrow tube and channel, which should be distinguished from the diffusivity of sound in an unbounded thermoviscous fluid (see, e.g. Morfey (2001)). The first line of (3.1) is the lowest equation, to which the second line gives the higher-order corrections of order $R^2\omega/\nu_e (\equiv |\delta_e|^{-2} \ll 1)$. To the lowest approximation, the gas is in perfect thermal contact with the wall so that the temperature disturbance vanishes. When (3.1) is assumed, it takes account of the small temperature disturbance so that the heat flux (given later by (3.116)) is present through the wall surface. Because the thermal contact is still good in this case, the stack acts as a regenerator, though the term "stack" is often used when the thermal contact is imperfect.

Using the lowest equation, the higher-order terms in the curl brackets may be expressed equivalently in various way as far as the order of $|\delta_e|^{-2}$ is concerned. Subtracting the lowest equation multiplied by an arbitrary constant c, in fact, they may be replaced by

$$\left\{\left[\frac{4}{3}\gamma - (\gamma-1)Pr - c\right]\frac{\partial p'}{\partial t} + c\frac{\partial}{\partial x}\left(\alpha_e\frac{\partial p'}{\partial x}\right) - [\frac{4}{3}\gamma(1+\beta+Pr) + c]\frac{\alpha_e}{T_e}\frac{\mathrm{d}T_e}{\mathrm{d}x}\frac{\partial p'}{\partial x}\right\}. \tag{3.2}$$

If c is chosen to be $4/3\gamma - (\gamma-1)Pr$, the coefficient of $\partial p'/\partial t$ is made to vanish. If c is chosen to be $-4/3\gamma(1+\beta+Pr)/2$ for the coefficients of the last two terms to become equal, the higher-order equation is written as

$$\frac{\partial p'}{\partial t} - \frac{\partial}{\partial x}\left(\alpha_e\frac{\partial p'}{\partial x}\right) + \frac{\alpha_e}{T_e}\frac{\mathrm{d}T_e}{\mathrm{d}x}\frac{\partial p'}{\partial x} + \frac{\alpha_e}{a_e^2}\frac{\partial}{\partial t}\left\{c\left[-\varpi\frac{\partial p'}{\partial t} + \frac{\partial}{\partial x}\left(\alpha_e\frac{\partial p'}{\partial x}\right) + \frac{\alpha_e}{T_e}\frac{\mathrm{d}T_e}{\mathrm{d}x}\frac{\partial p'}{\partial x}\right]\right\} = 0, \tag{3.3}$$

with $\varpi = [4\gamma/3(3+\beta+Pr) - 2(\gamma-1)Pr]/[4\gamma/3(1+\beta+Pr)]$, which is positive for air. The factor in the curl brackets represents another diffusion wave equation with diffusion time modified by ϖ. This equation describes diffusion propagating *down* the temperature gradient, which should be compared with that *up* the gradient governed by the lowest equation. Thus it is revealed that the higher-order equation contains two different diffusion wave mechanisms.

The present analysis makes use of (3.1) for the case of the circular pore of radius R_S with the higher-order terms rewritten as (3.2) by choosing $c = 4\gamma/3 - (\gamma-1)Pr$ in the following form:

$$\frac{\partial p'}{\partial t} - \frac{\partial}{\partial x}\left(\alpha_e \frac{\partial p'}{\partial x}\right) + \frac{\alpha_e}{T_e}\frac{\mathrm{d}T_e}{\mathrm{d}x}\frac{\partial p'}{\partial x} + \frac{\alpha_e}{a_e^2}\frac{\partial}{\partial t}\left\{\left[\frac{4}{3}\gamma - (\gamma-1)Pr\right]\frac{\partial}{\partial x}\left(\alpha_e\frac{\partial p'}{\partial x}\right)\right.$$
$$\left. - \left[\frac{4}{3}\gamma(2+\beta+Pr) - (\gamma-1)Pr\right]\frac{\alpha_e}{T_e}\frac{\mathrm{d}T_e}{\mathrm{d}x}\frac{\partial p'}{\partial x}\right\} = 0, \tag{3.4}$$

with α_e in the pore of radius R_S given by

$$\alpha_e = \frac{a_e^2 R_S^2}{8\gamma\nu_e}, \tag{3.5}$$

The shear viscosity and the heat conductivity follow as power law (2.3). If this power law is assumed, α_e is no longer independent of T_e. The temperature dependence of the quantities with the subscript e is given in terms of T_e/T_0 as follows:

$$\frac{a_e^2}{a_0^2} = \frac{T_e}{T_0}, \quad \frac{\nu_e}{\nu_0} = \left(\frac{T_e}{T_0}\right)^{1+\beta}, \quad \frac{\alpha_e}{\alpha_0} = \left(\frac{T_e}{T_0}\right)^{-\beta}. \tag{3.6}$$

For the spatial derivative of these quantities, it is convenient to use the following relations:

$$\frac{1}{a_e^2}\frac{\mathrm{d}a_e^2}{\mathrm{d}x} = \frac{1}{T_e}\frac{\mathrm{d}T_e}{\mathrm{d}x}, \quad \frac{1}{\nu_e}\frac{\mathrm{d}\nu_e}{\mathrm{d}x} = \frac{1+\beta}{T_e}\frac{\mathrm{d}T_e}{\mathrm{d}x}, \quad \frac{1}{\alpha_e}\frac{\mathrm{d}\alpha_e}{\mathrm{d}x} = -\frac{\beta}{T_e}\frac{\mathrm{d}T_e}{\mathrm{d}x}. \tag{3.7}$$

To solve (3.4), an Ansatz is introduced as follows:

$$\alpha_e\frac{\partial p'}{\partial x} = \frac{T_e}{T_0}g(t), \tag{3.8}$$

where $g(t)$ is an arbitrary function of t, which has a physical dimension of an energy flux density [W/m^2]. Letting $T_e/T_0 = \theta$, p' is expressed as

$$p' = \int_0^x \frac{\theta}{\alpha_e}\mathrm{d}x\, g(t) + i(t), \tag{3.9}$$

where $i(t)$ is an arbitrary function of t. Substituting (3.9) into (3.4), it follows that

$$\left[\int_0^x \frac{\theta}{\alpha_e}\mathrm{d}x - \frac{1}{6}(1+\beta+Pr)\frac{R_S^2}{\nu_e}\frac{\mathrm{d}\theta}{\mathrm{d}x}\right]\frac{\mathrm{d}g}{\mathrm{d}t} + \frac{\mathrm{d}i}{\mathrm{d}t} = 0. \tag{3.10}$$

Note that if the higher-order terms are ignored in (3.4), g must be independent of t and (3.8) becomes irrelevant to the present problem. It is only when the higher-order terms are taken into account that (3.8) has a significance.

Differentiating the factor bracketed in (3.10) with respect to x, it follows that

$$\theta^{1+\beta} - \frac{4}{3}\gamma(1+\beta+Pr)\frac{\alpha_0^2}{a_0^2}\frac{\mathrm{d}}{\mathrm{d}x}\left(\frac{1}{\theta^{1+\beta}}\frac{\mathrm{d}\theta}{\mathrm{d}x}\right) = 0, \tag{3.11}$$

where the last relation in (3.6) has been used. Integrating (3.11), it follows that

$$\theta - \frac{2}{3}\gamma(1+\beta+Pr)\frac{\alpha_0^2}{a_0^2}\left(\frac{1}{\theta^{1+\beta}}\frac{\mathrm{d}\theta}{\mathrm{d}x}\right)^2 = \text{const.}, \tag{3.12}$$

where the const. is arbitrary. Taking this constant to be zero, θ is obtained as

$$\theta \equiv \frac{T_e}{T_0} = \left(1 - \frac{x}{x_\infty}\right)^{-2/(1+2\beta)}, \tag{3.13}$$

where T_e/T_0 is assumed to take unity at $x = 0$, and x_∞ is given by

$$x_\infty = \frac{1}{1+2\beta}\sqrt{\frac{1+\beta+Pr}{24\gamma}}\frac{a_0 R_S^2}{\nu_0}. \tag{3.14}$$

If the const. in (3.12) is chosen to be unity, θ is obtained analytically for $\beta = 0.5$ as

$$\frac{T_e}{T_0} = \left(1 - \frac{x^2}{4x_\infty^2}\right)^{-1}. \tag{3.15}$$

In this case, the temperature increases slowly from $x = 0$ as $1+x^2/4x_\infty^2+\cdots$ for $x/x_\infty \ll 1$ compared with (3.13).

The following analysis assumes T_e/T_0 in (3.13) by restricting to a range in $x/x_\infty < 1$. For the atmospheric air at 15°C, $a_0 = 340$ m/s, $\gamma = 1.4$, $Pr = 0.72$, $\nu_0 = 1.45\times 10^{-5}$ m^2/s and $\beta = 0.5$ so that x_∞ takes $3.0 \times 10^6\, R_S^2$ m^{-1}. Supposing $R_S = 0.5$ mm, x_∞ is about 0.75 m. If β is chosen to be 0.5, for example, T_e/T_0 takes 2 for $x/x_\infty = 1/2$, and 3 for $x/x_\infty = 2/3$. To compare it with a parabolic distribution, T_e/T_0 is expanded in power series of x/x_∞ as

$$\frac{T_e}{T_0} = 1 + \frac{2}{1+2\beta}\left(\frac{x}{x_\infty}\right) + \frac{[1+2(1+2\beta)]}{(1+2\beta)^2}\left(\frac{x}{x_\infty}\right)^2 + \cdots. \tag{3.16}$$

It is found that (3.16) deviates from $[1+(1+2\beta)^{-1}x/x_\infty]^2$ by $2(1+2\beta)^{-1}(x/x_\infty)^2$.

For the temperature distribution given by (3.13), it follows that

$$\int_0^x \frac{\theta}{\alpha_e}\mathrm{d}x = \frac{(1+2\beta)x_\infty}{\alpha_0}\left[\left(1 - \frac{x}{x_\infty}\right)^{-1/(1+2\beta)} - 1\right]. \tag{3.17}$$

Using this and (3.13) into (3.10), it is found that i must be chosen to be $(1+2\beta)x_\infty g/\alpha_0$ plus an arbitrary constant in t. Thus p' is specified as

$$p' = \frac{\Gamma}{a_0}\left(1 - \frac{x}{x_\infty}\right)^{-1/(1+2\beta)} g(t) = \frac{\Gamma}{a_0}\left(\frac{T_e}{T_0}\right)^{1/2} g(t), \tag{3.18}$$

where Γ is defined by

$$\Gamma \equiv \frac{(1+2\beta)x_\infty a_0}{\alpha_0} = \sqrt{\frac{8\gamma(1+\beta+Pr)}{3}}. \tag{3.19}$$

As long as (3.13) is assumed, (3.18) is an exact solution to (3.4). However, this is insufficient to accommodate boundary conditions and another solution independent of it is required. Although (3.4) does not permit a solution $h(t)$ uniform in x, h being an arbitrary function of t, it is possible to construct a solution about it in the form of an asymptotic series of time derivatives of h as $p' = h(t) + w(x)\dot{h} + w^{(2)}(x)\ddot{h} + \cdots$. Here the dot designates differentiation with respect to t, and w and $w^{(2)}$ are functions of x to be determined so as to satisfy (3.4) consistently. The series is suggested by noting that the operator $(\alpha_e/a_e^2)\partial/\partial t$ in the higher-order term yields $R_S^2\omega/8\gamma\nu_e$, ω^{-1} being a typical time scale involved in variations of h like $\mathrm{e}^{\mathrm{i}\omega t}$, and the factor is small because the ratio of the pore radius to a typical thickness of the viscous diffusion layer $\sqrt{\nu_e/\omega}$ is smaller than unity. Substituting the series into (3.4), p' is evaluated up to the first order in $\dot{h}$ as

$$p' = h(t) + \Lambda\left(1 - \frac{x}{x_\infty}\right)^{2(1+\beta)/(1+2\beta)} \frac{R_S^2}{6\nu_0}\frac{\mathrm{d}h}{\mathrm{d}t} + \cdots = h(t) + \Lambda\frac{R_S^2}{6\nu_e}\frac{\mathrm{d}h}{\mathrm{d}t} + \cdots, \tag{3.20}$$

where Λ is defined by

$$\Lambda = \frac{1+\beta+Pr}{(1+\beta)(3+2\beta)}, \tag{3.21}$$

and higher-order terms than $R_S^2\omega/6\nu_e$ have been ignored. Summing (3.18) and (3.20), p' is expressed in terms of two unknown functions g and h in t as

$$p' = \frac{\Gamma}{a_0}\left(\frac{T_e}{T_0}\right)^{1/2} g + h + \Lambda\frac{R_S^2}{6\nu_e}\frac{\mathrm{d}h}{\mathrm{d}t}. \tag{3.22}$$

As the pressure in (3.22) is evaluated up to the first order of $R_S^2\omega/\nu_e$, the axial velocity $u'(r,x,t)$ in the pore is also taken up to terms of the same order, r being a radial coordinate in the pore. It is given as

$$u' = -\frac{1}{4\mu_e}\frac{\partial p'}{\partial x}(R_S^2 - r^2) + \frac{1}{64\rho_e\nu_e^2}\frac{\partial^2 p'}{\partial t\partial x}(R_S^2 - r^2)(3R_S^2 - r^2). \tag{3.23}$$

The lowest velocity profile is simply that of Poiseuille flow for an incompressible fluid. It should be remarked, however, that for the instability to occur, as will be shown later, the higher-order term becomes indispensable and then the velocity profile deviates from that of Poiseuille flow. The mean velocity averaged over the cross-section of the pore of radius R_S, denoted by $\overline{u'}$, is obtained as

$$\overline{u'} \equiv \frac{1}{\pi R_S^2}\int_0^{R_S} 2\pi r u' \mathrm{d}r = -\frac{R_S^2}{8\mu_e}\frac{\partial p'}{\partial x} + \frac{R_S^4}{48\rho_e\nu_e^2}\frac{\partial^2 p'}{\partial t\partial x}. \tag{3.24}$$

Here and hereafter the overbar is used to imply a mean value over the cross-section of a flow passage. Thus the mean mass flux density is given by

$$\rho_e\overline{u'} = -\frac{\gamma}{a_0^2}\left(g - \frac{R_S^2}{6\nu_e}\frac{\mathrm{d}g}{\mathrm{d}t}\right) + \frac{2(1+\beta)\gamma\Lambda}{\Gamma a_0}\left(\frac{T_e}{T_0}\right)^{-1/2}\frac{R_S^2}{6\nu_e}\frac{\mathrm{d}h}{\mathrm{d}t}, \tag{3.25}$$

where the last term results from the first term in (3.24) and the contribution from the second term is of higher order. Here this mass flux is per unit area and therefore 'density' was added. For brevity's sake, however, it will be omitted.

Supposing time-harmonic disturbances having an angular frequency ω, we set $[p', u', g, h] = \mathrm{Re}\{[P(x), U(x), G, H\,]\,\mathrm{e}^{\mathrm{i}\omega t}\}$, $\mathrm{Re}\{\cdots\}$ standing for taking the real part of each element in the vector, and P, U, G and H being complex amplitudes and G and H constants independent of x. Then it follows from (3.22) that

$$P = \frac{\Gamma}{a_0}\left(\frac{T_e}{T_0}\right)^{1/2} G + H + \mathrm{i}\zeta_e \Lambda H, \tag{3.26}$$

where ζ_e is a non-dimensional parameter for the ratio squared of the pore radius to a typical thickness of the viscous diffusion layer $\sqrt{\nu_e/\omega}$ defined by

$$\zeta_e = \frac{R_S^2 \omega}{6\nu_e} \quad \text{with} \quad \frac{\zeta_e}{\zeta_0} = \left(\frac{T_e}{T_0}\right)^{-(1+\beta)}, \tag{3.27}$$

where $|\zeta_e| \ll 1$. The mean mass flux is given by (3.25) as

$$\rho_e \overline{U} = -\frac{\gamma}{a_0^2}(1 - \mathrm{i}\zeta_e)G + \mathrm{i}\zeta_e \frac{2(1+\beta)\gamma\Lambda}{\Gamma a_0}\left(\frac{T_e}{T_0}\right)^{-1/2} H. \tag{3.28}$$

3.2.2 Relations for the gas in the buffer tube

In the buffer tube, the temperature decreases with x monotonically, and Ueda & Kato (2008) modelled this by an exponential function. As is demonstrated by Sugimoto & Yoshida (2007), on the other hand, (2.92) ($\varepsilon \to 0, j = 1$) is solvable analytically when the temperature distribution is parabolic in x. In view of this, we assume that the temperature distribution in the buffer tube is given by a parabolic function concave upward and follow their approach to obtain solutions. Description on the method of solutions is thus kept minimum, and for details, reference should be made to their paper. Since their analysis does not take account of the temperature dependence of the viscosity and the heat conductivity, the present analysis is new in the respect of inclusion of β. If β is set equal to zero, of course, their results will be recovered.

Assuming a time-harmonic disturbance for p' in the form of $\mathrm{Re}\{P(x)\mathrm{e}^{\mathrm{i}\omega t}\}$, and noting that the derivative of minus half-order of $\mathrm{e}^{\mathrm{i}\omega t}$ is simply given by $(\mathrm{i}\omega)^{-1/2}\mathrm{e}^{\mathrm{i}\omega t}$ [$\equiv (1 - \mathrm{i})(2\omega)^{-1/2}\mathrm{e}^{\mathrm{i}\omega t}$] for $\omega > 0$, (2.92) is reduced to the following equation:

$$(1 - 2C\delta_e)a_e^2 \frac{\mathrm{d}^2 P}{\mathrm{d}t^2} + [1 - 2(C + C_T)\delta_e]\frac{a_e^2}{T_e}\frac{\mathrm{d}T_e}{\mathrm{d}x}\frac{\mathrm{d}P}{\mathrm{d}x} + \omega^2 P = 0, \tag{3.29}$$

where δ_e is defined by

$$\delta_e = \frac{1}{R}\left(\frac{\nu_e}{\mathrm{i}\omega}\right)^{1/2} \quad \text{with} \quad \frac{\delta_e}{\delta_0} = \left(\frac{T_e}{T_0}\right)^{(1+\beta)/2}, \tag{3.30}$$

and $|\delta_e| \ll 1$. Following Sugimoto and Yoshida (2007) to introduce new valuables F and Z and define P as

$$P = \frac{F}{Z} \quad \text{with} \quad Z = (1 - K_\beta \delta_e)\frac{a_e}{a_0}, \tag{3.31}$$

(3.29) is recast into the following form of equation:

$$X\frac{\mathrm{d}}{\mathrm{d}x}\left(X\frac{\mathrm{d}F}{\mathrm{d}x}\right)+MX\frac{\mathrm{d}}{\mathrm{d}x}\left(\frac{a_e}{T_e}\frac{\mathrm{d}T_e}{\mathrm{d}x}\right)+YF=0, \tag{3.32}$$

with

$$X=(1-C\delta_e)a_e, \tag{3.33}$$

where K_β, M and Y are chosen to be determined so that (3.32) agrees with (3.29) up to the first order of δ_e.

From the coefficient of $\mathrm{d}P/\mathrm{d}x$, we have $M=-1/2$ and

$$K_\beta=\frac{1}{1+\beta}\left[2C_T-\left(1+\frac{\beta}{2}\right)C\right]=\frac{1}{1+\beta}(2C_{T\beta}-C), \tag{3.34}$$

with $C_{T\beta}$ defined by

$$C_{T\beta}=C_T-\frac{\beta}{4}C. \tag{3.35}$$

The subscript β in K_β, $C_{T\beta}$ and $k_\beta^\pm$ in (3.50) indicates account of the temperature dependence of the viscosity and the heat conductivity. When no dependence is taken into account, they are reduced to those without β. From the coefficient of P, we have

$$Y=\omega^2+C_{T\beta}\delta_e\left[a_e\frac{\mathrm{d}}{\mathrm{d}x}\left(\frac{a_e}{T_e}\frac{\mathrm{d}T_e}{\mathrm{d}x}\right)+\left(1+\frac{\beta}{2}\right)\left(\frac{a_e}{T_e}\frac{\mathrm{d}T_e}{\mathrm{d}x}\right)^2\right], \tag{3.36}$$

and

$$Z=\left[1-\frac{2C}{1+\beta}\left(\frac{C_{T\beta}}{C}-\frac{1}{2}\right)\delta_e\right]\frac{a_e}{a_0}. \tag{3.37}$$

When the pressure amplitude is available, the velocity amplitude U in the main-flow region is determined. In the outside of the boundary layer called a main-flow region, the diffusive effects are neglected. Then the equation of motion in the axial direction is given for the axial velocity $u'(x,t)$ as follows:

$$\rho_e\frac{\partial u'}{\partial t}=-\frac{\partial p'}{\partial x}. \tag{3.38}$$

In the boundary layer, on the other hand, the velocity must vanish on the tube wall so that the velocity defect results. Taking this defect into consideration, the mean velocity over the whole cross-section of the tube is expressed as follows (see (8) in Shimizu & Sugimoto (2010)):

$$\overline{u}=u'-\frac{2\sqrt{\nu_e}}{R}\frac{\partial^{-\frac{1}{2}}u'}{\partial t^{-\frac{1}{2}}}. \tag{3.39}$$

The velocity amplitude U in the main-flow region is

$$U=\frac{\mathrm{i}}{\rho_e\omega}\frac{\mathrm{d}P}{\mathrm{d}x}, \tag{3.40}$$

where $\mathrm{d}P/\mathrm{d}x$ is expressed in terms of F and Z as

$$\frac{\mathrm{d}P}{\mathrm{d}x}=\frac{1}{XZ}\left(X\frac{\mathrm{d}F}{\mathrm{d}x}-\frac{X}{Z}\frac{\mathrm{d}Z}{\mathrm{d}x}F\right). \tag{3.41}$$

Using (3.39) and (3.40), the mean mass flux $\rho_e\overline{U}$ is given by

$$\rho_e\overline{U} = \rho_e(1-2\delta_e)U = (1-2\delta_e)\frac{E}{XZ}, \tag{3.42}$$

with the definition of E given by

$$E \equiv \frac{\mathrm{i}}{\omega}\left(X\frac{\mathrm{d}F}{\mathrm{d}x} - \frac{X}{Z}\frac{\mathrm{d}Z}{\mathrm{d}x}F\right). \tag{3.43}$$

Suppose the temperature distribution in the buffer tube be in the form of parabola as

$$\frac{T_e}{T_0} = \left[1+\lambda\left(\frac{x_2-x}{L_B}\right)\right]^2, \tag{3.44}$$

where λ is a positive constant satisfying continuity of temperature at $x = x_1$, i.e. $T_1/T_0 = (1-L_S/x_\infty)^{-2/(1+2\beta)} = (1+\lambda)^2$. To solve (3.32), we introduce a complex axial coordinate ξ through $X\mathrm{d}/\mathrm{d}x = a_0\mathrm{d}/\mathrm{d}\xi$. Taking the hot end of the stack at $x = x_1(= L_S)$ to be located at $\xi = 0$, ξ is given by

$$\xi = -\frac{L_B}{\lambda}\left\{\log\left(\frac{\eta}{1+\lambda}\right) + \frac{b}{1+\beta}\left[\eta^{1+\beta} - (1+\lambda)^{1+\beta}\right]\right\}, \tag{3.45}$$

with $\eta = 1+\lambda\left(x_2-x\right)/L_B$ and

$$b = C\delta_0 = \frac{C}{R}\left(\frac{\nu_0}{\mathrm{i}\omega}\right)^{1/2}, \tag{3.46}$$

where $|b| \ll 1$.

For the parabolic temperature distribution, a solution to (3.32) expressed in terms of ξ is available by a successive approximation in b. Then F is obtained up to the first order of b as

$$\begin{aligned} F = {} & B^+\mathrm{e}^{\mathrm{i}k^+\xi} + B^-\mathrm{e}^{\mathrm{i}k^-\xi} \\ & - \mathrm{i}b\beta_F\frac{C_{T\beta}}{C}\lambda(1+\lambda)^{1+\beta}\left(\frac{B^+}{k_\beta^+L_B}\,\mathrm{e}^{\mathrm{i}k^+\xi} + \frac{B^-}{k_\beta^-L_B}\mathrm{e}^{\mathrm{i}k^-\xi}\right)\mathrm{e}^{-(1+\beta)\lambda\xi/L_B}, \end{aligned} \tag{3.47}$$

while E is obtained similarly as

$$\begin{aligned} E = {} & \frac{a_0}{\omega}\Bigg[k^-B^+\mathrm{e}^{\mathrm{i}k^+\xi} + k^+B^-\mathrm{e}^{\mathrm{i}k^-\xi} \\ & + \mathrm{i}b\beta_E\frac{C_{T\beta}}{C}\lambda(1+\lambda)^{1+\beta}\left(\frac{k^-B^+}{k_\beta^+L_B}\,\mathrm{e}^{\mathrm{i}k^+\xi} + \frac{k^+B^-}{k_\beta^-L_B}\,\mathrm{e}^{\mathrm{i}k^-\xi}\right)\mathrm{e}^{-(1+\beta)\lambda\xi/L_B}\Bigg], \end{aligned} \tag{3.48}$$

where $k^\pm$ are defined as

$$k^\pm L_B = \frac{\mathrm{i}}{2}\lambda \pm \psi, \tag{3.49}$$

with $\psi = [(\omega L_B/a_0)^2 - \lambda^2/4]^{1/2}$, $k_\beta^\pm$ are defined as

$$k_\beta^\pm L_B = k^\pm L_B + \frac{\mathrm{i}}{2}\beta\lambda = \frac{\mathrm{i}}{2}(1+\beta)\lambda \pm \psi, \tag{3.50}$$

and β_F and β_E are defined, respectively, by

$$\beta_F = \frac{2+\beta}{1+\beta} \quad \text{and} \quad \beta_E = \frac{\beta}{1+\beta}. \tag{3.51}$$

Here and hereafter the symbols $\pm$ and $\mp$ are understood to be ordered vertically.

3.2.3 Relations for the gas in the section without the temperature gradient

In the section except for the stack and the buffer tube, the temperature of the gas is uniform at the room temperature T_0. Then (3.29) is simply reduced to

$$(1 - 2C\delta_0)a_0^2\frac{\mathrm{d}^2P}{\mathrm{d}x^2} + \omega^2 P = 0, \tag{3.52}$$

and the solution is readily available as

$$P = D^+\mathrm{e}^{\mathrm{i}k(x-x_2)} + D^-\mathrm{e}^{-\mathrm{i}k(x-x_2)}, \tag{3.53}$$

with the wavenumber k given by

$$k = \frac{\omega}{(1-2C\delta_0)^{1/2}a_0} = \frac{\omega}{X_0}. \tag{3.54}$$

No confusion would occur of k in (3.54) with the thermal conductivity.

Using (3.53) in (3.38), the velocity amplitude is given by

$$U = -\frac{1}{\rho_0 X_0}D^+\mathrm{e}^{\mathrm{i}k(x-x_2)} + \frac{1}{\rho_0 X_0}D^-\mathrm{e}^{-\mathrm{i}k(x-x_2)}, \tag{3.55}$$

and the mean mass flux averaged over the cross-section of the tube is given by

$$\rho_0\overline{U} = \rho_0(1-2\delta_0)U. \tag{3.56}$$

3.2.4 Matching conditions at the junctions between sections

To determine the unknowns G, H, $B^\pm$ and $D^\pm$ to fix the solution valid throughout the tube, matching conditions are required at each junction between the sections. Among them, the conditions at both ends of the stack are delicate. A domain in the vicinity of the left end of the stack is illustrated in figure 9 in a scale comparable with the pore radius. Although there should be drawn many pores, the figure is very simplified. In reality, heat exchangers are placed on both ends of the stack with a small gap apart for heat to flow to or from external hot or cold reservoirs. But because the heat exchangers are not taken into account in the present model, they are drawn in broken lines.

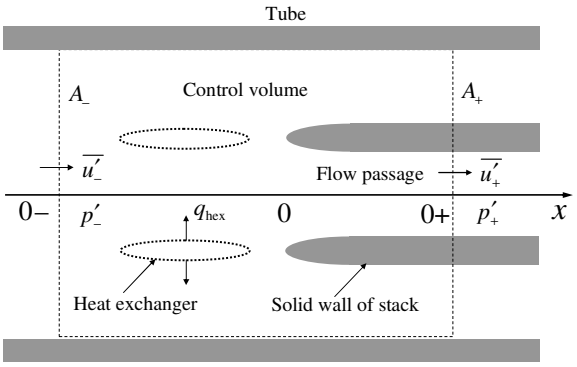

Figure 9: Illustration of a control volume containing the left end of the stack at $x = 0$ and virtual heat exchangers, bounded by the walls of the tube, the stack and the heat exchangers and two planes at $x = 0-$ and $x = 0+$ taken in matching regions, where the number of the pores and the heat exchangers is reduced significantly for simplicity and the heat exchangers are very short axially. Since the heat exchangers are not taken into account in the present model, they are drawn in broken curves. The subscripts + and − indicate values at $x = 0+$ and $x = 0-$, respectively, the control volume being small in comparison with a volume associated with a wavelength, and $q_{\rm hex}$ represents symbolically a heat flux from the heat exchangers.

To consider matching conditions, an idea of the method of matched asymptotic expansions may be applied usefully because complicated end behaviours are expected to be limited in the vicinity of the end and decayed away from it. This is seen in the experimental results by Berson & Blanc-Benon (2007) and Berson et al. Taking the origin $x = 0$ at the left end of the stack, take a control volume bounded by the walls of the tube, the stack, the heat exchangers and two planes at $x = 0-$ and $x = 0+$ chosen arbitrarily in so-called matching regions. The virtual heat exchanger is included in this volume.

The theories of thick and thin diffusion layers are assumed to be valid in $x \ll 0-$ and in $0+ \ll x$, respectively. The left matching region, represented by $0-$, is estimated to be located away from the left end of the heat exchangers by a distance comparable with the tube radius. This is estimated by an evanescent mode appearing near an obstacle and decaying in the form of $\exp(j_1 x/R)$ for $x < 0$, j_1 (≈ 3.83) being the smallest root of the Bessel function of first order $J_1(j_1) = 0$. The right matching region, represented by $0+$, is estimated to be located at a position comparable with R_S for an inlet flow into the pore.

For this volume, consider the mass, axial momentum and energy fluxes through the planes. Because the heat exchangers are short axially and located closely to the stack end, the control volume bounded by the two planes is small enough in comparison with a volume associated with a wavelength and the gas therein may be treated as being incompressible. Then it is obvious that the mass flux must be continuous. In the linear theory, it requires that $[\rho_e \overline{u'} A_e]_-^+ = 0$ where $[\cdots]_-^+$ means difference of a value of $[\cdots]$ at $x = 0+$ from the one at $x = 0-$ and A_e denotes the whole cross-sectional area of the flow passages at x; A at $x = 0-$ and A_S at $x = 0+$. Because ρ_e is continuous, it is reduced to $[\overline{u'} A_e]_-^+ = 0$.

As for the momentum flux, some remarks are necessary. When the gas flows into the pores or out of them, the flow is constricted or expanded so that vortical motions usually

occur due to separation of flows. These effects on the pressure are quadratic in the velocity. In addition, the heat exchangers may also give rise not only to such a quadratic pressure difference but also to a linear skin friction in a flow of a very low Reynolds number. Thus the pressure is not required to be continuous, in general. As long as the linear theory is concerned, however, the pressure may be set to be continuous if the skin friction on the heat exchangers were ignored because they are short.

Thirdly the energy flux must satisfy a balance of enthalpy and heat fluxes given by $[\overline{(\rho_e+\rho')(h_e+h')u'}A_e]_-^+ = q_{\rm hex}$, h_e and h' being, respectively, a specific enthalpy in the quiescent state and its excess quantity (h not to be confused with h defined in (3.20)) and $q_{\rm hex}$ being a heat flux from the heat exchangers. Here the axial energy flux transporting the kinetic energy is discarded in quadratic theory, while the axial flux of stress power $-v\sigma$, v and σ being, respectively, the velocity vector and the viscous stress tensor, and the excess axial heat flux by conduction are small. The heat flux from the walls of the tube and the stack is also discarded because the surface area is negligible.

Using $h_e = c_pT_e$ and the continuity in mass flux $[\overline{(\rho_e+\rho')u'}A_e]_-^+ = 0$ in full expression, the balance of the energy flux is reduced to $[\rho_e\overline{h'u'}A_e]_-^+ = q_{\rm hex}$. Invoking the thermodynamic relation, $h' = T_eS' + p'/\rho_e$, S' being an excess specific entropy, the condition is written as $[(p'\overline{u'} + \rho_eT_e\overline{S'u'})A_e]_-^+ = q_{\rm hex}$. Thus the energy flux consists of the acoustic energy flux (acoustic intensity) $p'\overline{u'}$ and the entropy (heat) flux $\rho_eT_e\overline{S'u'}$. On the plane at $x = 0-$, S' may be negligible because the main-flow region is regarded as being adiabatic and contributions from the boundary layer remains to be small. On the plane at $x = 0+$, on the other hand, S' cannot be ignored because the entropy flux is present. Since the gas in the pore undergoes isothermal change $T'/T_e = 0$ to the lowest order, it follows that $\rho_eT_eS'u' = -p'u'$ so that it cancels with the acoustic energy flux. In this consequence, $p'\overline{u'}A$ at $x = 0-$ may be set equal to $-q_{\rm hex}$ at $x = 0$. Thus the matching condition for the energy flux may be used to evaluate the heat flux $q_{\rm hex}$. The same arguments are applied to the junction at $x = x_1$.

Across the junction $x = x_2$, it suffices to impose continuity of the mass flux and the pressure in the linear theory. Although both conditions may be trivial, the latter may also be derived from discussions of the energy flux. Because the adiabatic processes are assumed in the main-flow region, the continuity of energy flux requires that $[p'\overline{u'}A_e]_-^+ = 0$. Using the continuity of mass flux, this is reduced to the continuity of pressure. Thus the matching conditions at $x = x_2$ are the continuity in pressure and mass flux. In addition, the periodic boundary condition is imposed at $x = 0$ and $x = L$ because of the toroidal geometry.

Consider the matching conditions at $x = x_1$. The left end of the buffer tube is located at $\xi = 0$ where Z takes the value Z_1 given by

$$Z_1 = (1+\lambda)\left[1 - b\frac{K_\beta}{C}(1+\lambda)^{1+\beta}\right]. \tag{3.57}$$

Then the right end at $x = x_2$ is located at $\xi = \xi_2$ given by

$$\xi_2 = \frac{L_B}{\lambda}\left\{\log(1+\lambda) + \frac{b}{1+\beta}\Big[(1+\lambda)^{1+\beta} - 1\Big]\right\}, \tag{3.58}$$

where Z takes the value of Z_2 given by

$$Z_2 = Z_0 = 1 - b\frac{K_\beta}{C}. \tag{3.59}$$

Here and hereafter the subscripts 1 and 2 imply values at $x = x_1$ and $x = x_2$, respectively, while the subscript 0 implies a value at $x = 0$ as well as a value defined already at the room temperature or in a quiescent state.

The continuity in pressure and mass flux across the junction at $x = x_1$ requires, respectively,

$$\frac{\Gamma}{a_0}(1+\lambda)G + H + \mathrm{i}\zeta_1 \Lambda H = \left.\frac{F}{Z}\right|_{x=x_1}, \tag{3.60}$$

and

$$\left[-\frac{\gamma}{a_0^2}(1-\mathrm{i}\zeta_1)G + \mathrm{i}\zeta_1 \frac{2(1+\beta)\gamma\Lambda}{\Gamma(1+\lambda)a_0}H\right] A_S = (1-2\delta_e)\left.\frac{E}{XZ}\right|_{x=x_1} A, \tag{3.61}$$

where A_S and A denote again the total cross-section area of all pores in the stack and the cross-sectional area of the tube in the outside of the stack, respectively. The continuity in pressure and in mass flux across the junction at $x = x_2$ requires, respectively,

$$\left.\frac{F}{Z}\right|_{x=x_2} = D^+ + D^-, \tag{3.62}$$

and

$$(1-2\delta_e)\left.\frac{E}{XZ}\right|_{x=x_2} A = \frac{(1-2\delta_0)}{X_0}\left(-D^+ + D^-\right) A. \tag{3.63}$$

At the junction $x = L$, which corresponds to $x = 0$ by periodicity, the continuity in pressure and mass flux across this junction requires, respectively,

$$D^+ \mathrm{e}^{\mathrm{i}k(L-x_2)} + D^- \mathrm{e}^{-\mathrm{i}k(L-x_2)} = \frac{\Gamma}{a_0} G + H + \mathrm{i}\zeta_0 \Lambda H, \tag{3.64}$$

and

$$\begin{aligned} &\frac{(1-2\delta_0)}{X_0}\left[-D^+ \mathrm{e}^{\mathrm{i}k(L-x_2)} + D^- \mathrm{e}^{-\mathrm{i}k(L-x_2)}\right] A \\ &= \left[-\frac{\gamma}{a_0^2}(1-\mathrm{i}\zeta_0)G + \mathrm{i}\zeta_0 \frac{2(1+\beta)\gamma\Lambda}{\Gamma a_0} H\right] A_S. \end{aligned} \tag{3.65}$$

The six conditions from (3.60) to (3.65) are used to determine six unknowns G, H, $B^\pm$ and $D^\pm$.

3.2.5 Reduction of unknowns for derivation of frequency equation

Using (3.60) and (3.61), we start with removing G and H in (3.64) and (3.65), and then eliminate D^+ and D^- to reduce the number of equations to two. Equation (3.61) is expressed as

$$\frac{\gamma}{a_0} G_H = -\frac{1}{\varphi}\left(\frac{1-2\delta_1}{1-\mathrm{i}\zeta_1}\right)\frac{a_0 E_1}{X_1 Z_1}, \tag{3.66}$$

with

$$G_H = G - \mathrm{i}\zeta_1 \frac{2(1+\beta)\Lambda a_0}{\Gamma(1+\lambda)} H, \tag{3.67}$$

where a term in ζ_1^2 has been ignored and φ denotes the porosity of stack defined by

$$\varphi \equiv \frac{A_S}{A}, \tag{3.68}$$

which is usually smaller than unity. Eliminating G in (3.60) by use of (3.67), H is related to G_H through

$$[1 + \mathrm{i}\zeta_1(3 + 2\beta)\Lambda]\, H = \frac{F_1}{Z_1} - \frac{\Gamma}{a_0}(1 + \lambda)G_H. \tag{3.69}$$

Substituting (3.66) for G_H on the right-hand side, G_H and H have been expressed in terms of the other unknowns.

Employing these expressions to eliminate G and H in (3.64), it follows that

$$Z_0 D^+ \mathrm{e}^{\mathrm{i}k(L-x_2)} + Z_0 D^- \mathrm{e}^{-\mathrm{i}k(L-x_2)} = \frac{Z_0}{Z_1}\Big[\mathrm{e}^{\mathrm{i}\zeta_1 c} F_1 + \mathcal{F} E_1\Big], \tag{3.70}$$

with Z_0/Z_1, c (different from that used in (3.2)) and $\mathcal{F}$ given, respectively, by

$$\frac{Z_0}{Z_1} = \frac{1}{1+\lambda}\left\{1 + b\frac{K_\beta}{C}\Big[(1+\lambda)^{1+\beta} - 1\Big]\right\}, \tag{3.71}$$

$$c = \Lambda\left[(1+\lambda)^{2(1+\beta)} - 1 - \frac{2(1+\beta)\lambda}{1+\lambda}\right], \tag{3.72}$$

and

$$\begin{aligned}\mathcal{F} &= \frac{\Gamma\lambda}{\varphi\gamma}\left(\frac{1-2\delta_1}{1-\mathrm{i}\zeta_1}\right)\frac{a_0}{X_1}\,\mathrm{e}^{\mathrm{i}\zeta_1(1+1/\lambda)c} \\ &= \frac{\Gamma\lambda}{\varphi\gamma(1+\lambda)}\left[1 + b\left(1 - \frac{2}{C}\right)(1+\lambda)^{1+\beta} + \mathrm{i}\zeta_1\right]\mathrm{e}^{\mathrm{i}\zeta_1(1+1/\lambda)c},\end{aligned} \tag{3.73}$$

where F_1 and E_1 denote, respectively, $F(\xi_1)$ and $E(\xi_1)$, and their explicit expressions are given, respectively, by (3.47) and (3.48) as

$$F_1 = f_1^+ B^+ + f_1^- B^-, \tag{3.74}$$

with

$$f_1^\pm = 1 - \mathrm{i}b\beta_F \frac{C_{T\beta}}{C}\frac{\lambda(1+\lambda)^{1+\beta}}{k_\beta^\pm L_B}, \tag{3.75}$$

and

$$E_1 = \frac{a_0 k^-}{\omega} e_1^+ B^+ + \frac{a_0 k^+}{\omega} e_1^- B^-, \tag{3.76}$$

with

$$e_1^\pm = 1 + \mathrm{i}b\beta_E \frac{C_{T\beta}}{C}\frac{\lambda(1+\lambda)^{1+\beta}}{k_\beta^\pm L_B}. \tag{3.77}$$

Here note that $1 + \mathrm{i}\zeta_1 c$ has been expressed compactly as $\mathrm{e}^{\mathrm{i}\zeta_1 c}$, but this will be reverted to the original expression in final results. Similar compact expressions are used for other quantities.

Similarly the other equation (3.65) is rewritten as

$$-Z_0 D^+ \mathrm{e}^{\mathrm{i}k(L-x_2)} + Z_0 D^- \mathrm{e}^{-\mathrm{i}k(L-x_2)} = \frac{Z_0}{Z_1}\left(\mathrm{i}\zeta_1 d F_1 + \mathcal{G} E_1\right), \tag{3.78}$$

with

$$\begin{aligned}\mathcal{G} &= \left(\frac{1-2\delta_1}{1-2\delta_0}\right)\left(\frac{1-\mathrm{i}\zeta_0}{1-\mathrm{i}\zeta_1}\right)\frac{X_0}{X_1}\mathrm{e}^{\mathrm{i}\zeta_1\Gamma(1+\lambda)d/\varphi\gamma} \\ &= \frac{1}{(1+\lambda)}\left\{1 + b\left(1-\frac{2}{C}\right)\left[(1+\lambda)^{1+\beta}-1\right] + \mathrm{i}\Big(\zeta_1-\zeta_0\Big)\right\}\mathrm{e}^{\mathrm{i}\zeta_1\Gamma(1+\lambda)d/\varphi\gamma},\end{aligned} \tag{3.79}$$

and

$$d = \frac{2\varphi(1+\beta)\gamma\Lambda}{\Gamma}\left[(1+\lambda)^{2+2\beta} - \frac{1}{1+\lambda}\right]. \tag{3.80}$$

Next (3.62) and (3.63) are rewritten, respectively, as

$$Z_0(D^+ + D^-) = F(\xi_2) \equiv F_2, \tag{3.81}$$

and

$$Z_0(-D^+ + D^-) = E(\xi_2) \equiv E_2, \tag{3.82}$$

where F_2 and E_2 are given, respectively, by

$$F_2 = f_2^+ B^+ \mathrm{e}^{\mathrm{i}k^+\xi_2} + f_2^- B^- \mathrm{e}^{\mathrm{i}k^-\xi_2}, \tag{3.83}$$

with

$$f_2^\pm = 1 - \mathrm{i}b\beta_F \frac{C_{T\beta}}{C}\frac{\lambda \mathrm{e}^{-b[(1+\lambda)^{1+\beta}-1]}}{k_\beta^\pm L_B}, \tag{3.84}$$

and

$$E_2 = \frac{a_0 k^-}{\omega} e_2^+ B^+ \mathrm{e}^{\mathrm{i}k^+\xi_2} + \frac{a_0 k^+}{\omega} e_2^- B^- \mathrm{e}^{\mathrm{i}k^-\xi_2}, \tag{3.85}$$

with

$$e_2^\pm = 1 + \mathrm{i}b\beta_E \frac{C_{T\beta}}{C}\frac{\lambda \mathrm{e}^{-b[(1+\lambda)^{1+\beta}-1]}}{k_\beta^\pm L_B}. \tag{3.86}$$

Adding and subtracting (3.81) and (3.82), and using (3.70) and (3.78), it follows that

$$2Z_0 D^+ \mathrm{e}^{+\mathrm{i}k(L-x_2)} = (F_2 - E_2)\mathrm{e}^{+\mathrm{i}k(L-x_2)} = \frac{Z_0}{Z_1}\left[\mathrm{e}^{\mathrm{i}\zeta_1(c-d)}F_1 + (\mathcal{F}-\mathcal{G})E_1\right], \tag{3.87}$$

and

$$2Z_0 D^- \mathrm{e}^{-\mathrm{i}k(L-x_2)} = (F_2 + E_2)\mathrm{e}^{-\mathrm{i}k(L-x_2)} = \frac{Z_0}{Z_1}\left[\mathrm{e}^{\mathrm{i}\zeta_1(c+d)}F_1 + (\mathcal{F}+\mathcal{G})E_1\right]. \tag{3.88}$$

Using (3.81) and (3.82) to express $Z_0 D^+$ and $Z_0 D^-$ in terms of B^+ and B^-, (3.87) and (3.88) are written in the matrix form as

$$\begin{bmatrix} W_{+1}^+ & W_{+1}^- \\ \\ W_{-1}^+ & W_{-1}^- \end{bmatrix}\begin{bmatrix} B^+ \\ \\ B^- \end{bmatrix} = 0, \tag{3.89}$$

with

$$W_j^{\pm} = \left(f_2^{\pm} - j\frac{a_0 k^{\mp}}{\omega} e_2^{\pm} \right) \mathrm{e}^{\mathrm{i}k^{\pm}\xi_2} \mathrm{e}^{\mathrm{i}jk(L-x_2)} - \frac{Z_0}{Z_1} \left[\mathrm{e}^{\mathrm{i}\zeta_1(c-jd)} f_1^{\pm} + (\mathcal{F} - j\mathcal{G}) \frac{a_0 k^{\mp}}{\omega} e_1^{\pm} \right], \tag{3.90}$$

j being $+1$ or -1. From the non-trivial condition for $B^{\pm}$, the frequency equation is derived as follows:

$$\begin{aligned} &(I^{+}\mathrm{e}^{\mathrm{i}k^{+}\xi_2} - I^{-}\mathrm{e}^{\mathrm{i}k^{-}\xi_2})[\mathrm{e}^{+\mathrm{i}k(L-x_2)} - \mathrm{e}^{-\mathrm{i}k(L-x_2)}] \\ &+ (J^{+}\mathrm{e}^{\mathrm{i}k^{+}\xi_2} - J^{-}\mathrm{e}^{\mathrm{i}k^{-}\xi_2})[\mathrm{e}^{+\mathrm{i}k(L-x_2)} + \mathrm{e}^{-\mathrm{i}k(L-x_2)}] + K = 0, \end{aligned} \tag{3.91}$$

with

$$I^{\pm} = -f_1^{\mp} f_2^{\pm} - \mathcal{F}\frac{a_0 k^{\pm}}{\omega} f_2^{\pm} e_1^{\mp} - \mathcal{G} e_1^{\mp} e_2^{\pm} - \mathrm{i}\zeta_1 \left(f_1^{\mp} f_2^{\pm} c - \frac{a_0 k^{\mp}}{\omega} f_1^{\mp} e_2^{\pm} d \right), \tag{3.92}$$

$$J^{\pm} = \frac{a_0 k^{\mp}}{\omega} f_1^{\mp} e_2^{\pm} - \mathcal{F} e_1^{\mp} e_2^{\pm} - \mathcal{G}\frac{a_0 k^{\pm}}{\omega} f_2^{\pm} e_1^{\mp} + \mathrm{i}\zeta_1 \left(\frac{a_0 k^{\mp}}{\omega} f_1^{\mp} e_2^{\pm} c - f_1^{\mp} f_2^{\pm} d \right), \tag{3.93}$$

$$\begin{aligned} K = {} & 2\left(\frac{Z_0}{Z_1}\right)^{-1} \left(\frac{a_0 k^{+}}{\omega} f_2^{+} e_2^{-} - \frac{a_0 k^{-}}{\omega} f_2^{-} e_2^{+} \right) \mathrm{e}^{\mathrm{i}(k^{+}+k^{-})\xi_2} \\ & + 2\frac{Z_0}{Z_1}\Big[\mathcal{G} + \mathrm{i}\zeta_1(\mathcal{G}c - \mathcal{F}d) \Big] \left(\frac{a_0 k^{+}}{\omega} f_1^{+} e_1^{-} - \frac{a_0 k^{-}}{\omega} f_1^{-} e_1^{+} \right), \end{aligned} \tag{3.94}$$

and $\zeta_1 = (1+\lambda)^{-2(1+\beta)}\zeta_0$, where the relation $a_0^2 k^{+} k^{-}/\omega^2 = -1$ has been used.

Expanding the products in $I^{\pm}$, $J^{\pm}$ and K up to the first order in ζ_0, ζ_1 and b, it follows that

$$\begin{aligned} I^{\pm} = {} & -\Big[1 - \mathrm{i}b\beta_F\Big(s_1^{\mp} + s_2^{\pm}\Big)\Big] - \frac{\Gamma\lambda}{\varphi\gamma(1+\lambda)}\frac{a_0 k^{\pm}}{\omega}\Big[1 + b\tau_1 + \mathrm{i}b\Big(\beta_E s_1^{\mp} - \beta_F s_2^{\pm}\Big)\Big] \\ & - \frac{1}{(1+\lambda)}\Big[1 + b\Big(\tau_1 - \tau_2\Big) + \mathrm{i}b\beta_E\Big(s_1^{\mp} + s_2^{\pm}\Big)\Big] \\ & - \mathrm{i}\zeta_1\left[\frac{\Gamma}{\varphi\gamma}\Big(\frac{a_0 k^{\pm}}{\omega}c + d\Big) + c - \frac{a_0 k^{\mp}}{\omega}d\right], \end{aligned} \tag{3.95}$$

$$\begin{aligned} J^{\pm} = {} & \frac{a_0 k^{\mp}}{\omega}\Big[1 - \mathrm{i}b\Big(\beta_F s_1^{\mp} - \beta_E s_2^{\pm}\Big)\Big] - \frac{\Gamma\lambda}{\varphi\gamma(1+\lambda)}\Big[1 + b\tau_1 + \mathrm{i}b\beta_E\Big(s_1^{\mp} + s_2^{\pm}\Big)\Big] \\ & - \frac{1}{(1+\lambda)}\frac{a_0 k^{\pm}}{\omega}\Big[1 + b\Big(\tau_1 - \tau_2\Big) + \mathrm{i}b\Big(\beta_E s_1^{\mp} - \beta_F s_2^{\pm}\Big)\Big] \\ & - \mathrm{i}\zeta_1\left[\frac{\Gamma}{\varphi\gamma}\Big(c + \frac{a_0 k\pm}{\omega}d\Big) - \frac{a_0 k^{\mp}}{\omega}c + d\right], \end{aligned} \tag{3.96}$$

$$\begin{aligned} K = {} & \frac{4a_0}{\omega L_B}\psi\Bigg\{(1+\lambda)\Big[1 - b\Big(\chi_1 - \chi_2\Big)\Big]\mathrm{e}^{\mathrm{i}(k^{+}+k^{-})\xi_2} \\ & + \frac{1}{(1+\lambda)^2}\Big[1 + b\Big(\chi_1 - \chi_2 + \tau_1 - \tau_2\Big)\Big] + \frac{\mathrm{i}\zeta_1}{(1+\lambda)^2}\left(c + \frac{\Gamma}{\varphi\gamma}d\right)\Bigg\}, \end{aligned} \tag{3.97}$$

where use has been made of the following notations:

$$s_1^{\pm} = \frac{C_{T\beta}}{C}\frac{\lambda(1+\lambda)^{1+\beta}}{k_\beta^{\pm} L_B}, \quad s_2^{\pm} = \frac{C_{T\beta}}{C}\frac{\lambda \mathrm{e}^{-b[(1+\lambda)^{1+\beta}-1]}}{k_\beta^{\pm} L_B}, \tag{3.98}$$

$$\tau_1 = \left(1 - \frac{2}{C}\right)(1+\lambda)^{1+\beta} + \mathrm{i}b^{-1}\zeta_1, \quad \tau_2 = 1 - \frac{2}{C} + \mathrm{i}b^{-1}\zeta_0, \tag{3.99}$$

and

$$\chi_1 = \frac{K_\beta}{C}(1+\lambda)^{1+\beta}, \quad \chi_2 = \frac{K_\beta}{C}. \tag{3.100}$$

Here it is convenient to note the relation:

$$\frac{a_0 k^+}{\omega} f_1^+ e_1^- - \frac{a_0 k^-}{\omega} f_1^- e_1^+ = \frac{2a_0}{\omega L_B}\psi. \tag{3.101}$$

This relation holds up to the order of b and also when the subscript 1 is replaced by 2.

Hence the frequency equation (3.91) is now available from the matching conditions at three junctions between the sections. If β is set equal to be zero, the result will be simplified considerably. It is remarked that the frequency equation does not involve the stack length L_S explicitly.

3.3 Marginal conditions

3.3.1 Frequency equation in the limits of thick and thin diffusion layers

Before solving the frequency equation (3.91), we examine a solution in both limits of thick and thin diffusion layers as $\zeta_0 \to 0$ ($\zeta_1 \to 0$) and $b \to 0$. Then the frequency equation becomes

$$\begin{aligned}
&\mathrm{i}\frac{\Gamma\lambda}{\varphi\gamma(1+\lambda)}\left[\left(\frac{\lambda}{2}\sin\phi - \psi\cos\phi\right)\sin\sigma - \sigma_B \sin\phi\cos\sigma\right] \\
&+\left[1 + \frac{1}{(1+\lambda)}\right]\sigma_B \sin\phi\sin\sigma + \left[\frac{1}{(1+\lambda)}\left(\frac{\lambda}{2}\sin\phi - \psi\cos\phi\right)\right. \\
&\left.-\frac{\lambda}{2}\sin\phi - \psi\cos\phi\right]\cos\sigma + \sqrt{1+\lambda}\left[1 + \frac{1}{(1+\lambda)^2}\right]\psi = 0,
\end{aligned} \tag{3.102}$$

with

$$\sigma = \frac{\omega(L - L_S - L_B)}{a_0}, \quad \sigma_B = \frac{\omega L_B}{a_0}, \quad \phi = \psi\log\frac{(1+\lambda)}{\lambda}. \tag{3.103}$$

In a special case without the temperature gradient, i.e. $\lambda \to 0$, (3.102) is reduced to $\cos(\sigma + \sigma_B) - 1 = 0$ because $\phi = \psi = \sigma_B$. Thus $\omega L/a_0$ is given by 2π, 4π, $\cdots$, which correspond, respectively, to cases that the length of the looped tube coincides with one wavelength, two wavelengths, and so on. These modes of oscillations are called the one-wave mode, the two-wave mode, and so on.

In a general case with the temperature gradient, it is noticed that (3.102) has a trivial solution $\phi = \psi = 0$. However, this solution $\sigma_B = \lambda/2$ is not physically acceptable. Besides this, roots for ω will be complex. If ω takes a real solution, ψ becomes either real or imaginary, depending on the sign of $\sigma_B^2 - \lambda^2/4$. When ψ takes a real value, the first line

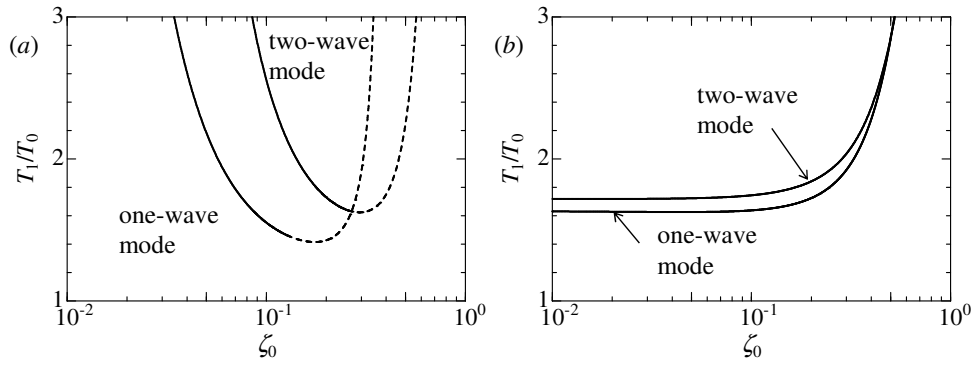

Figure 10: Marginal conditions for the temperature ratio T_1/T_0 in the one-wave mode and the two-wave mode against $\zeta_0 (= R_S^2\omega/6\nu_0)$. In (a), the curves are drawn by taking the porosity proportional to the pore's cross-sectional area with the total number of the pores fixed, the curves being broken when the porosity exceeds unity, while in (b), the curves are drawn by changing the pore radius with the porosity φ fixed at 0.67.

in (3.102) takes an imaginary value, whereas the other takes real values. When ψ takes an imaginary value, on the contrary, the reverse situation occurs. In fact, it is graphically confirmed that there are no real solutions for both real and imaginary parts to vanish simultaneously. If real solutions are to exist, then this is due to the small parameters ζ_0 and b.

3.3.2 Solutions to the frequency equation

We now proceed to seek a real solution of ω to (3.91) with (3.95) to (3.97). Plotting values of the real and imaginary parts of (3.91) over the plane of λ and σ, a domain for a real solution of σ to exist can be found. By trial and error, one set of solutions for λ and σ is first sought numerically by Newton's method for an appropriate combination of λ and σ, with values of the other parameters fixed. If only the value of R_S is changed slightly, another set of solutions is obtained, and repeating this procedure, curves will be drawn. In view of the experiments by Ueda & Kato (2008), we take a looped tube of $R = 20$ mm, $L_B = 0.6$ m, and $L - L_S = 2.76$ m filled with atmospheric air. For the exponent β, we take $\beta = 0.5$ for mathematical simplicity. However, it turns out that its influence on the marginal conditions is so small that β may be set to be zero as long as the temperature ratio T_1/T_0 is less than 3.

Figure 10 shows the curves for the marginal conditions where the horizontal and vertical axes denote, respectively, the non-dimensional parameter ζ_0 and the temperature ratio T_1/T_0. At a fixed value of the horizontal axis, the instability occurs if the temperature ratio exceeds the curve. The looped tube is expected to have the one-wave, the two-wave modes and so on, even when the temperature gradient exist. In figure 10, two curves are drawn for the one-wave and two-wave modes. Because the two-wave mode has about twice the frequency of the one-wave mode, it is remarked that the values of the radius and the porosity are different even for the same value of ζ_0.

The curves are drawn in the following way. Starting with the case with the pore

radius $R_S = 0.1$ mm and the porosity $\varphi = 0.67$, the real frequency σ and the temperature ratio T_1/T_0 are sought. Then there are found two sets of the solution, one set being $\sigma+\sigma_B = 6.30$, $T_1/T_0 = 1.63$ and $\zeta_0 = 0.086$ for $L_S = 0.011$ m, and the other $\sigma+\sigma_B = 12.8$, $T_1/T_0 = 1.81$ and $\zeta_0 = 0.175$ for $L_S = 0.013$ m. The pore radius and the stack length found are smaller than those in the experiments. At the room temperature 15°C, in passing, the frequency $\omega/2\pi$ is 124 Hz for the one-wave mode and 252 Hz for the two-wave mode. While the former agrees with a_0/L (=123 Hz) well, the latter frequency is a little higher than $2a_0/L$ (=245 Hz). These frequencies do not change significantly with the pore radius and the temperature ratio. The curves in figure 10(a) are drawn by changing R_S but with the total number of pores fixed implicitly, and choosing φ proportional to the pore's cross-sectional area. Because the value of φ is usually smaller than unity, the solid curves are changed into broken ones in the range of $\varphi > 1$.

In figure 10(b), the curves are drawn with the value of φ fixed at 0.67 so that the number of pores varies along the curve. If the pores are assumed to be distributed uniformly over the cross-section of the stack, the pores and the wall surrounding them are divided into many identical 'cells' except for those in the vicinity of the periphery of the stack. Further if the number of cells is large enough, the porosity may be represented by the ratio of the cross-sectional area of the single pore to that of each cell. In other word, the porosity may be represented by its local value of the cell. For $R_S = 0.1$ mm and $\varphi = 0.67$, one side of the square cell is calculated to be of length 0.22 mm. This corresponds to 13,800 cells per square inches, which is larger by one order than 1,600 cells now available in ceramic stacks. For $\varphi = 0.67$ and $\zeta_0 = 0.3$ in figure 10(b), for example, $R_S = 0.19$ mm and one side of the cell is of length 0.41 mm so that there are about 3,900 cells per square inches. The number of cells changes in proportion to φ/R_S^2.

Figure 10(a) shows that as R_S and $\varphi(< 1)$ increases so that the wall becomes thinner, the temperature ratio decreases. Figure 10(b) shows that the temperature ratio does not change appreciably for $\zeta_0 < 0.1$ even if the pore radius is decreased and the number of cells is increased as long as the porosity is fixed. From both figures, it is seen that the temperature ratio for the one-wave and two-wave modes may exchange. The ratio for the one-wave mode is lower than that of the two-wave mode for a small value of ζ_0, but this relation reverses as ζ_0 increases in figure 10(a), though $\varphi > 1$. In any case, it is found that the porosity plays a crucial role in determining the temperature ratio.

3.3.3 Effects of the porosity of the stack

Figure 10 shows the qualitative features of the marginal conditions but it gives no quantitative information generally on the porosity and the number of pores, though the specific value of the number is meaningless. Combination of the two curves shown in figures 10(a) and 10(b) for the one-wave mode yields an information as to how the pore radius and the porosity affect the marginal conditions. This is drawn in figure 11. In figure 11(a), the leftmost solid curve corresponds to the one in figure 11(a) and five solid (and broken in part for $\varphi > 1$) curves represent the marginal conditions with the number of pores reduced consecutively to the right by 1/2, 1/3, 1/4 and 1/5 of that for the leftmost solid curve, while six dotted curves represent the marginal conditions with the value of porosity φ increased from 0.5 to 1 by step 0.1. Figure 11(b) is simply a blow-up of figure 11(a) near the minimum temperature ratio. It is found that the more the number of pores, the

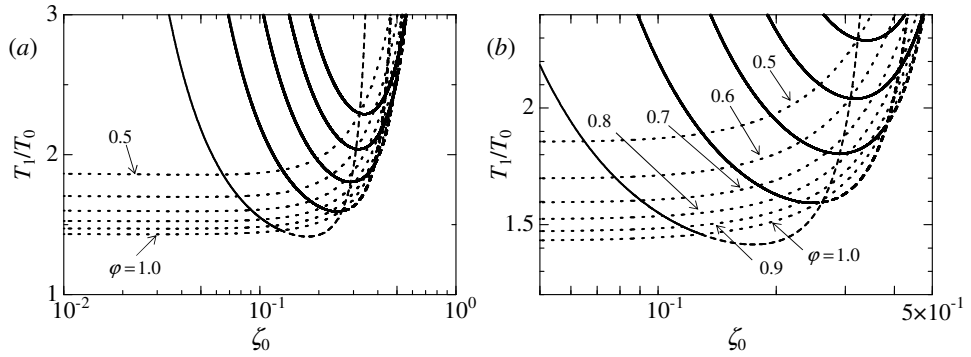

Figure 11: Marginal conditions for the temperature ratio T_1/T_0 in the one-wave mode against $\zeta_0(= R_S^2\omega/6\nu_0)$ for various values of the porosity of the stack and of the number of pores in (a), and (b) is blown up in the vicinity of the minimum temperature ratio in (a). The leftmost solid curve corresponds to the one in figure 10(a) and five solid (and broken in part for $\varphi > 1$) curves represent the marginal conditions with the number of pores reduced to the right consecutively by 1/2, 1/3, 1/4 and 1/5 of that for the leftmost solid curve, while six dotted curves represent the marginal conditions with the value of porosity φ increased from 0.5 to 1 by step 0.1.

lower the temperature ratio needed for instability of the gas. In fact, the instability may occur for T_1/T_0 greater than about 1.4 for $\varphi < 1$.

To understand a relation between the marginal curves with the total number of pores fixed and the ones with the porosity fixed, figure 12(a) depicts the marginal surface for the one-wave mode determined by the frequency equation (3.91) in the three-dimensional space over the plane $(\zeta_0, T_1/T_0)$ by taking φ vertically. The ranges in T_1/T_0 and φ are taken unrealistically large and small, respectively. The surface appears to have a horn rightward as φ tends to decrease (upward). The red curves show several contours on which φ is fixed at different values. They corresponds to the dotted curves in figure 11. As the value of φ becomes smaller, the contours become smaller but tend to a closed loop. The blue curve shows a contour with the total number of pores fixed, i.e. with the value of φ proportional to R_S^2. Figure 12(b) shows the projection of the curves onto the base plane. The curves in the rectangular domain enclosed by the dotted lines correspond to the ones shown in figure 10.

For the two-wave mode as well, a similar surface is drawn. As can be seen from figure 10(b), it intersects with the surface for the one-wave mode. It should be remarked that the intersection does not imply coexistence of the one-wave and two-wave modes, because both the tube radius and the angular frequency are different even at the same point of ζ_0.

3.3.4 Effects of the buffer tube's length

We examine effects of the buffer tube's length L_B on the marginal conditions with the length $L - L_S$ fixed at 2.76 m. Three cases are chosen with $L_B = 0.4$ m, 0.6 m and 0.8 m, though the case with $L_B = 0.6$ m is the same as was examined. Figures 13(a) and 13(b) depict the marginal conditions for the three values of L_B with the porosity of the stack proportional to the pore's cross-sectional area and the total number fixed for the

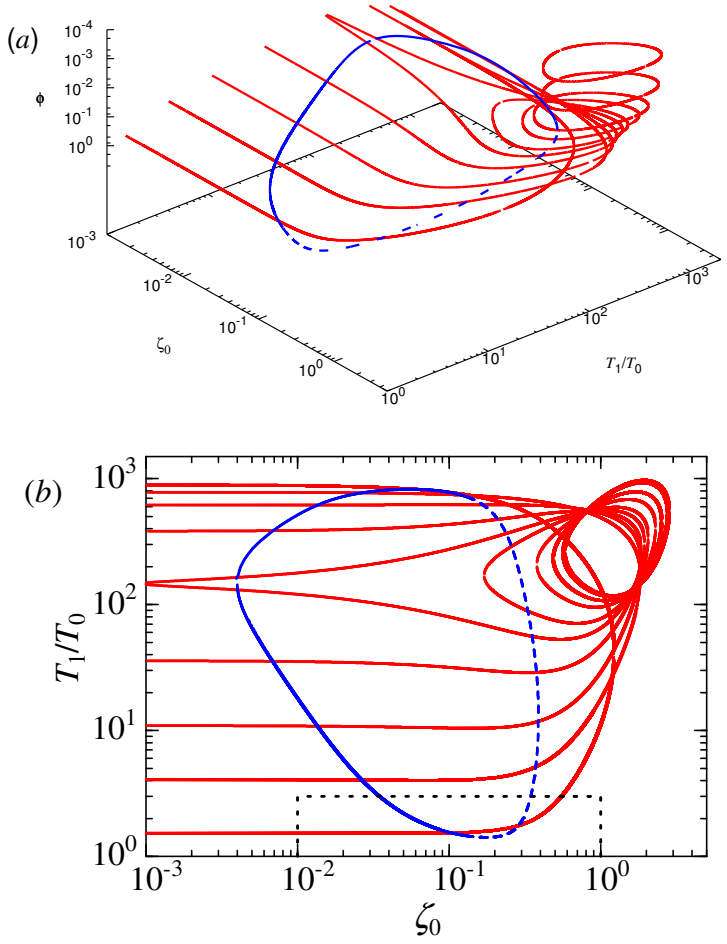

Figure 12: Three-dimensional illustration of a marginal surface for the one-wave mode determined by the frequency equation (3.91) over the plane $(\zeta_0, T_1/T_0)$ with φ taken vertically in (a) and its projection onto the base plane in (b). The red curves show contours on which the value of φ is held constant, while the blue curve shows a contour on which the value of φ is taken proportional to R_S^2. The curves in the rectangular domain enclosed by the dotted line correspond to the ones shown in figure 10.

one-wave mode and two-wave mode, respectively. The solid curves are changed into the broken ones when the porosity exceeds unity.

Figures 14(a) and 14(b) depict the marginal conditions for the three values of L_B with the porosity of the stack held at 0.67 for the one-wave mode and two-wave mode, respectively. It is seen in figures 13(a) and 14(a) for the one-wave mode that the longer the buffer tube becomes, the lower the marginal temperature ratio becomes. This result qualitatively agrees with the experimental result by Ueda & Kato (2008). For the two-wave mode, however, it is seen in figures 13(b) and 14(b) that the results for the one-wave mode do not hold and the length appears to yield no significant difference.

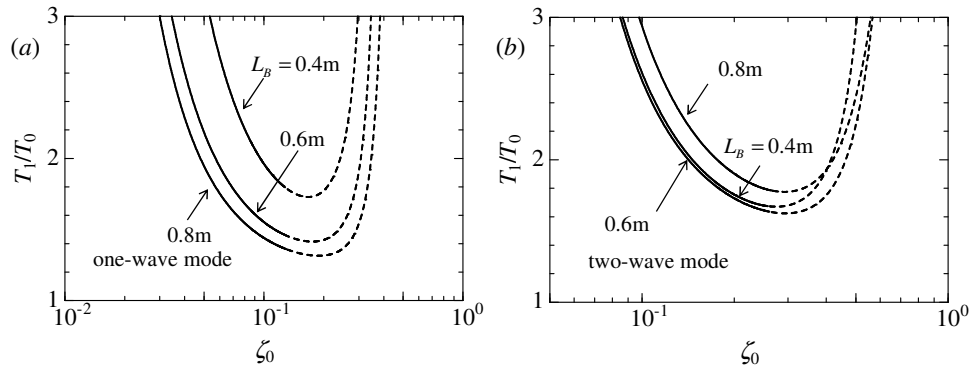

Figure 13: Marginal conditions for the temperature ration T_1/T_0 against $\zeta_0 (= R_S^2\omega/6\nu_0)$ in three cases of the buffer tube's length 0.4 m, 0.6 m and 0.8 m with $L - L_S$ held at 2.76 m, where (a) and (b) depict, respectively, the conditions for the one-wave and two-wave modes with the porosity of the stack proportional to the pore's cross-sectional area and the total number fixed. The solid curves are changed into the broken curves when the porosity φ exceeds unity.

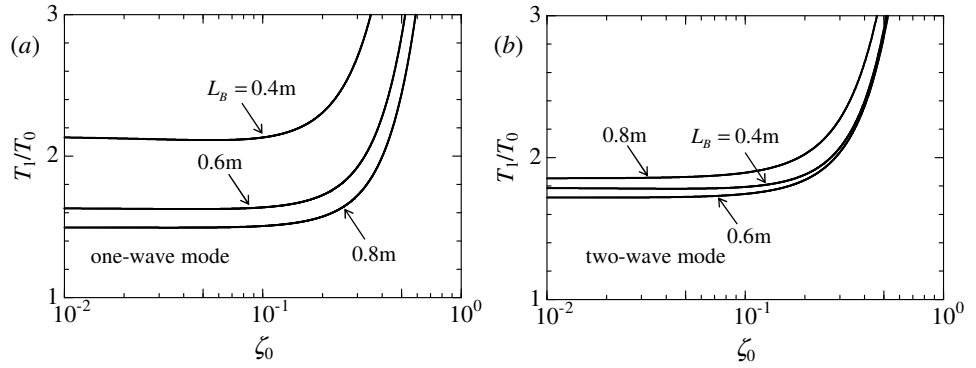

Figure 14: Marginal conditions for T_1/T_0 against $\zeta_0 (= R_S^2\omega/6\nu_0)$ in three cases of the buffer tube's length 0.4 m, 0.6 m and 0.8 m with $L - L_S$ held at 2.76 m, where (a) and (b) depict, respectively, the conditions for the one-wave and two-wave modes with the porosity φ at 0.67.

3.4 Mode of oscillation

3.4.1 One-wave mode of oscillations

Now that the frequency at the marginal state is available, spatial and temporal variations of physical quantities are calculated by using the analytical solutions. Firstly we examine those in the one-wave mode of oscillations. For the marginal state given by $\zeta_0 = 0.3$ in figure 10(b) for $\varphi = 0.67$, figures 15(a) and 15(b) depict, respectively, the spatial profiles of the excess pressure p' and the mean axial velocity $\overline{u'}$ calculated by (3.24) and (3.39) at every one-eighth of the period $2\pi/\omega$. This marginal state occurs at $\sigma + \sigma_B = 6.24$ and $T_1/T_0 = 1.92$ for $R_S = 0.19$ mm, $L_S = 0.049$ m and $L_B = 0.6$ m. The frequency $\omega/2\pi$ is 122 Hz. In figure 15, the stack and the buffer tube are located in the sections $0 < x/L < 0.0175$ and $0.0175 < x/L < 0.23$, respectively.

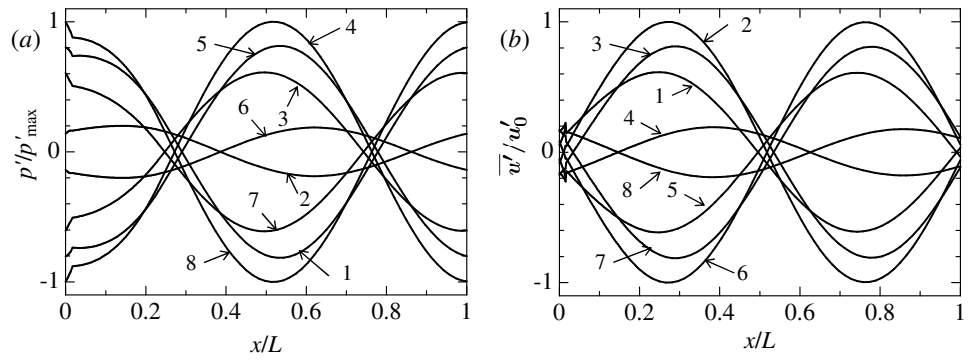

Figure 15: Spatial and temporal profiles of the excess pressure $p'/p_{\max}$ in (a) and the mean axial velocity $\overline{u'}/u'_0$ in (b) with $u'_0 = p'_{\max}/\rho_0 a_0$ in the one-wave mode for the case $\zeta_0 = 0.3$ at every one-eighth of the period $2\pi/\omega$, where the numbers $1, 2, 3, \cdots, 8$ attached to the curves represent the times at $1/8, 2/8, 3/8, \cdots, 8/8$-th period.

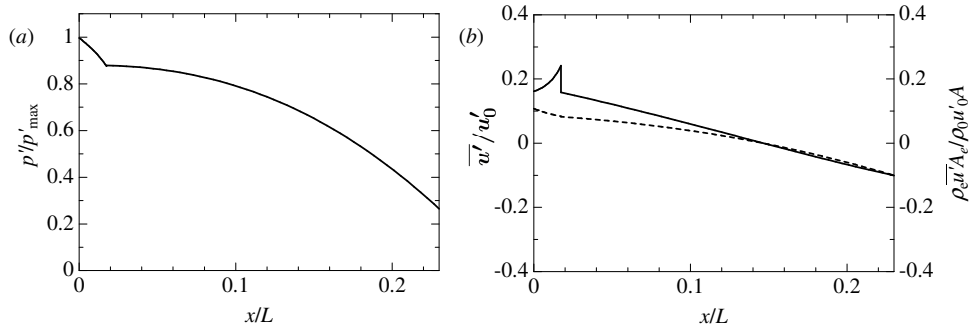

Figure 16: Blow-up of the profiles at 8/8-th period in figure 15 for the excess pressure $p'/p'_{\max}$ in (a) and the mean axial velocity $\overline{u'}/u'_0$ in (b) with $u'_0 = p'_{\max}/\rho_0 a_0$ in the sections of the stack and the buffer tube for the case $\zeta_0 = 0.3$ where the mass flux $\rho_e \overline{u'} A_e/\rho_0 u'_0 A$ is also drawn in the broken curve.

The numbers $1, 2, 3, \cdots, 8$ attached to the curves designate respective profiles at the times $1/8, 2/8, 3/8, \cdots, 8/8$-th period. For one period, the pressure attains the maximum at the left end of the stack $x/L = 0$, though its magnitude is determined up to a scale factor in the linear theory. Letting the maximum pressure at $x = 0$ be $p'_{\max}$, the vertical axis in figure 15(a) measures $p'/p'_{\max}$. Once the typical magnitude has been set to be $p'_{\max}$, the other quantities are to be determined consistently by it. In figure 15(b), the velocity $\overline{u'}$ is normalized by u'_0 given in terms of $p'_{\max}$ and a typical acoustic impedance $\rho_0 a_0$ as $p'_{\max}/\rho_0 a_0$.

Because the section of the stack is too short for the profiles to be visible in figure 15, the profiles at the 8/8-th period are blown up in figure 16 including those in the buffer tube. In figure 16(a), the pressure is continuous across the junction $x/L = 0.0175$ between the stack and the buffer tube, but its gradient is discontinuous there. In figure 16(b), the velocity in the stack is larger than that in the other sections and jumps at both ends of

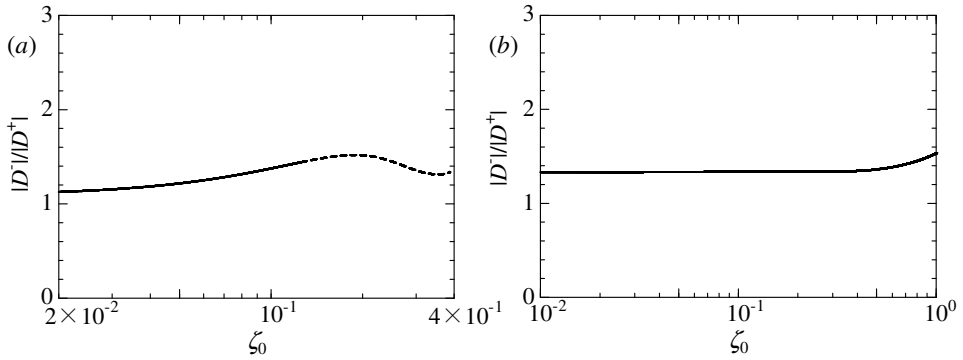

Figure 17: Ratio of the amplitude $|D^-|$ of the wave propagating in the positive sense of the x-axis to the amplitude $|D^+|$ of the wave in the negative sense against $\zeta_0 (= R_S^2\omega/6\nu_0)$, where (a) and (b) correspond to the marginal conditions for the one-wave mode shown in figures $10(a)$ and $10(b)$, respectively, with the porosity of the stack set proportional to the pore's cross-sectional area and the number of pores held constant, and with the porosity fixed at 0.67, the solid curve being broken when the porosity exceeds unity.

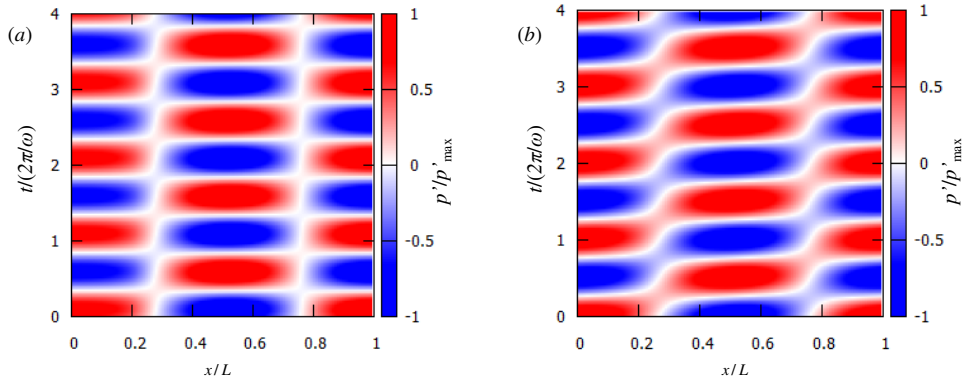

Figure 18: Contour maps of the pressure distribution $p'/p'_{\max}$ in the looped tube over the plane of the space x/L and the time $t/(2\pi/\omega)$ at the marginal states where (a) and (b) represent, respectively, the cases with $\zeta_0 = 0.02$ and $\zeta_0 = 0.12$ in figure $17(a)$.

the stack because of constriction of the cross-sectional area. However, the mass flux is continuous everywhere as required by the matching conditions. This is seen in the profile of the mass flux $\rho_e\overline{u'}A_e/\rho_0 u_0' A$ in the broken curves, where A_e takes A_S in the section of the stack and A in the other sections. The velocity increases with x while the mass flux decreases gently. At the junction $x/L = 0.23$ between the buffer tube and the tube without the temperature gradient, no such discontinuity occurs. In the buffer tube, the mass flux decreases with x.

Overall the profiles in figure 15 have no definite nodes and antinodes. Such a mode of oscillations can neither be classified as a standing wave nor a traveling wave purely in one direction. The fields in the buffer tube and in the section without the temperature gradient consist of two waves propagating in the positive and negative sense of the x-axis.

Figures 17(a) and 17(b) depict the ratio $|D^-|/|D^+|$ for the amplitude $|D^-|$ propagating in the positive sense of the x-axis to $|D^+|$ in the negative sense against ζ_0, corresponding to the marginal conditions shown in figures 10(a) and 10(b), respectively. In figure 17(a), the ratio is drawn with the porosity of the stack set proportional to the pore's cross-sectional area and the number of pores held constant, where the solid curve is broken when the porosity φ exceeds unity.

It is seen that the ratio increases with ζ_0 but a peak appears near $\zeta_0 \approx 0.2$ corresponding to the minimum temperature ratio in figure 10(a), though $\varphi > 1$. For $\varphi < 1$, the ratio tends to increase with the porosity. In figure 17(b), the ratio is drawn with the porosity of the stack fixed at 0.67. The ratio tends to increase with ζ_0 but very gently. It is found from these results that the porosity affects not only the temperature ratio at the marginal state but also the ratio of wave amplitudes propagating in the positive and negative sense of the x-axis.

To visualize the pressure field continuously over several periods, figure 18 depicts the contour maps of the pressure distribution at the marginal state specified by $\zeta_0 = 0.02$ and 0.12 in figure 18(a), which correspond, respectively, to the case that the traveling component in the positive sense is excited least and most, respectively. The horizontal and vertical axes measure, respectively, the axial coordinate x/L and the time $t/(2\pi/\omega)$ normalized. The pressure level $p'/p'_{\max}$ is given in the colour bar. Several streaks are seen in each figure. In figure 18(a), they are lying almost horizontally and nodes are visible, whereas in figure 18(b), they are wavy and inclined upward to the right. This suggests that the field in figure 18(a) is almost a standing wave while the one in figure 18(b) is a traveling wave.

Consider the pressure field in the section without the temperature gradient. It consists of the sum of two harmonic waves, i.e. $p' = |D^+|\cos(kx+\omega t+\theta^+)+|D^-|\cos(-kx+\omega t+\theta^-)$, where $\theta^\pm$ are phases of the waves, respectively, and the lossy effects are so small that k may be set equal to ω/a_0 by (3.54). The sum is expressed as

$$p' = D(t)\cos[kx - \Phi(t)], \tag{3.104}$$

with the amplitude D and the phase Φ given, respectively, by

$$D = \sqrt{|D^+|^2 + |D^-|^2 + 2|D^+||D^-|\cos(2\omega t + \theta^+ + \theta^-)}\,, \tag{3.105}$$

and

$$\tan\Phi = -\frac{|D^+|\sin(\omega t + \theta^+) - |D^-|\sin(\omega t + \theta^-)}{|D^+|\cos(\omega t + \theta^+) + |D^-|\cos(\omega t + \theta^-)}. \tag{3.106}$$

This shows that when two harmonic waves are propagating in both senses, the instantaneous profile of p' is sinusoidal in x but with its amplitude and phase modulated in t. The phase is propagated at a velocity $v_{\rm ph}$ given by

$$v_{\rm ph} \equiv \frac{\mathrm{d}\Phi}{\mathrm{d}t} = -\omega\left(\frac{|D^+|^2 - |D^-|^2}{D^2}\right). \tag{3.107}$$

If $|D^+| = |D^-|$, then $D = 2|D^+|\cos[\omega t+(\theta^+ +\theta^-)/2]$ and the phase remains stationary. This is the case of a standing wave. If the amplitude of wave propagating in the positive sense of the x-axis is larger than that in the negative sense, i.e. $|D^-| > |D^+|$, then the phase Φ is propagated in the positive sense with a speed dependent on t. When the

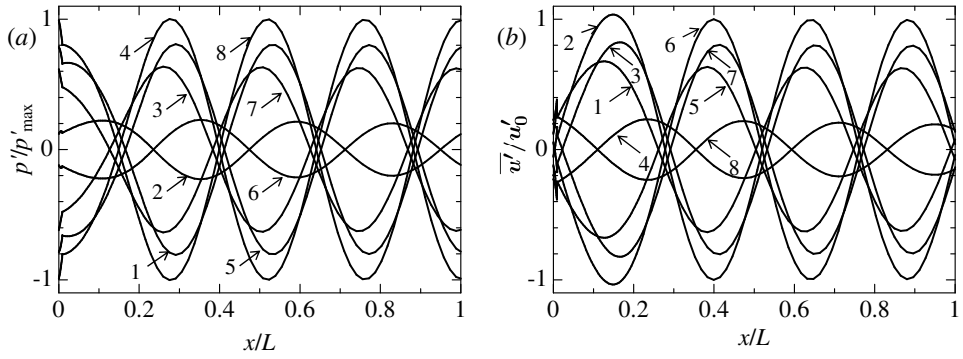

Figure 19: Spatial and temporal profiles of the excess pressure $p'/p_{\max}$ in (a) and the axial velocity u'/u'_0 in (b) with $u'_0 = p'_{\max}/\rho_0 a_0$ in the two-wave mode for the case $\zeta_0 = 0.3$ at every one-eighth of the period $2\pi/\omega$, where the numbers $1, 2, 3, \cdots, 8$ attached to the curves represent the times at $1/8, 2/8, 3/8, \cdots, 8/8$-th period.

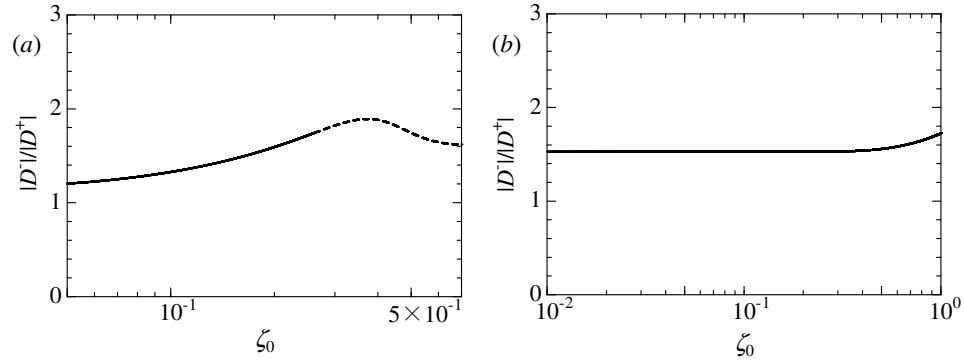

Figure 20: Ratio of the amplitude $|D^-|$ of the wave propagating in the positive sense of the x-axis to the amplitude $|D^+|$ of the wave in the negative sense against $\zeta_0 (= R_S^2\omega/6\nu_0)$, where (a) and (b) correspond to the marginal conditions for the two-wave mode shown in figures $10(a)$ and $10(b)$, respectively, with the porosity of the stack set proportional to the pore's cross-sectional area and the number of pores held constant, and with the porosity fixed at 0.67, the solid curve being broken when the porosity exceeds unity.

amplitude D is large (small), $v_{\rm ph}$ is small (large). This explains why the streaks appear to be inclined and wavy.

3.4.2 Two-wave mode of oscillations

Next we examine the case of the two-wave mode of oscillations. Just as in figure 15, figure 19 depicts spatial and temporal profiles of the excess pressure and the mean axial velocity at every one-eighth of the time period $2\pi/\omega$ at $\zeta_0 = 0.3$ in figure $10(b)$ for $\varphi = 0.67$. Even if ζ_0 is chosen to be the same as in the one-wave mode, the condition is different from it. For $R_S = 0.13$ mm, $L_S = 0.025$ m and $L_B = 0.6$ m, this marginal state occurs at

$\sigma+\sigma_B = 12.8$ and $T_1/T_0 = 2.04$. Then the frequency $\omega/2\pi$ is 251 Hz. Except for that two peaks and troughs are seen along the tube, no special features are found in the profiles in comparison with with the case of the one-wave mode. The pressure takes the maximum at $x = 0$ Figure 20 depicts the ratio of the amplitude $|D^-|$ of the wave propagating in the positive sense of the x-axis to the amplitude $|D^+|$ of the wave in the negative sense against $\zeta_0(= R_S^2\omega/6\nu_0)$, where (a) and (b) correspond to the marginal conditions in figures $10(a)$ and $10(b)$, respectively, with the porosity of the stack set proportional to the pore's cross-sectional area and the number of pores held constant, and with the porosity fixed at 0.67, the solid curve being broken when the porosity exceeds unity. For the two-wave mode as well, the ratio does not change appreciably.

3.5 Spatial distribution of mean acoustic energy flux

In this section, we examine a mean acoustic energy flux averaged over one period. This is defined per unit area of the cross-section as follows:

$$\widetilde{I} \equiv \frac{\omega}{2\pi}\int_t^{t+2\pi/\omega} p'\,\overline{u'}\mathrm{d}t = \frac{1}{2}\mathrm{Re}\{P\overline{U}^*\}, \tag{3.108}$$

where the tilde implies a mean over the period and the asterisk denotes the complex conjugate. Over the cross-sectional area of all pores in the stack, the total flux is calculated by multiplying the product of P in (3.26) and $\overline{U}^*$ obtained from (3.28) with φA so that the flux per unit cross-sectional area of the tube A is given by

$$-\frac{\varphi\gamma}{2\rho_0 a_0^2}\frac{T_e}{T_0}\mathrm{Re}\Bigg\{(1+\mathrm{i}\zeta_e)\left[\frac{\Gamma}{a_0}\left(\frac{T_e}{T_0}\right)^{1/2}|G|^2 + G^*H\right] + \mathrm{i}\zeta_e\Lambda G^*H \\ +\mathrm{i}\zeta_e\frac{2(1+\beta)\Lambda a_0}{\Gamma}\left[\frac{\Gamma}{a_0}GH^* + \left(\frac{T_e}{T_0}\right)^{-1/2}|H|^2\right]\Bigg\}, \tag{3.109}$$

up to the first order of ζ_e, while in the buffer tube, the flux is given by using (3.42) as

$$\frac{1}{2}\mathrm{Re}\left\{\frac{1}{\rho_e a_e}\left(\frac{1-2\delta_e}{1-C\delta_e}\right)\frac{F^*E}{|Z|^2}\right\}. \tag{3.110}$$

In the section without the temperature gradient, (3.108) is calculated by (3.53) and (3.56) as

$$-\frac{1}{2\rho_0 a_0}\Bigg\{\Big[1+\frac{1}{\sqrt{2}}\Big(1-\frac{2}{C}\Big)|b|\Big]\Big(\left|D^+\right|^2\mathrm{e}^{2k_i(x-x_2)} - \left|D^-\right|^2\mathrm{e}^{-2k_i(x-x_2)}\Big) \\ +\sqrt{2}\Big(1-\frac{2}{C}\Big)|b|\,\mathrm{Im}\{D^+D^{-*}\mathrm{e}^{2\mathrm{i}k_r(x-x_2)}\}\Bigg\}, \tag{3.111}$$

where k_r and $-k_i$ denote, respectively, real and imaginary parts of k defined by (3.54) to the first order in b as

$$k = \frac{\omega}{a_0}\left(1+\frac{1-\mathrm{i}}{\sqrt{2}}|b|\right) \equiv k_r - \mathrm{i}k_i, \tag{3.112}$$

and $\mathrm{Im}\{\cdots\}$ stands for taking the imaginary part of $\{\cdots\}$. The first line of (3.111) represents the decay of mean acoustic energy fluxes transported independently by the

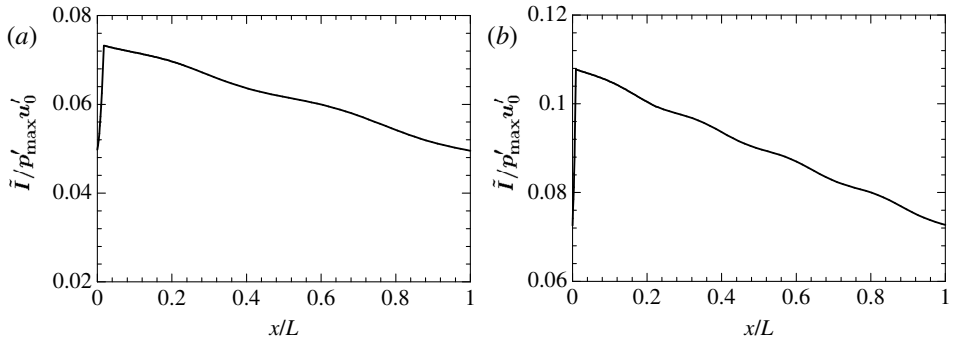

Figure 21: Spatial distribution of the mean acoustic energy flux $\widetilde{I}/p'_{\max}u'_0$ with $u'_0 = p'_{\max}/\rho_0 a_0$ per unit tube's cross-sectional area where (a) and (b) are the cases of the one-wave and two-wave modes, respectively, with $\zeta_0 = 0.3$ in figure 10(b) for $\varphi = 0.67$.

waves D^+ and D^-, while the second line represents the flux due to the weak coupling between them by the diffusion effects.

Figures 21(a) and 21(b) show the spatial distribution of the mean acoustic energy flux $\tilde{I}$ per unit area of the cross-section normalized by $p_{\max}u'_0$ for the one-wave mode and two-wave mode, respectively, in the case of $\zeta_0 = 0.3$ shown in figure 10(b) for $\varphi = 0.67$. It takes a positive value which means that the flux flows in the positive sense of the x-axis everywhere. It is seen that the flux increases in the stack, whereas it decreases slowly in the buffer tube and the section without the temperature gradient. The flux at $x = L$ coincides with the one at $x = 0$ to the first order of ζ_0 and b. The difference is of quadratic order and almost invisible in figure 21, though there may appear to be a gap especially in figure 21(b). The decrease by the lossy effects due to the boundary layer is compensated by the increase in the stack.

While the mean acoustic energy flux is calculated specifically by (3.109) to (3.111), we consider it from a general viewpoint. It can be shown that

$$\frac{\partial}{\partial t}\left(\frac{\rho_e\overline{u'}^{\,2}}{2} + \frac{p'^2}{2\rho_e a_e^2}\right) + \frac{\partial}{\partial x}(p'\overline{u'}) = \frac{2}{R}\left(\overline{u's} + \frac{p'q}{c_p\rho_e T_e}\right), \tag{3.113}$$

where s and q denote the shear stress on the gas exerted by the wall and the heat flux into the gas through it, respectively, and $q/c_p\rho_e T_e$ has a dimension of velocity. Averaging (3.113) over one period, it follows that

$$\frac{\mathrm{d}\widetilde{I}}{\mathrm{d}x} = \frac{2}{R}\left(\widetilde{\overline{u's}} + \frac{\widetilde{p'q}}{c_p\rho_e T_e}\right), \tag{3.114}$$

Equations (3.113) and (3.114) are the general relations derived from the thermoacoustic-wave equation for a circular tube of radius R.

In the case for thick diffusion layer for the pore of radius R_S, s and q are given, respectively, by

$$\frac{2}{R_S}s = \frac{\partial p'}{\partial x} - \frac{R_S^2}{8\nu_e}\frac{\partial^2 p'}{\partial t\partial x} + \left(\frac{R_S^4}{48\nu_e^2}\frac{\partial^3 p'}{\partial t^2\partial x}\right). \tag{3.115}$$

and

$$\frac{2}{R_S}q = -\frac{\partial p'}{\partial t} - \left(\frac{\gamma}{\gamma-1}\right)\frac{\alpha_e}{T_e}\frac{\mathrm{d}T_e}{\mathrm{d}x}\frac{\partial p'}{\partial x} + \frac{R_S^2}{\nu_e}\frac{\partial}{\partial t}\left[\frac{Pr}{8}\frac{\partial p'}{\partial t} + \frac{1}{6}\left(\frac{\gamma}{\gamma-1}\right)(1+Pr)\frac{\alpha_e}{T_e}\frac{\mathrm{d}T_e}{\mathrm{d}x}\frac{\partial p'}{\partial x}\right]. \tag{3.116}$$

The expressions (3.115) and (3.116) are obtained by specifying higher-order terms in (5.26) and (5.27) in I. Although the third term in (3.115) is unnecessary in the present context, attention is drawn to that (3.4) is derived by taking account of the terms up to this order. In fact, substitution of (3.115) and (3.116) into (2.37) in I with $1/2H$ replaced by $2/R_S$ yields (3.4). In this process, it is found that the second term on the left-hand side of (2.37) in I cancels with the lowest term due to the shear stress. This is why s must be specified up to the term of next higher order so as to close (3.4) consistently including the terms of order $R_S^2\omega/\nu_e$.

Using (3.115) and (3.116), (3.114) can be expressed as

$$\frac{\mathrm{d}\widetilde{I}}{\mathrm{d}x} = -\frac{R_S^2}{8\mu_e}\left[\Big(\widetilde{\frac{\partial p'}{\partial x}}\Big)^2 + \frac{1}{T_e}\frac{\mathrm{d}T_e}{\mathrm{d}x}\widetilde{p'\frac{\partial p'}{\partial x}}\right] - \frac{R_S^2}{8\mu_e a_e^2}\left[(\gamma-1)Pr\Big(\widetilde{\frac{\partial p'}{\partial t}}\Big)^2 + \frac{4}{3}\gamma(1+Pr)\frac{\alpha_e}{T_e}\frac{\mathrm{d}T_e}{\mathrm{d}x}\widetilde{\frac{\partial p'}{\partial t}\frac{\partial p'}{\partial x}}\right], \tag{3.117}$$

where the relation $1/c_p\rho_e T_e = (\gamma-1)/\rho_e a_e^2$ has been used. The contribution from $\overline{u'}s$ results only in the first term in the first square brackets, which is always negative so that the shear stress never contributes to increase in the acoustic energy flux in the positive sense of the x axis. The other terms are contributed from $p'q/c_p\rho_e T_e$. If the temperature gradient is absent, only the first term in the second brackets remains but does not contribute to increase because this terms results from the simple heat conduction. The other terms may take a positive or negative value depending on the magnitude of the gradient and the mean values of $-p'\partial p'/\partial x$ and $-\partial p'/\partial t\cdot\partial p'/\partial x$. When the temperature gradient is present, the shear stress participates in the heat flux (see (2.46) in I). Since $-\partial p'/\partial x$ is proportional to the axial velocity to the lowest relation, the former mean may be interpreted as the mean power associated with $p'\overline{u'}$ through the heat flux, while the latter may be interpreted as the product of s and q.

In the theory of thin diffusion layer, on the other hand, $\widetilde{I}$ is given by

$$\frac{\mathrm{d}\widetilde{I}}{\mathrm{d}x} = \frac{2}{R}\widetilde{p'v_b}, \tag{3.118}$$

where v_b is given by

$$v_b = \sqrt{\nu_e}\left[C\frac{\partial^{-\frac{1}{2}}}{\partial t^{-\frac{1}{2}}}\left(\frac{\partial u'}{\partial x}\right) + \frac{C_T}{T_e}\frac{\mathrm{d}T_e}{\mathrm{d}x}\frac{\partial^{-\frac{1}{2}}u'}{\partial t^{-\frac{1}{2}}}\right]. \tag{3.119}$$

In the buffer tube, it is found numerically that the temperature gradient does not contribute to increase the flux. Since two waves coexist there, the temperature gradient acts favourably for the wave propagating in the negative sense of x to increase its energy

flux. However, because this wave is weaker than that propagating in the positive sense, the net energy flux turns out to be decayed.

Using (3.118), a reason why the marginal temperature ratio is reduced for a longer buffer tube may be explained. For the wave propagating in the positive sense, the temperature gradient acts adversely to decrease the energy flux. Because the gradient becomes gentler in a longer tube, such a loss in the energy flux may be reduced so that the marginal temperature ratio becomes lower. In the section without the temperature gradient, it is found that the mean of $p'v_b$ takes a negative value by noting that $\partial u'/\partial x$ is replaced by the lossless relation $-(\rho_e a_e^2)^{-1}\partial p'/\partial t$ and using $p'v_b = \mathrm{Re}\{PV_b^*\}/2$ for a time-harmonic disturbance, V_b being a complex amplitude of v_b.

In the present problem, the decay in the acoustic energy flux results from the loss in the buffer tube and in the section without the temperature gradient. Because no other loads are applied, it is exactly balanced by the generation in the stack. If the acoustic system in the tube is loaded by inserting another stack, for example, the loss will be increased so that marginal conditions will be modified (Guedra & Penelet (2012)). Even in such a case, (3.114) is applicable everywhere. While the mean of $\overline{u}'s$ is always negative, it happens that the mean of $p'q$ may take a positive value depending on the temperature gradient. However, q cannot be imposed independently of p' but related to it via (2.46) in I. Although mechanisms of instability are not yet given transparently, it has been revealed that a phase difference between p' and $\overline{u'}$ and that between s and q are responsible for them in the case of a thick diffusion layer.

3.6 Conclusion of marginal conditions

The stability analysis for the onset of thermoacoustic oscillations in a gas-filled, looped tube with a stack subject to a temperature gradient and acting as a regenerator has been developed based on the asymptotic theory of thick diffusion layer for the gas in the stack and the one of thin diffusion layer for the gas in the other section of the tube, respectively. Given the plausible and mathematically tractable temperature distributions on the walls of the stack and the buffer tube, analytical solutions have been obtained by taking account of the temperature dependence of the shear viscosity and the heat conductivity. The frequency equation has been derived without recourse to numerical methods to determine the marginal conditions. The marginal curves obtained numerically for the temperature ratio appear to correspond to the left branch obtained by the experiments by Yazaki *et al.* (1998) and Ueda & Kato (2008). Although the marginal conditions obtained by them have been given for the temperature ratio in terms of the ratio of the pore radius to the thickness of diffusion layer in the stack, it has been revealed that they cannot be determined without specifying the porosity of the stack. Hence the marginal curves should be extended to a surface woven by the porosity.

4 Comparison of the results by Rott's theory and asymptotic theories

In §3, marginal conditions in looped tube are obtained by asymptotic theories. It is shown that thick diffusion layer theory gives the left branches of marginal curves and unveiled the behavior like gas oscillation and energy flux in looped tube. However, availability of thick diffusion layer theory should be confirmed for the future study for extention to nonlinear problem. Therefore marginal conditions obtained by analytical solutions based on asymptotic theories in §3 are compared with those by Rott's theory which has no limitation of the thickness of diffusion layer. Because Rott's equation is difficult to solve analytically for smooth temperature distributions, it is solved numerically by Runge-Kutta method combined with a shooting method. We now derive marginal conditions by solving Rott's equation numerically to compare with the ones obtained in the preceding section. For a pore of small radius, i.e. ζ_0 is small, the conditions by the analytical solutions are expected to be in accordance with those based on Rott's equation. Using Runge-Kutta method, the boundary-value problem is solved by imposing a spatially periodic condition for the looped tube. A shooting method is adopted to this end. This method is that, starting with probable values initially, the complex pressure amplitude and its spatial derivative are sought combined with a Newton's method to satisfy the periodic boundary conditions.

4.1 Rott's equation and dimensionless parameters

The thermoacoustic-wave equation is capable of describing a spatio-temporal behavior of any disturbance in p' in the framework of the linear theory. If p' is assumed to be time-harmonic in the form of $P(x)\exp(\mathrm{i}\omega t)$, the thermoacoustic-wave equation is reduced to an ordinary differential equation derived by Rott. Following the notation by Rott, differential equation for the complex pressure amplitude P in the circular tube is given in the following form:

$$\frac{\mathrm{d}}{\mathrm{d}x}\left[a_e^2(1-f_1)\frac{\mathrm{d}P}{\mathrm{d}x}\right] - \frac{f_2-f_1}{1-Pr}\frac{a_e^2}{T_e}\frac{\mathrm{d}T_e}{\mathrm{d}x}\frac{\mathrm{d}P}{\mathrm{d}x} + \omega^2[1+(\gamma-1)f_2]P = 0. \tag{4.1}$$

where f_1 and f_2 are defined as

$$f(\eta_e) = \frac{2I_1(\eta_e)}{\eta_e I_0(\eta_e)}, \tag{4.2}$$

and

$$f_2 = f_1(\sqrt{Pr}\eta_e), \tag{4.3}$$

with η_e given by

$$\eta_e = \delta_e^{-1} = R\left(\frac{\nu_e}{\mathrm{i}\omega}\right)^{-1/2} \tag{4.4}$$

Before calculation, we change Rott's equation into non-dimensional one. We introduce a nondimensional pressure and a coordinate,

$$P^* = \frac{P}{P_0}, \quad x^* = \frac{x}{L} \tag{4.5}$$

and the pressure derivative is set as

$$\frac{\mathrm{d}P^*}{\mathrm{d}x^*} = Z^*. \tag{4.6}$$

Using Z^*, Rott's equation is expressed by two equations

$$\frac{\mathrm{d}Z^*}{\mathrm{d}x^*} = -\frac{(1-f_1) + \mathrm{d}f_1/\mathrm{d}x^* - (f_2-f_1)/(1-Pr)}{1-f_1}\frac{1}{T_e}\frac{\mathrm{d}T_e}{\mathrm{d}x^*}\frac{\mathrm{d}P^*}{\mathrm{d}x^*}$$
$$-\sigma_0^2\left(\frac{T_e}{T_0}\right)^{-1}\frac{[1+(\gamma-1)f_2]}{1-f_1}P^*, \tag{4.7}$$

where σ_0 and ζ_R is dimension-less parameter defined as

$$\sigma_0 = \frac{\omega^2 L^2}{a_0^2}, \zeta_R = \frac{1}{R}\sqrt{\frac{\nu_0 L}{a_0}} \tag{4.8}$$

This system of equations is solved by Runge-Kutta method. Using these parameters, thickness of diffusion layer to tube radius δ_e is expressed as

$$\delta_e = \frac{1}{R}\left(\frac{\nu_e}{\mathrm{i}\omega}\right)^{1/2} = \frac{1-\mathrm{i}}{\sqrt{2}}\frac{\zeta_R}{\sqrt{\sigma_0}}\left(\frac{T_e}{T_0}\right)^{(1+\beta)/2} \tag{4.9}$$

In the stack, thickness of diffusion layer to the pore radius δ_S is expressed as

$$\delta_S = \frac{1}{R_S}\left(\frac{\nu_e}{\mathrm{i}\omega}\right)^{1/2} = \phi_r\delta_e, \tag{4.10}$$

where ϕ_r is the ratio of tube radius to pore radius in the stack defined as

$$\frac{R}{R_s} = \phi_r. \tag{4.11}$$

4.2 Method of calculating marginal conditions by shooting method

Combinations of parameters which satisfy periodic boundary conditions with real frequency give marginal conditions. We give the initial condition at $x = x_0$ (x_0 is located at the section without temperature gradient). Without any loss of generality, P^* may be set to be unity as

$$P^*|_{x=x_0} = 1, \tag{4.12}$$

while $\mathrm{d}P^*/\mathrm{d}x$ is taken arbitrarily. Under these conditions, Rott's equation is solved toward $x = x_0 + L$ by the 4th order Runge-Kutta method to seek the pressure amplitude and its derivative. The periodic boundary conditions require

$$P^*|_{x=x_0+L} = P^*|_{x=x_0}(=1), \tag{4.13}$$

and

$$\overline{U^*}|_{x=x_0+L} = \overline{U^*}|_{x=x_0}, \tag{4.14}$$

where $\overline{U}$ is the mean velocity averaged over the cross-section defined as

$$\overline{U} = \frac{\mathrm{i}}{\omega\rho_e}\frac{\mathrm{d}P}{\mathrm{d}x}\left[1 - 2\frac{I_1(\eta_e)}{\eta_e I_0(\eta_e)}\right] \tag{4.15}$$

At $x = x_0 + L$, matching condition of velocity for periodic boundary is written as

$$Z^*|_{x=x_0+L} = Z^*|_{x=x_0}. \tag{4.16}$$

At ends of the stack at $x = x_1$ and $x = x_2$ is imposed the continuity of pressure and mass flux as

$$\rho_e A\overline{U^*}|_{x=x_1} = \rho_e A_S \overline{U_S^*}|_{x=x_1} \tag{4.17}$$

We seek the combinations of parameters which satisfy periodic boundary conditions (4.13) and (4.16), but P^* is complex. So the conditions to be satisfied are given as

$$\begin{aligned}
\mathrm{Re}\{P^*|_{x=x_0}\} &= \mathrm{Re}\{P^*|_{x=x_0+L}\} \\
\mathrm{Im}\{P^*|_{x=x_0}\} &= \mathrm{Im}\{P^*|_{x=x_0+L}\} \\
\mathrm{Re}\{Z^*|_{x=x_0}\} &= \mathrm{Re}\{Z^*|_{x=x_0+L}\} \\
\mathrm{Im}\{Z^*|_{x=x_0}\} &= \mathrm{Im}\{Z^*|_{x=x_0+L}\}.
\end{aligned} \tag{4.18}$$

When geometry of looped tube, i.e. length outside of stack, tube radius, pore radius and porosity, is given, nondimensional parameters to be varied are following four parameters:

$$\begin{gathered}
\sigma_0\left(=\frac{\omega L}{a_0}\right), \quad \lambda\left(=\sqrt{T_1/T_0}-1\right) \\
\mathrm{Re}\{Z^*|_{x=x_0}\}, \quad \mathrm{Im}\{Z^*|_{x=x_0}\}
\end{gathered} \tag{4.19}$$

These are non-dimensional frequency with real omega, temperature ratio, and real and imaginary part of the derivative of pressure at $x = 0$. We have already known that the pressure and velocity oscillate in the form neither of a standing wave nor of a traveling wave purely in the looped tube. So because the derivative of pressure at $x = 0$ is underspecified, they are variable parameters. Boundary conditions (4.13) and (4.16) give four variable and four equations F^n $(n = 1, 2, 3, 4)$ as followings:

$$\begin{aligned}
F^1 &= \mathrm{Re}\{P^*|_{x=x_0+L}(\sigma_0, \lambda, \mathrm{Re}\{Z_0^*\}, \mathrm{Im}\{Z_0^*\})\} - \mathrm{Re}\{P^*|_{x=x_0}\} = 0 \\
F^2 &= \mathrm{Im}\{P^*|_{x=x_0+L}(\sigma_0, \lambda, \mathrm{Re}\{Z_0^*\}, \mathrm{Im}\{Z_0^*\})\} - \mathrm{Im}\{P^*|_{x=x_0}\} = 0 \\
F^3 &= \mathrm{Re}\{Z^*|_{x=x_0+L}(\sigma_0, \lambda, \mathrm{Re}\{Z_0^*\}, \mathrm{Im}\{Z_0^*\})\} - \mathrm{Re}\{Z^*|_{x=x_0}\} = 0 \\
F^4 &= \mathrm{Im}\{Z^*|_{x=x_0+L}(\sigma_0, \lambda, \mathrm{Re}\{Z_0^*\}, \mathrm{Im}\{Z_0^*\})\} - \mathrm{Im}\{Z^*|_{x=x_0}\} = 0
\end{aligned} \tag{4.20}$$

We seek the solution of these equations by the Newton method. Rewriting four variables (4.19) as

$$(v_1, v_2, v_3, v_4) = (\sigma_0, \lambda, \mathrm{Re}\{Z_0^*\}, \mathrm{Im}\{Z_0^*\}) \tag{4.21}$$

When the variables are changed slightly to $v_n + \Delta v_n$ so as to satisfy the equations $F^n = 0$, relations are expressed as

$$F^n(v_1, v_2, v_3, v_4) + \frac{\partial F^n}{\partial v_1}\Delta v_1 + \frac{\partial F^n}{\partial v_2}\Delta v_2 + \frac{\partial F^n}{\partial v_3}\Delta v_3 + \frac{\partial F^n}{\partial v_4}\Delta v_4 = 0. \tag{4.22}$$

From these relations, the system of equations for the four variables is derived as

$$\begin{pmatrix} F_1^1 & F_2^1 & F_3^1 & F_4^1 \\ F_1^2 & F_2^2 & F_3^2 & F_4^2 \\ F_1^3 & F_2^3 & F_3^3 & F_4^3 \\ F_1^4 & F_2^4 & F_3^4 & F_4^4 \end{pmatrix} \begin{pmatrix} \Delta v_1 \\ \Delta v_2 \\ \Delta v_3 \\ \Delta v_4 \end{pmatrix} = - \begin{pmatrix} F^1 \\ F^2 \\ F^3 \\ F^4 \end{pmatrix}, \tag{4.23}$$

where F_i^n is partial differentiation defined as

$$F_i^n = \frac{\partial}{\partial v_i} F^n(v_1, v_2, v_3, v_4). \tag{4.24}$$

Here these partial differentiations are evaluated numerically by finite difference as

$$\frac{\partial F^n}{\partial v_1} \approx \frac{F^n(v_1 + \Delta v_1, v_2, v_3, v_4) - F^n(v_1, v_2, v_3, v_4)}{\Delta v_1}. \tag{4.25}$$

Solving the system of equation (4.23), Δv_n is derived and the variables are updated as $v_i^j + \Delta v_i^j \to v_i^{j+1}$, where v_i^j is the j-th step in the Newton-method. As the calculation progresses, v approaches the solution. So the partial derivatives by finite difference to derive v_i^{j+1} are calculated by the values at v_i^j and v_i^{j-1}. When difference between v_i^j and v_i^{j-1} is small enough, we take parameters at this point as marginal condition.

4.3 Marginal conditions

For the same temperature distribution as assumed in the analytical solution, marginal conditions are obtained for the same geometry: $L - L_S = 2.16$m, $L_B = 0.6$m, $R = 20$mm. At first, we set the pore radius R_S as 0.1mm and porosity $\varphi = 0.67$. Note again that given the temperature ratio in the analytical solution, the length of stack is determined by the pore radius and temperature ratio, so the total length of looped tube is slightly changed.

We seek the combination of parameters which satisfy the condition that the length of the looped tube coincides with one wavelength by shooting method and plot the relation between pore radius, frequency and temperature ratio. As the pore radius is changed slightly, i.e. ϕ_r is changed, next marginal condition is obtained. Repeating this process, full marginal conditions are available and the marginal curves are plotted.

Figure 22(a) and 22(b) compare the marginal curves obtained by the analytical solution and by numerical method using Rott's theory. In these figures, curves in red represent the results by the approximated theory, while curves in black the results by Rott's theory.

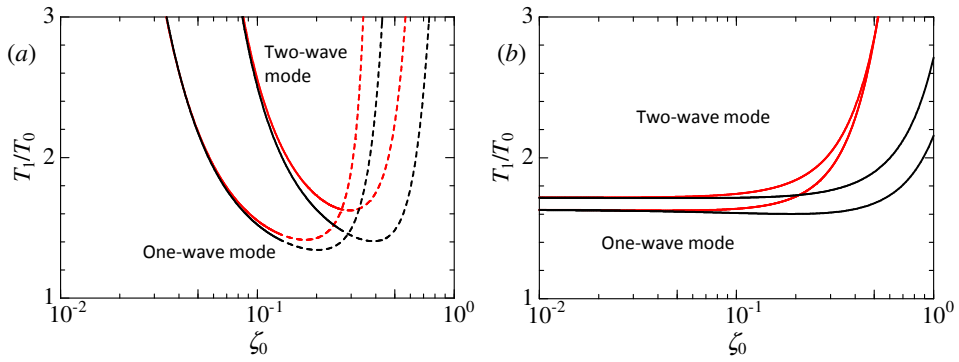

Figure 22: Marginal conditions for temperature ratio T_1/T_0 for the one-wave mode against ζ_0. Red curves are results derived by analytical solution based on approximate theory. Black curves are results by shooting method based on Rott's theory. In (a), the curves are drawn by taking the porosity proportional to the pore's cross-sectional area with the total number of the pores fixed, the curves being broken when the porosity exceeds unity, while in (b), the curves are drawn by changing the pore radius with the porosity φ fixed at 0.67.

In (a), the curves are drawn by taking the porosity proportional to the pore's cross-sectional area with the total number of the pores fixed, the curves being broken when the porosity exceeds unity, while in (b), the curves are drawn by changing the pore radius with the porosity φ fixed at 0.67. As R_S is smaller, especially smaller than 0.1, results from approximate theory coincide well with those by Rott's theory. It is found that the approximate thermoacoustic wave equation used in the stack is appropriate for the case of thin pore radius, though these results have been expected. When the initial frequency is chosen about twice the one for the one-wave mode, marginal conditions for the two wave mode are also obtained. For the two-wave mode as well, the good agreements are obtained for small pore radius.

Figure 23(a) and 23(b) show the graphs for the one-wave mode as to how the pore radius and the porosity affect the marginal conditions. In figure 23(a), the leftmost red and black curves correspond to the ones in figure 22(a) and other four red and black (broken in part for $\varphi > 1$) curves represent the marginal conditions with the number of pores reduced consecutively to the right by 1/2, 1/3, 1/4 and 1/5 of that for the leftmost curves. In figure 23(b) six red and black curves represent the marginal conditions with the value of porosity φ increased from 0.5 to 1 by step 0.1. In these figures, the results by the approximate theory are shown in red and the ones by Rott's theory are shown in black. In (a), the results by the approximate theory agree with those by Rott's theory for small pore radius, but for large pore radius, the lowest temperature ratio for each curve is different between the approximate and Rott's theories. However, the temperature ratio and ζ_0 at the bottom of temperature ratio are larger as the number of pores becomes small. In (b), the temperature ratio by Rott's theory is smaller than that by the approximate theory for the large value of ζ_0.

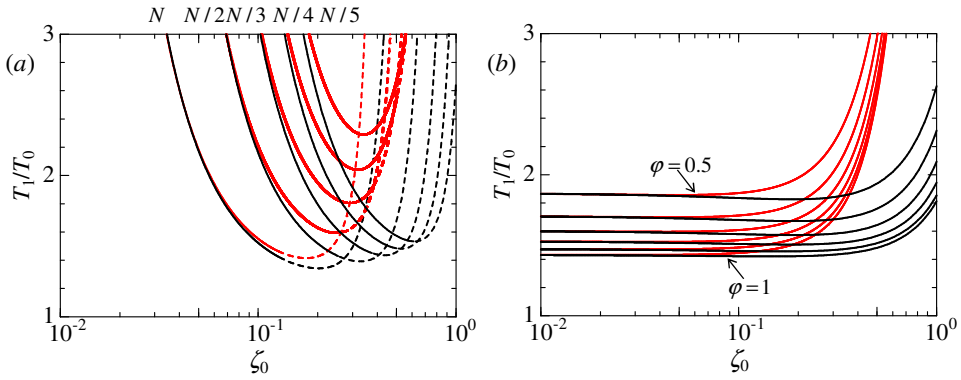

Figure 23: Marginal conditions for temperature ratio T_1/T_0 for the one-wave and two-wave mode against ζ_0 . Red curves are results derived by analytical solution based on approximate theory. Black curves are results by shooting method based on Rott's theory. In figure 23(a), the leftmost red and black curves corresponds to the one in figure 22(a) and five red and black (broken in part for $\varphi > 1$) curves represent the marginal conditions with the number of pores reduced consecutively to the right by 1/2, 1/3, 1/4 and 1/5 of that for the leftmost curves. In figure 23(b) six red and black curves represent the marginal conditions with the value of porosity φ increased from 0.5 to 1 by step 0.1.

4.4 Pressure and velocity distribution

Next we compare the results of pressure and velocity distributions with the analytical solutions. Figure 24 shows the pressure and velocity distributions along the center line of the looped tube calculated by the shooting method at $\zeta_0 = 0.3$ and porosity $\varphi = 0.67$. In this figure, the stack and buffer tube are located in the section $0 \leq x \leq 0.015$ and $0.015 \leq x \leq 0.229$. Figure 24(a) shows the pressure distribution where the vertical axis measures P/P_0, where P_0 is chosen to be the pressure at $x = 0$. In figure 24(b), the velocity U is normalized by U_0 given in terms of P_0 and a typical acoustic impedance $\rho_0 a_0$ as $P_0/\rho_0 a_0$.

Because the section of the stack is too short for the profiles to be visible in figure 24, the profiles are blown up in figure 25 including those in the buffer tube. In figure 24(a), the pressure is continuous across the junction $x/L = 0.015$ between the stack and the buffer tube, but its gradient is discontinuous there. In figure 24(b), the velocity in the stack is larger than that in the other sections and jumps at both ends of the stack because of constriction of the cross-sectional area. But the mass flux is continuous everywhere as required by the matching conditions. This is seen in the profile of the mass flux $\rho_e U A_e/\rho_0 U_0 A$ in the broken curves, where A_e takes A_S in the section of the stack and A in the other sections. The velocity increases with x while the mass flux decreases gently. Because temperature ratio has a difference between approximate theory and Rott's theory (temperature ratio by Rott's theory is smaller than that of approximate theory), the length of the stack for Rott's theory is smaller than that of approximate theory. So distributions by approximate theory and Rott's theory are not plotted at the same time. However, figures 15 and 24 have the same features as the analytical solutions. Figure 26(a) and 26(b) show the pressure and velocity distributions for the two-wave mode. Qualitative

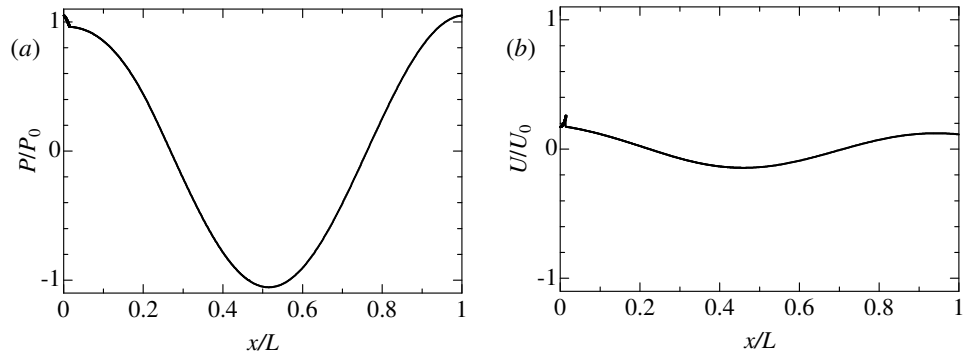

Figure 24: Spatial and temporal profiles of the pressure P/P_0 in (a) and the mean axial velocity U/U_0 in (b) with $U_0 = P_0/\rho_0 a_0$ in the one-wave mode for the case $\zeta_0 = 0.3$.

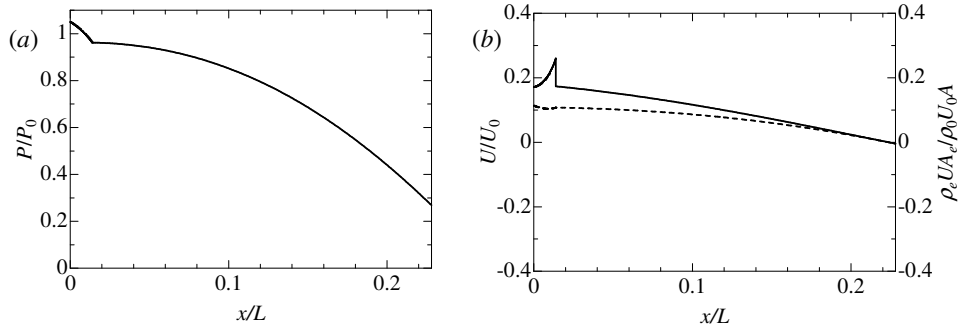

Figure 25: Blow-up of figure 23 for the pressure P/P_0 in (a) and the mean axial velocity U/U_0 in (b) with $U_0 = P_0/\rho_0 a_0$ in the sections of the stack and the buffer tube for the case $\zeta_0 = 0.3$ where the mass flux $\rho_e U A_e/\rho_0 U_0 A$ is also drawn in the broken curve.

difference is not shown between the one-wave and two-wave mode. These have common feature that the top of the antinode of pressure is located at the cold end of the stack. This is already shown in analytical solution of approximate theory.

4.5 Marginal conditions for the case of parabolic temperature distribution

We have shown that the results by the approximate theory agree with that of Rott's theory for the case of small ζ_0. However, the temperature distribution is determined by the pore radius of stack and temperature ratio so the total length of looped tube is different for the different ζ_0 on marginal conditions. Therefore effects of the length of the stack on the marginal conditions should be examined. Now that the marginal conditions are available numerically for any temperature ratio by the shooting method, the case of a parabolic temperature distribution in the stack is considered to fix the length of the stack. We set geometry of looped tube as $L = 2.8$m, $L_B = 560$mm, $R = 20$mm, $L_S = 56$mm, and set

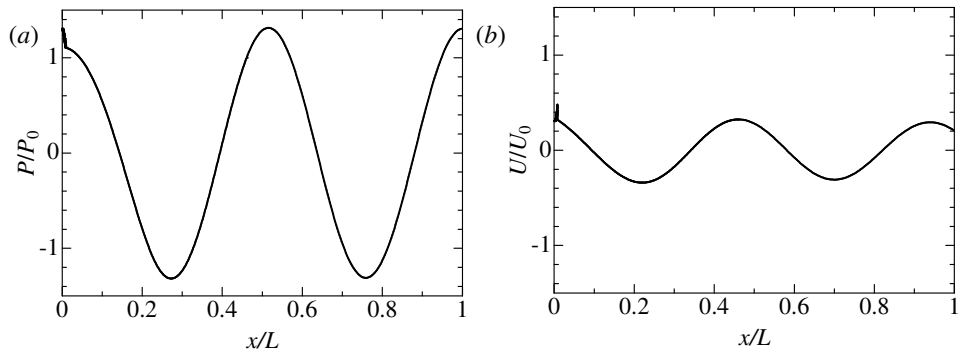

Figure 26: Spatial and temporal profiles of the pressure P/P_0 in (a) and the mean axial velocity U/U_0 in (b) with $U_0 = P_0/\rho_0 a_0$ in the one-wave mode for the case $\zeta_0 = 0.3$.

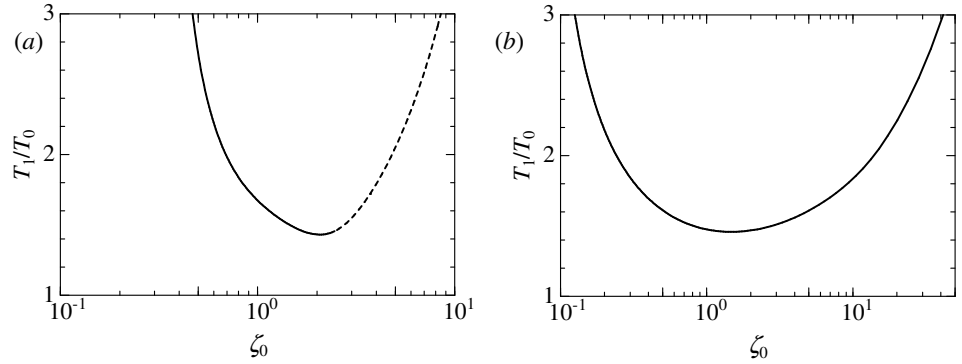

Figure 27: Marginal conditions for temperature ratio T_1/T_0 for the one-wave mode against ζ_0. In (a), the curves are drawn by taking the porosity proportional to the pore's cross-sectional area with the total number of the pores fixed, the curves being broken when the porosity exceeds unity, while in (b), the curves are drawn by changing the pore radius with the porosity φ fixed at 0.67.

$\beta = 0.5, Pr = 0.7, \gamma = 1.4$.

In this case as well, two types of marginal curves are shown. Figure 27(a) and 27(b) show the curves drawn by taking the porosity proportional to the pore's cross-sectional area with the total number of the pores fixed, the curves being broken when the porosity exceeds unity, and the curves drawn by changing the pore radius with the porosity φ fixed at 0.67, respectively. The curve with the porosity of the stack proportional to the pore radius squared has a larger variation of the temperature ratio than the curve with porosity fixed. This is the same feature as the temperature distribution for the analytical solution. In (b), however, the temperature ratio of the marginal curve with the porosity fixed becomes higher as the ζ_0 becomes smaller, whereas the temperature ratio by the analytical solution is almost constant. This difference is explained by the following results.

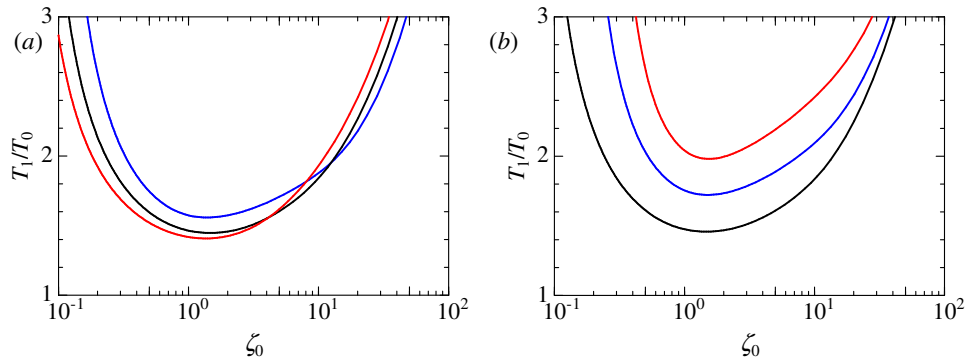

Figure 28: Marginal conditions for temperature ratio T_1/T_0 for the one-wave mode against ζ_0. In (a) the marginal curves with various value of porosity are plotted. Blue, black and red curves are φ=0.5, 0.7, 0.9, respectively. The other geometry of looped tube is fixed as $L = 2.8$m, $L_S = 56$mm, $L_B = 560$mm, $R = 20$mm. In (b) marginal curves with the various length of the stack are plotted. Black, blue and red curves correspond to the length of the stack $L_S = 56$mm,112mm,168mm, respectively. The other geometry of looped tube is fixed as $L = 2.8$m, $L_B = 560$mm, $R = 20$mm, $\varphi = 0.67$.

4.6 Effects of the porosity and the length of stack

We now examine the effects of the porosity and the length of the stack on marginal conditions for the parabolic temperature distribution in the stack. Figure 28(a) shows the marginal curves with various values of porosity. Blue, black and red curves show the curves with $\varphi = 0.5, 0.7, 0.9$, respectively. Geometry of looped tube is fixed as $L = 2.8$m, $L_B = 560$mm, $R = 20$mm, $L_S = 56$mm. Figure 28(b) shows the marginal curves with the various lengths of the stack. Black, blue and red curves correspond to the length of the stack $L_S = 56$mm,112mm,168mm, respectively. The other geometry of looped tube is fixed as $L = 2.8$m, $L_B = 560$mm, $\varphi = 0.67$. In figure 28 (a), the temperature ratio is larger as the porosity becomes smaller for the smaller ζ_0, while for lager ζ_0, the temperature ratio is smaller as the porosity becomes small. In figure 28(b), the temperature ratio is smaller as the length of the stack becomes short. Essentially, the marginal curves of the looped tube have the form like a bowl, and so have the bottom of temperature ratio at a certain ζ_0. In the case of using the temperature distribution of analytical solution, as ζ_0 becomes smaller, i.e. the pore radius of stack becomes smaller, the length of the stack becomes short through the definition of temperature distribution. In other words, the temperature gradient increases as the pore radius becomes smaller. Therefore the temperature ratio of marginal curves for the analytical solution with the porosity of the stack fixed does not change in the small ζ_0 region. But in the case with porosity proportional to the pore radius, porosity becomes small as ζ_0 becomes small, i.e. pore radius becomes small, so the temperature ratio becomes higher.

5 Conclusion

At first, we examined the effects of the thermal conduction in the wall on the thermoacoustic-wave equation and its approximated theory. The effects appear through the parameter ε and Ge defined by the square root of the product of two ratios, one being the ratio of the heat capacities per volume and the other the ratio of the thermal conductivities and defined by the relative thickness of the wall, respectively. Usually, the value of ε is very small so that the effects of heat condition have been taken into account to the first order of ε. However it has been unveiled that when the geometry parameter takes special values, the expansion exhibits nonuniformity, i.e. resonance, and then the effects become enhanced up to the order of $\sqrt{\varepsilon}$. In thin diffusion layer theory, the effects of heat condition appear only through ε, however in the thick diffusion layer theory, they appear through ε and Ge. The effects of heat conduction in wall may be neglected as long as the value of ε is small enough. But it may happen that the effects appear enhanced, depending through Ge on the geometry of the tubes, and the combination between the gas and the solid. For the case of thick diffusion layer, the effects of heat conduction do not introduce new terms in form but modify only the coefficients. This is a useful knowledge in deriving marginal conditions.

Marginal conditions for the onset of thermoacoustic oscillations in a gas-filled, looped tube has been developed based on the asymptotic theory of thick diffusion layer for the gas in the stack and the one of thin diffusion layer for the gas in the other section of the tube, respectively. For simplicity, ε is assumed to be enough small for the effects of thermal conductivity in wall to be negligible. The marginal curves obtained numerically for the temperature ratio appear to correspond to the left branch obtained by the experiments by Yazaki and Ueda and Kato. It has been revealed that marginal conditions cannot be determined without specifying the porosity of the stack. Hence the marginal curves should be extended to a surface woven by the porosity.

Using the marginal conditions available, the mode of oscillations in the tube has also been clarified not only for the one-wave but also for two-wave modes. It has been revealed that the wave propagating in the positive sense from the stack's cold end to the hot end thought it is greater than that propagating in the opposite sense, so that the acoustic field as a whole appears to be a travelling wave propagating in the positive sense. In accordance with this, the mean acoustic energy flux flows in the same sense everywhere. It is only in the stack that the flux is generated by the action of the thermoviscous diffusion.

The theories of thick and thin diffusion layer are characterized by two small parameters ζ_0 and $|b|$ representing the ratio squared of the pore radius to the thickness of diffusion layer and the ratio of the thickness to the tube radius, respectively. Although they are assumed much smaller than unity, the results appear to be applicable even when the parameters become comparable with unity. In fact, when the present result is considered together with the result by Shimizu et al, the full marginal curves appear to be covered almost by those in the limits $\zeta_0 \sim 1$ and $|b| \sim 1$ beyond the valid range of the asymptotic theories. Hence it is concluded that the approximate theories of thick and thin diffusion layers are relatively simple and useful in understanding and predicting the thermoacoustic phenomena.

Marginal conditions are derived by Rott's theory and compared with those of the analytical solution based on asymptotic theories. For small ζ_0, marginal curves agree with

each other as we expected. It is shown that thick diffusion layer theory give the good approximation for the small radius. Using parabolic temperature distribution, marginal curves are calculated in order to examine the effects of the length of stack. It is shown that temperature ratio is smaller as the length of stack becomes short. Marginal conditions are affected not only by the pore radius, porosity of the stack but also the length of the stack.

In the future study, analysis by thermoacoustic-wave equation with heat conduction in wall should be considered. For example, using asymptotic equations which take account of influence of heat conduction, effects on marginal conditions of looped tube may be examined. It seems to be difficult to solve the analytical solution to the equations with heat conduction but they are expected to be solved by modifying each coefficient. The factor given by ε and Ge may affect the marginal curves because the value of Ge varies depending on the geometry of stack.

Because availability of asymptotic theories is confirmed in §4, thick diffusion layer theory is expected to the nonlinear problem.

References

Abramowitz, M. & Stegun, I. A. 1972 *Handbook of Mathematical Functions.* Dover.

American Institute of Physics. 1982 *AIP Handbook 3rd ed.* pp.**4**-105–118, **4**-142–162. McGraw-Hill.

Backhaus, S. & Swift, G. W. 1999 A thermoacoustic Stirling heat engine. Nature **399**, 335–338.

Backhaus, S. & Swift, G. W. 2000 A thermoacoustic-Stirling heat engine: Detailed study. *J. Acoust. Soc. Am.* **107**, 3148–3166.

Berson, A. & Blanc-Benon, Ph. 2007 Nonperiodicity of the flow within the gap of a thermoacoustic couple at high amplitudes. *JASA Express Lett.* **122**, EL122–EL127.

Berson, A., Michard, M. & Blanc-Benon, Ph. 2008 Measurement of acoustic velocity in the stack of a thermoacoustic refrigerator using particle image velocimetry. *Heat Mass Transfer.* **44**, 1015–1023.

Garrett, S. L. 2004 Thermoacoustic engines and refrigerators. *Am. J. Phys.* **72**, 11–17.

Gel'fand, I. M. & Shilov, G. E. 1964 *Generalized Functions.* Vol.1. pp. 115–122. Academic Press.

Gopinath, A., Tait, N. L. & Garrett, S. L. 1998 *Thermoacoustic streaming in a resonant channel: The time averaged temperature distribution. J. Acoust. Soc. Am.* **103**, 1388–1405.

Guedra, M. & Penelet, G. 2012 On the use of a complex frequency for the description of thermoacoustic engines. *Acust. Acta Acust.* **98**, 232–241.

Guedra, M., Penelet, G., Lotton, P. & Dalmont, J-P. 2011 Theoretical prediction of the onset of thermoacoustic instability from the experimental transfer matrix of a thermoacoustic core. *J. Acoust. Soc. Am.* **130**, 145–152.

Henry, P. S. H. 1931 *The tube effect in sound-velocity measurements. Proc. Phys. Soc.* **43**, 340–361.

Incropera, F. P. & DeWitt, D. P. 1990 *Fundamentals of Heat and Mass Transfer.* Appendix A. John Wiley & Sons.

Karpov, S. & Prosperetti, A. 2002 *A nonlinear model of thermoacoustic devices. J. Acoust. Soc. Am.* **112**, 1431–1444.

Kirchhoff, G. 1868 Ueber den Einfluß der Wärmeleitung in einem Gase auf die Schallbewegung. *Ann. Phys. Chem.* **134**, 177–193.

Lieuwen, T. C. 2012 *Unsteady Combustor Physics.* Chapter 6. Cambridge Univ. Press.

Marx, D. & Blanc-Benon, Ph. 2004 *Numerical simulation of stack–heat exchangers coupling in a thermoacoustic refrigerator. AIAA J.* **42**, 1338–1347.

Marx, D. & Blanc-Benon, Ph. 2005 *Numerical calculation of the temperature difference between the extremities of a thermoacoustic stack plate. Cryogenics* **45**, 163–172.

Morfey, C. L. 2001 *Dictionary of Acoustics.* p.112. Academic Press.

Ooura, T. & Mori, M. 1991 The double exponential formula for oscillatory functions over the half infinite interval. *J. Compt. Appl. Math.* **38**, 353–360.

Penelet, G., Job, S., Gusev, V., Lotton, P. & Bruneau, M. 2005 Dependence of sound amplification on temperature distribution in annular thermoacoustic engines. *Acust. Acta Acust.* **91**, 567–577.

Rayleigh, Lord 1945 *The Theory of Sound Vol.2.* pp. 319–328. Dover.

Rott, N. 1969 Damped and thermally driven acoustic oscillations in wide and narrow tubes *Z. Angew. Math. Phys.* **20**, 230–243.

Rott, N. 1973 Thermally driven acoustic oscillations. Part II: Stability limit for helium. *Z. Angew. Math. Phys.* **24**, 54–72.

Shimizu, D. & Sugimoto, N. 2010 Numerical study of thermoacoustic Taconis oscillations. *J. Appl. Phys.* **107**, 1–11.

Shimizu, D., Nishikawa, K. & Sugimoto, N. 2012 Numerical simulations of thermoacoustic oscillations in a looped tube. In *19th Intl. Symp. on Nonlinear Acoustics.* (ed. T. Kamakura & N. Sugimoto). NONLINEAR ACOUSTICS–State-of-the-Art and Perspectives, AIP Conf. Proc. #1474, pp. 299–302. AIP.

Sugimoto, N. 2010 Thermoacoustic-wave equations for gas in a channel and a tube subject to temperature gradient. *J. Fluid Mech.* **658**, 89–116.

Sugimoto, N. & Yoshida, M. 2007 Marginal condition for the onset of thermoacoustic oscillations of a gas in a tube. *Phys. Fluids* **19**, 074101 1–13.

Sugimoto, N. & Shimizu, D. 2008 Boundary-layer theory for Taconis oscillations in a helium-filled tube. *Phys. Fluids* **20**, 104102 1–11.

Sugimoto, N. & Takeuchi, R. 2009 Marginal conditions for thermoacoustic oscillations in resonators. *Proc. R. Soc. A.* **465**, 3531–3552.

Swift, G. W. 1988 Thermoacoustic engines. *J. Acoust. Soc. Am.* **84**, 1145–1180.

Swift, G. W. 2002 *Thermoacoustics: A Unifying Perspective for Some Engines and Refrigerators.* Acoustical Society of America.

Taconis, K. W., Beenakker, J. J. M., Nier, A. O. C. & Aldrich, L. T. 1949 Measurements concerning the vapour-liquid equilibrium of solutions of He^3 in He^4 below $2.19°K$. *Physica* **15**, 733–739.

Turns, S. R. 2006 *Thermal–Fluid Sciences An Integrated Approach.* Cambridge University Press.

Ueda, Y. & Kato, C. 2008 Stability analysis of thermally induced spontaneous gas oscillations in a straight and looped tube. *J. Acoust. Soc. Am.* **124**, 851–858.

Yazaki, T., Iwata, A., Maekawa, T. & Tominaga, A. 1998 Traveling wave thermoacoustic engine in a looped tube. *Phys. Rev. Lett.* **81**, 3128–3131.

Yazaki, T., Biwa, T. & Tominaga, A. 2002 A pistonless Stirling cooler. *Appl. Phys. Lett.* **80**, 157–159.

Zhou, Y., Hirao, K., Watari, K., Yamauchi, Y. & Kanzaki, S. 2004 Thermal conductivity of silicon carbide densified with rare-earth oxide additives. *J. Eur. Ceram. Soc.* **24**, 265–270.

Acknowledgments

I would like to express my sincere gratitude to Professor Nobumasa Sugimoto for his support, discussions and advices. I also thank all members of Sugimoto laboratory for their help. They provided me this precious study opportunity in Sugimoto laboratory.

I also would like to express my gratitude to Professor Genta Kawahara and Professor Satoyuki Kawano for their invaluable comments and careful inspection of the thesis.

Finally, I would like to extend my grateful thanks to my parents for their understanding, support and encouragement throughout my study.

List of publications

N. Sugimoto & H. Hyodo 2012 “Effects of heat conduction in wall on thermoacoustic-wave propagation,” *J.Fluid Mech.* **697**, pp 60–91, (2012)

H. Hyodo & N. Sugimoto 2014 “Stability analysis for the onset of thermoacoustic oscillations in a gas-filled, looped tube,” *J.Fluid Mech.* **741**, pp 585–618, (2014)

Presentations at international conferences

N. Sugimoto & H. Hyodo 2012 “Diffusive effects on acoustic wave propagation in a gas-filled channel subject to temperature gradient,” *Proceedings of XXIII International Congress on Theoretical and Applied Mechanics* (eds. Y. Bai & J. Wang) FM 60–91, (2012)

H. Hyodo & N. Sugimoto 2013 “Marginal conditions of thermoacoustic oscillations in a looped tube based on thick and thin diffusion layer theories,” *Proceedings of the 21st Congress on Acoustics*, (POMA —ICA 2013, 19, 045085 (2013)), *J. Acoust. Soc. Am.* , 133(5) Pt.2,(2013)

Presentations at domestic conferences

兵頭弘晃, 杉本信正, “温度勾配のある平行壁面間の音の伝播に及ぼす壁の熱伝導性の効果,” 第 60 回　理論応用力学講演会，東京工業大学，OS05-11，2011 年 3 月 8 日

兵頭弘晃, 杉本信正, “ 温度勾配のある平板間の音の伝播を記述する熱音響波動方程式とそれに及ぼす壁の熱伝導の効果 ”，京都大学数理解析研究所，共同研究集会，京都大学，講究録 #1800「非線形波動現象の研究の新たな進展」,pp236-248，2011 年 10 月 14 日

兵頭弘晃，杉本信正 :“ 厚い拡散層近似を用いたループ管における熱音響振動の臨界条件 ”，第 61 回理論応用力学研究会，東京大学，OS13-08，2012 年 3 月 9 日

兵頭弘晃，杉本信正 :“ ループ管内のスタック内気体に対して厚い拡散層近似を用いた場合の熱音響不安定の臨界条件 ”，日本流体力学会年会 2012，高知大学，230，2012 年 9 月 17 日

兵頭弘晃，杉本信正 :“ 境界層および厚い拡散層近似を用いたループ管内の熱音響振動の安定性解析 ”，京都大学数理解析研究所，共同研究集会，京都大学，講究録 #1847「非線形波動現象の数理と応用」，pp1-9，2012 年 10 月 16 日

兵頭弘晃 :“ ループ管のスタックに厚い拡散層近似を用いた場合の熱音響振動の臨界条件 ”，　応用熱音響研究会，東北大学東京分室，2013 年 3 月 16 日

兵頭弘晃，杉本信正 :“ 拡散層厚さに応じた近似理論によるループ管内の熱音響振動の解析 ”，京都大学数理解析研究所，共同研究集会，京都大学，2013 年 10 月 16 日